The role of the cadherin *fmi-1/flamingo* in the development of the D-type GABAergic neurons

By

Submitted to the graduate degree program in Molecular Biosciences
and the Graduate Faculty of the University of Kansas in partial fulfillment of the requirements
for the degree of Doctor of Philosophy.

_____

Chairperson − Brian Ackley

_____

Erik Lundquist

_____

Robert Ward

_____

Stuart Macdonald

_____

John Karanicolas

_____

John Kelly

Date Defended: November 1, 2012

The Dissertation Committee for Elvis Huarcaya Najarro
certifies that this is the approved version of the following dissertation:

The role of the cadherin *fmi-1/flamingo* in the development of the D-type GABAergic neurons

_____

Chairperson – Brian Ackley

Date approved: November 1, 2012

Abstract

Cadherin proteins are cell adhesion molecules involved in multiple aspects of the development of the nervous system. A subgroup of these proteins, called protocadherin, has been recently shown to play key roles during the formation of neuronal networks in various animal models. In the model nematode *Caenorhabditis elegans*, there is only one protocadherin protein, called *fmi-1,* which has not being fully characterized. Here, I describe the cellular and molecular characterization of the cadherin *fmi-1/flamingo* in the development of the D-type GABAergic neurons.

Mutant alleles for *fmi-1* were originally isolated during a genetic screen looking for genes that regulate synaptic morphology in the D-type GABAergic neurons, which are comprised of DD and VD neurons. In fact, *fmi-1* animals display synaptic defects, which include reduced synapse number and aberrant synapse size and morphology, as well as an abnormal accumulation of synaptic vesicles at non-synaptic regions. Electron microscopy data reinforce these observations. Although synaptic defects were present in both the ventral nerve cord (VNC) and the dorsal nerve cord (DNC), it appears that synapses corresponding to the VD neurons are primary affected by *fmi-1* mutations. Furthermore, transcriptional analysis suggests that *fmi-1* is not present in the VD neurons. In fact, expression of *fmi-1* under a promoter that is not active in the VD neurons was able to partially rescue these defects. Therefore, in this cellular context, *fmi-1* might be acting cell non-autonomously.

Mutations in *fmi-1* also cause neurite growth defects in the VD neurons along the anteroposterior (A/P) axis. I have developed a VD-specific marker to visualize and score these defects. VD neurons in *fmi-1* animals display two different types of neurite defects. First, an anterior ventral neurite (AVN), which will become the axon, fails to extend fully in the VNC.

Second, VD neurons display a posterior ventral neurite (PVN) instead of a normal anterior neurite, which causes commissure patterning defects along the anteroposterior axis (A/P axis). These defects arose during the early development of the VD neurons and they appear not to be caused by defects in cell division or cell fate specification.

Fly and vertebrate homologues of *fmi-1* can work as part of the planar cell polarity (PCP) pathway. We found that mutations in two core components of the PCP pathway, *vang -1* and *prkl-1*, do not display *fmi-1*-like defects in the VD neurons. Therefore, *fmi-1* might be working independently from the PCP pathway to regulate directional neurite growth in these neurons.

Finally, I also describe genetic interactions between *fmi-1* and two components of the Wnt pathway, *lin-17/frizzled* and *dsh-1/disheveled*. Epistasis analyses suggest that *lin-17* and *dsh-1* work in a pathway distinct from that of *fmi-1* to regulate directional neurite growth in the VD neurons along the A/P axis.

In summary, *fmi-1* plays multiple roles during the development of the D-type GABAergic neurons. Interestingly, *fmi-1* and the Wnt pathway work redundantly to regulate VD neurite growth along the A/P axis in the VNC in *C. elegans*.

Acknowledgements

No challenging journey such as the one to become a scientist can be achieved without the support of key individuals. I would like to thank my parents, Aurelio Huarcaya Huamán y Flora Najarro Arce, for all their invaluable encouragement and support, for believing that getting an education is as important as getting food in one's belly. I would like also express gratitude to my brothers and sisters. Every one of them is an example of endurance and resilience against obstacles in life. Also, thank you to all my nephews and nieces for making me smile and telling me that they are proud of me. I would like to express special gratitude to my brother in law, Gonzalo Prieto Cámero, who took me under his wing as a mentee during the early years of college in Perú.

My best friend, my beautiful wife Sara Elizabeth Billings, deserves and will deserve all the credit for my success. It has been really important to have her as a counterbalance in my life and bring calm times to it. Thank you for everything.

I think of science as a type of art. If one wants to learn how to do the best possible art, one should find the best teachers. I have been very lucky to have three such teachers. I would like to express my sincere gratitude to my mentor Dr. Brian Ackley for giving me the opportunity to work in his lab. His scientific enthusiasm can only be surpassed by his qualities as a human being. Second, I would like to thank Dr. Michael Herman for teaching me how to work with *C. elegans*. Last but not least, I would like to acknowledge Dr. Erik Lundquist for all of his support.

Finally, I would like to thank the members of the Ackley lab, especially Raymond Caylor for his friendship and also the members of my committee for all their helpful suggestions.

Table of Contents

List of figures

List of Tables

Chapter I:

Introduction

Neurons are among the most specialized cells in the animal kingdom. They process and transmit information by electrical and chemical signaling. They contain highly specialized compartments to carry out their functions such as dendrites and axons, which typically are involved in receiving and transmitting information, respectively. Neurons do not work in isolation, but instead form networks. The formation of neuronal networks has traditionally been separated into different steps, including cell generation, cell migration, neurite growth and differentiation to form dendrites or axons, and finally synapse formation.

The use of model organisms has been important to uncover the cellular and molecular mechanisms that are essential for the formation of neuronal networks. The model nematode, *Caenorhabditis elegans*, has been especially important in this regard because of its relatively simple nervous system. In the adult hermaphrodite, the nervous system contains 302 neurons. In addition, *C. elegans* is a transparent organism, which allows researchers to label and visualized neurons in live animals. Furthermore, because of its short life span, *C. elegans* can be readily used to perform genetic experiments. For all these reasons, *C. elegans* is an excellent model organism to study the molecular and cellular mechanisms involved in the formation of neuronal circuits, particularly in axon growth and synaptogenesis.

Proper formation of neuronal networks requires cell-cell interactions. Cadherin proteins constitute one of the largest families of cell adhesion molecules and are involved in the mediation of neuronal interactions during the formation of the nervous system. In *C. elegans*, there are twelve genes that encode for thirteen cadherin molecules, including a single protocadherin called *fmi-1/flamingo*. Unlike classical cadherins, which are characterized by the presence of cadherin domains and an intracellular catenin-binding site, the domain composition of *fmi-1* includes nine cadherin domains, six EGF domains, two laminin G domains and one GPS

cleavage site. In addition, *fmi-1* also contains a seven-transmembrane domain and a small intracellular domain (Steimel et al., 2010, Najarro et al., 2012). Because of the presence of these protein domains, *fmi-1* is predicted to work as either an adhesion protein or as a receptor (Steimel et al., 2010, Najarro et al., 2012).

Homologs of *fmi-1* have previously shown to modulate different aspects of the development of the nervous system. For example, disruption of *flamingo*, the single *Drosophila* homolog of *fmi-1*, causes target selection defects of photoreceptor axons, dendritic defects and synapse formation defects formation (Gao et al., 2000, Curtin et al., 2003, Lee et al., 2003, Senti et al., 2003, Shima et al., 2004, Formstone and Mason, 2005, Tissir et al., 2005, Chen and Clandinin, 2008, Lewis et al., 2011). Unlike Drosophila, vertebrates have three *fmi-1* homologs called *celsr-1* to *3,* and loss-of-function mutations in these genes cause defects during the formation of neuronal networks (Berger-Muller and Suzuki, 2011). For instance, mutations in *celsr-3* cause axon growth and guidance defects along the anteroposterior (A/P) axis in the mouse and rat systems (Fenstermaker et al., 2010, Shafer et al., 2011). Interestingly, in these contexts, *celsr-3* appears to work in a planar cell polarity (PCP)-like pathway (Fenstermaker et al., 2010, Shafer et al., 2011). In addition, *celsr-3* appears to work cell autonomously here (Fenstermaker et al., 2010, Shafer et al., 2011). *flamingo* has also being shown to be part of the PCP pathway, however, in the *Drosophila* system, *flamingo* can also work independently from this pathway and a cell non-autonomous fashion (Lee et al., 2003, Senti et al., 2003, Chen and Clandinin, 2008).

In *C. elegans*, the axon bundles in the ventral nerve cord (VNC) can be separated into two axon tracks, the left and right axon tracks which run longitudinally along the A/P axis (Hutter, 2003). *fmi-1* has been shown to be important for axon track formation. In fact, *fmi-1* mutant

3

animals display axonal defects such as axon guidance and axon growth defects in the pioneer and pioneer follower neurons respectively (Steimel et al., 2010). Interestingly, mutations in two core components of PCP pathway, *vang-1* and *prkl-1*, do not display *fmi-1*-like defects in axon track formation suggesting that, in this context, *fmi-1* might be working independently from the PCP pathway (Steimel et al., 2010). The same study also shows that *fmi-1* might be acting cell autonomously and cell-non autonomously in the pioneer and pioneer follower neurons respectively to regulate axon guidance and growth in these neurons (Steimel et al., 2010). Overall, these data suggest that *fmi-1* has conserved functions similar to its vertebrate and *Drosophila* counterparts during the formation of the nervous system.

One question that remained unanswered in this previous study is whether *fmi-1* also has synaptic functions or other novel functions. We are using the D-type GABAergic neurons to uncover these potential *fmi-1* functions. The D-type GABAergic neurons are comprised of two types of neurons, the DD and VD neurons respectively (Hall and Russell, 1991, Knobel et al., 1999). Both types of neurons typically display a characteristic horizontal H-shape morphology (Hall and Russell, 1991, Knobel et al., 1999). The DD neurons are comprised of six neurons that are born during late embryogenesis and they make inhibitory synapses onto muscles located in the dorsal nerve cord (Hall and Russell, 1991, Knobel et al., 1999). In contrast, the thirteen postembryonically born VD neurons make inhibitory synapses onto ventral muscles (Hall and Russell, 1991, Knobel et al., 1999). The D-type GABAergic neurons, along with the cholinergic neurons, control the characteristic sinusoidal movement of the worm (Hall and Russell, 1991, Knobel et al., 1999). Because of its simplicity, the GABAergic system is an ideal model for understanding different aspects of the formation of the nervous system including synaptogenesis and axon growth (White, 1986, Hall and Russell, 1991). In addition, genetic tools to visualize

cellular and subcellular structures in the GABAergic neurons have been developed during the past few years. For example, *Punc-25::gfp* and *Punc-25::snb-1::gfp* genetic constructs can be used to visualized DD and VD neurons and the presynaptic sites of these neurons respectively (Jin et al., 1999, Zhen and Jin, 1999). Moreover, DD neurons can be specifically labeled using *Pflp-13::gfp* (Kim and Li, 2004) However, until just recently, it was not possible to specifically label the VD neurons. Here, I describe the engineering and use of *Punc-55::gfp* construct which allow visualization of the VD neurons at the single cell resolution.

We have found that mutations in *fmi-1* regulate synaptic morphology in the D-type GABAergic neurons. The types of synaptic defects include reduced synapse number, aberrant synapse size and morphology, as well as an abnormal accumulation of synaptic vesicles at non-synaptic regions. The VD neurons appear to be primarily affected by the loss of *fmi-1* even though we did not detect presence of *fmi-1* in these cells. Therefore, *fmi-1* could be acting cell-non autonomously to regulate synaptic morphology in the VD neurons. We also found that another cadherin, *cdh-4*, is present in the VD neurons and that it might be working in the *fmi-1* pathway to regulate synaptic morphology.

During the early development of the VD neurons, an anterior ventral neurite (AVN), the future VD axon, grows anteriorly away from the cell body positioned in the VNC. Little is known about the mechanism or mechanisms that control this early directional growth along the A/P axis. We have used a new VD marker, *Punc-55::gfp*, and found that *fmi-1* is important for this early anterior neurite growth. AVN in *fmi-1* animals fail to extend fully and some VD neurons display a posterior ventral neurite (PVN) instead of a normal anterior neurite, which causes commissure patterning defects along the anteroposterior axis (A/P axis). Mutations in *prkl-1* and *vang-1*, two core components of the PCP pathway, did not display *fmi-1*-like defects,

suggesting that, in this cellular context, *fmi-1* might be working in a novel pathway to regulate the direction of VD neurite growth along the A/P axis.

Previous observations have implicated the Wnt pathway in axon guidance and growth along the A/P axis. Similarly, we have found that mutations in components of this pathway cause neurite growth defects in the VD neurons. In fact, we discovered genetic interactions between *fmi-1* and two components of the Wnt pathway, *lin-17/frizzled* and *dsh-1/disheveled*. Further analyses indicate that *lin-17* and *dsh-1* work in a pathway distinct from that of *fmi-1* to regulate directional neurite growth in the VD neurons.

In summary, we have discovered that *fmi-1* plays multiple roles during the development of the D-type GABAergic neurons. *fmi-1* animals display defects in synaptic morphology in the DD and VD neurons. Furthermore, VD neurons display directional neurite growth defects along the A/P axis which are enhanced when components of the Wnt pathway are mutated, suggesting that redundant pathways regulate VD neurite growth along the A/P axis in the VNC in *C. elegans*, ensuring a reliable and robust formation of neuronal circuits.

Chapter II:

The *C. elegans* Flamingo cadherin *fmi-1* regulates GABAergic neuronal development

2.1 Abstract

In a genetic screen for regulators of synaptic morphology, we identified the single *C. elegans* flamingo-like cadherin *fmi-1*. *fmi-1* mutants exhibit defective axon pathfinding, reduced synapse number, aberrant synapse size and morphology, as well as an abnormal accumulation of synaptic vesicles at non-synaptic regions. FMI-1 is primarily expressed in the nervous system, however, it is not expressed in the Ventral cord D-type (VD) GABAergic motorneurons, which are defective in *fmi-1* mutants. The axon and synapse defects of VD neurons could be rescued when *fmi-1* was expressed exclusively in non-VD, neighboring neurons, suggesting cell non-autonomy action of FMI-1. FMI-1 protein lacking its intracellular domain retained its ability to rescue the vesicle accumulation defects of GABAergic motorneurons, indicating the extracellular domain (ECD) was sufficient for FMI-1 function in GABAergic NMJ development. Mutations in *cdh-4*, a Fat-like cadherin, cause similar defects in GABAergic motorneurons. *cdh-4* is expressed by the VD neurons, and appears to function in the same genetic pathway as *fmi-1* to regulate GABAergic neuron development. Thus, *fmi-1* and *cdh-4* cadherins might act together to regulate synapse development and axon pathfinding.

2.2 Introduction

Patterning of the nervous system requires interactions between neurons and their environment. Multiple secreted factors and cell adhesion molecules have been demonstrated to coordinate axon guidance, target selection and synapse formation (Shen et al., 2004, Colon-Ramos et al., 2007, Inaki et al., 2007). The *C. elegans* neuromuscular system has a simple architecture with stereotyped synaptic positioning (White, 1986), making it attractive to elucidate the molecular mechanisms that underlie neural circuit formation (Jin, 2005, Richmond, 2005). Body wall muscles are innervated by both excitatory (cholinergic) and inhibitory (GABAergic) motorneurons, with NMJs formed coordinately with 2 cholinergic NMJs per 1 GABAergic. The cholinergic neurons make synapses onto the muscles (NMJs) and on the GABAergic neurons, but the GABAergic neurons predominantly form NMJs (White, 1986, Hall and Russell, 1991).

In a screen for GABAergic motor neuron synapse defective mutants we recovered two loss-of-function alleles in *fmi-1,* the single *C. elegans* flamingo-like non-classical cadherin. Flamingo was isolated as a component of the planar cell polarity (PCP) pathway in Drosophila, where it functions with Frizzled, in parallel to Fat and Dachsous (Lu et al., 1999, Usui et al., 1999, Casal et al., 2006). Several studies have shown roles for *flamingo* and the vertebrate orthologs (Celsr1-3) in nervous system formation, indicating these molecules are functionally conserved. *flamingo* and Celsr disrupted animals have developmental defects in target selection, dendrite extension, axon outgrowth, synapse development and circuit formation (Gao et al., 2000, Curtin et al., 2003, Lee et al., 2003, Senti et al., 2003, Shima et al., 2004, Formstone and Mason, 2005, Tissir et al., 2005, Chen and Clandinin, 2008, Lewis et al., 2011). In the Drosophila neuromuscular system, Flamingo exhibits functions after development to prevent the formation of inappropriate ectopic synapses and inhibit axonal degradation (Bao et al., 2007).

9

Flamingo belongs to the class-B2 family of G-protein coupled receptors (GPCRs), which includes other molecules that function at synapses, *e.g.* latrophilins (Sudhof, 2001). Unlike classical GPCRs however there is no evidence that Flamingo binds directly to G-proteins, although there is evidence for indirect interactions with G-proteins (Shima et al., 2007). Overall, the downstream signaling pathways by which Flamingo/Celsr molecules exert their influence are unclear. In multiple contexts, *flamingo* mutants are not phenocopied by PCP mutations, implicating that Flamingo may use different signaling pathways in these events (Gao et al., 2000, Lee et al., 2003). Where it has been examined Flamingo binds homophilically between cells, but intriguingly, functions cell non-autonomously in retinal neurons to regulate level-specific target selection (Chen and Clandinin, 2008).

Here we show that *fmi-1* loss of function causes specific patterning defects in the GABAergic VD neurons. Interestingly, FMI-1 is not expressed in the VD neurons themselves, rather in the adjacent cholinergic motor neurons. Expression of FMI-1 in the cholinergic neurons can specifically rescue the synaptic patterning defects in VD neurons. We provide additional evidence suggesting that *fmi-1* interacts genetically with the Fat-like cadherin, *cdh-4*, which is expressed in the VD neurons. Thus, the *fmi-1* and *cdh-4* cadherins might function together in VD neuron development.

2.3 Results

fmi-1 mutations cause synapse defects

We recovered two alleles, *ju43* and *ju58,* in a visual screen for mutants with altered synaptic vesicles clustering at the GABAergic NMJs using the *juIs1[Punc-25 SNB-1::GFP]* reporter. Compared to the uniformly sized and distributed fluorescent puncta in the wild type animals (puncta area 0.8 μm^2, 25.7 puncta/100 μm), these mutants showed enlarged, aberrantly shaped accumulations of GFP-labeled vesicles (Table 1, Figure 1), with extended regions lacking fluorescent puncta (*ju43* – 1.2 μm^2, 22.6 puncta/100 μm and *ju58* – 1.5 μm^2, 19.2 puncta/100 μm). Overall, the NMJs formed on the ventral body wall muscles were more severely disrupted in *ju43* (1.1 μm^2, 21.7 puncta/100 μm) and *ju58* (1.8 μm^2, 17.6 puncta/100 μm) than those along the dorsal muscles, although defects were noticeable in the dorsal cord (*ju43* – 1.3 μm^2, 23.4 puncta/100 μm and *ju58* – 1.2 μm^2, 21.7 puncta/100 μm). Because the VD and DD class of GABAergic neurons innervate the ventral and dorsal muscles, respectively, these observations suggest that the DD and VD neurons may be differentially affected by the *ju43* and *ju58* mutations.

We mapped *ju43* and *ju58* to the right arm of linkage group V close to the locus encoding the single *flamingo* cadherin-domain containing protein (F15B9.7/*cdh-6*/*fmi-1*) (Pettitt, 2005). We further identified molecular changes in both alleles (see below). We analyzed additional alleles of *fmi-1*, including a deletion allele *tm306* (Figure 2) isolated by the National Bioresource Project (http://www.shigen.nig.ac.jp/c.elegans/index.jsp), *gm188,* isolated in a screen for HSN migration defects and *rh308* isolated in a screen for pioneer axon guidance defects (Steimel et al., 2010) and observed that all exhibited grossly similar patterns of synaptic defects (Table 1). The *fmi-1* coding region spans ~17 kb and is predicted to contain 25 exons (Figure 2). We

generated a full-length cDNA for *fmi-1* (~7.7 kb), using primers directed at the predicted translational start and stop sites (see Materials and Methods); sequence analyses of this cDNA confirmed the exon-intron junctions of *fmi-1*. We determined the molecular nature of each of the mutations. The *gm188* and *ju43* lesions are missense mutations that result in amino acid changes in highly conserved glycines present in the 7th Cadherin domain and first LamG domain, respectively, in the ECD (Figure 2). The *ju58* mutation causes a premature stop and *tm306* deletes a portion of the coding region and introduces a premature stop codon (Figure 2). We partially rescued the defects using a fosmid genomic clone covering the *fmi-1* locus (Figure 1). The ventral cord SNB-1::GFP puncta, corresponding to VD neurons, in *ju58* animals had an apparent area of 1.80 μm^2 with 17.6 puncta/100 μm, while *ju58* animals containing the *fmi-1* fosmid formed puncta of 1.15 μm^2, with 19.9 puncta/100 μm, which was a significant improvement (p<0.05). To determine if the expression of *fmi-1* fosmid might cause defects in wild-type animals, we crossed the rescuing extrachromosomal array away from *ju58* and found the animals had normally sized puncta (0.9 μm^2), with a small increase in the number of puncta formed (25.7 ventral cord puncta/100 μm – *juIs1* vs. 26.5 puncta /100 μm – *juIs1+fmi-1)*, but the effect was not statistically significant (p>0.05). The rescue of *ju58* by transgenic expression suggests that the altered SNB-1::GFP patterning was likely due to a loss of *fmi-1* function.

The body wall muscles receive extensive cholinergic inputs from the cholinergic motor neurons. A synaptic vesicle marker for the cholinergic motor neurons (*nuIs94[Punc-129 GFP::SNB-1]*) displayed differences in *fmi-1* mutants as well (Figure 1, Table 1). In wild-type *nuIs94* animals, SNB-1::GFP were clustered in a relatively even sized and shaped pattern along the dorsal and ventral cords. In *ju58* animals the dorsal cord SNB-1::GFP puncta were slightly larger (1.03 μm^2 – WT vs. 1.17 μm^2 – *ju58*, *p*=0.002), while the puncta in the ventral cord were

approximately the same sizes (0.90 μm^2 – WT vs. 0.98 μm^2 – *ju58*, *p*>0.05). In *ju58* animals, there were occasional fluorescent puncta gaps not commonly observed in the wild-type animals, leading to a slight reduction in the total puncta formed (wt 26.7 puncta/100 μm vs. *ju58* 23.8/100 μm, p<0.05). Overall, the SNB-1::GFP marker in GABAergic neurons appeared to be more severely affected by *fmi-1* mutations than in cholinergic neurons.

fmi-1 synaptic defects occur during development

In our screen and subsequent analyses we primarily scored synapses in young adults. For the regions of the nerve cord lacking synaptic puncta, we asked whether these gaps could be due to a degeneration of synapses that were formed earlier in development, as has been reported for *Drosophila flamingo* mutant (Bao et al., 2007). The 13 VD motorneurons form and begin to establish NMJs during the first larval stage (L1). From L2 until adult the animals grow ~3-5 fold in length, and because no new VD neurons are born, the axons must elongate and add synapses during development. We therefore examined wild type and *fmi-1* mutant animals in stages L2, L3 and L4. We found that the *fmi-1* mutants had regions of the ventral cord lacking synaptic puncta as early as L2 (Figure 3). We did not see a significant change in the frequency of regions in the nerve cord lacking vesicles in younger vs. older animals (L2 – 1.2 gaps/ventral cord, L3 – 1.5, L4 – 1.5, Adult – 1.7, F=1.02, *p*=0.4, N=25 animals/stage). Therefore, we conclude that the absent synapses are more likely due to developmental defects in these neurons.

We further examined the gaps present in the SNB-1::GFP accumulation in VD neurons. In *fmi*-1 mutants, we identified two types of gaps in the SNB-1::GFP pattern in VD neurons; class I, where the gap occurred from a point in the line of synapses and then extended to the next cell body (Figure 3A-F) and class II, where synaptic puncta were present both anterior and posterior

13

of the SNB-1::GFP gap. The transport of synaptic material distal to the class II gap from the cell body suggests that either the axon is intact between those two points, or that the distal puncta arose from another neuron. In *fmi-1(tm306);juIs1* (SNB-1::GFP) animals (N=30) we found 1.4±0.77 gaps/animal. Of those, 42/57 gaps were class I, while 15/57 appeared to be class II. To address whether VD neurons had axon extension defects we examined the VD axons using a *Punc-55::gfp* reporter. 88% of *fmi-1(tm306)* mutants [1.26±0.85 gaps per animal (N=24)] exhibited axon extension defects in the VD neurons, compared to zero gaps in wild type. This analysis suggests that axon extension likely underlies the majority of the SNB-1::GFP gaps found in VD neurons, while a minority could arise from synaptic patterning defects within axons.

Additionally, we asked whether the SNB-1::GFP puncta morphology changes in VD (enlarged size) were affected by proximity to gaps. We calculated the average area of fluorescent SNB-1::GFP puncta within 10 µm of a gap versus those that were further than 10 µm. We observed no significant effect of being near a gap on the size of the puncta [*tm306* – (1.75±.40 near a gap vs. 1.42±0.15 distal, *p* =0.49) and *rh308* – (1.59±.60 near a gap vs. 2.03±0.42 distal, *p* =0.59)]. Thus, we concluded that the morphological aberrations in SNB-1::GFP accumulation likely represent an additional contribution of FMI-1 to VD neuronal development.

fmi-1 contributes to VD active zone development

To determine if other synaptic proteins were affected by loss of *fmi-1*, we examined the active zone proteins SYD-2 (Zhen and Jin, 1999) and UNC-10 (Koushika et al., 2001) in *fmi-1* mutants. We visualized the GABAergic active zones using a SYD-2::GFP reporter (Yeh et al., 2005), and found disruptions in the pattern of accumulation, including enlarged, misshapen puncta as well as areas lacking SYD-2 (Figure 3G,H). By wholemount immunostaining using

anti-UNC-10 antisera, we found that global UNC-10 accumulation within the nervous system was relatively normal (Figure 3I,J). The latter observation does not rule out subtle changes of UNC-10 in specific neurons, or a role for FMI-1 in directing the delivery of synaptic materials. Overall, *fmi-1* has a broader role in GABAergic synapse development, not limited to vesicle accumulation.

Synaptic components accumulate in non-synaptic sites in fmi-1 mutants

We examined the nervous system of *fmi-1(ju43)* and *fmi-1(ju58)* animals using ultrastructural analysis, and compared dorsal cord motor neuron synapses to similar regions of a wild-type animal (Figure 4). We calculated the length of the active zones and vesicle clustering domains, as well as the number of synaptic vesicles per synapse in the dorsal cord (Table 2). We found that in both *fmi-1* mutant alleles (N=1/genotype), the length of the GABAergic synapses, defined as a continuous series of sections containing clusters of synaptic vesicles surrounding the active zone, was approximately half that of the wild type, and that there was an ~50% reduction in the total number of vesicles present at the presynaptic terminals. However, the number of SVs in sections containing presynaptic density was not significantly different between *fmi-1* and wild type. We also noticed differences in the morphology of synaptic vesicles at the GABAergic NMJs in the *fmi-1* mutants. In wild type synaptic vesicles at GABAergic NMJs were of mostly equal size (30-50 nm) and were internally clear. By contrast the vesicles in the *fmi-1* mutants were enlarged, and often had electron dense material within the vesicles (Figure 4).

Within the segment of nerve cords we examined, the cholinergic synapses were more affected in the *ju43* than *ju58* background. In *ju43* animals the cholinergic synapses were longer than wild type (WT 618 nm vs. *ju43* 922.5 nm), but had approximately the same number of

synaptic vesicles as wild type. In *ju43* mutants cholinergic synapses also had a disrupted morphology whereby they formed NMJs containing multiple presynaptic densities, and some synapses appeared to be misplaced away from muscle targets (Figure 4).

The discrepancy between the ultrastructural results (smaller synapses) and fluorescent measurement of SNB-1::GFP (enlarged puncta) suggests that the GFP labeled material may not be present at synapses (defined by the presence of an active zone), or that the enlarged puncta, which appeared contiguous at the light microscopy level, may include closely positioned but separate synapses. The former phenotype has been observed previously in *unc-16* mutants where synaptic materials become trapped in enlarged cisternae within the axons (Brown et al., 2009). The observation of electron dense materials within vesicles might also reflect a failure in the assembly of active zone components at the plasma membrane, consistent with the SYD-2::GFP results. Overall it would appear that *fmi-1* mutations had a complex effect on synapse formation.

fmi-1 mutants exhibit axon guidance and fasciculation defects

We examined the axonal morphology of the GABAergic motorneurons with two GFP markers, *juIs145* and *juIs76* (Huang et al., 2002, Wu et al., 2007). These mark the DD neurons and DD/VD neurons respectively (Figure 5, Table 3). We observed multiple defects in the outgrowth of the VD and DD neurons, including errors in the left or right side of the ventral cord on which the commissural axon exits (L/R decision − 2% of the animals had defects in WT vs. 48% in *ju43* and 67% *tm306*) and the ability of the neurons to remain tightly bundled (defasciculations − 0% of WT animals vs. 50% of *ju43* and 36% of *tm306*) (Figure 5, Table 3). *fmi-1* animals also exhibited failures in longitudinal axon extension (Figure 5) in both DDs (*juIs76* observed in L1 animals) and VDs (see above) (Table 4). Only 4% of wild type animals

16

exhibited a gap between the cell body of a DD and the process from the next DD posterior (i.e. cell body of DD2 and axon of DD3). In *fmi-1* mutants we found multiple gaps (~2/animal) in >70% of animals examined. Also, similar defects were observed for the cholinergic neurons using the *juIs14* GFP marker (Figure 5) (Huang et al., 2003). Transgenic expression of a functional FMI-1::GFP rescued the axon extension phenotypes observed in *fmi-1(tm306);juIs76* L1 animals (*tm306lhIs9* – 30% gaps, 0.36±0.60/animal (N=33) vs. (*tm306* – 73% of animals, 1.72±1.17 gaps/animal, N=30) (Table 4).

Axon guidance phenotypes were also observed in the ultrastructural analysis. Wild type animals had, on average, 12.6 processes in the dorsal cord and 52.4 in the ventral cord (right bundle). *ju43* animals had a significant increase in the number of processes in the dorsal cord, 15.6, and a significant decrease in the ventral cord, 47.6 ($p < 0.05$). In *ju58* animals the dorsal cord was normal, 12.4 processes, but the ventral cord had a significant decrease, 44.4 ($p < 0.05$). These differences could be due to premature termination, inappropriate posterior extension, or from axons crossing into the contralateral bundle, as has been described here and previously (Steimel et al., 2010). Overall our evidence shows that mutations in *fmi-1* can cause defects in the synapse and axon patterning of both cholinergic and GABAergic motorneurons. However, defects in the morphology of synapses and accumulation of synaptic materials were present in intact axons that appeared to develop normally (Figures 3,4), suggesting that *fmi-1* may affect both axon outgrowth and synaptogenesis.

Axon guidance defects are FMI-1 dose-dependent

We also found that overexpression of Flamingo induced axon outgrowth errors, which has also been reported in Drosophila (Chen and Clandinin, 2008). Our FMI-1::GFP integrant, *lhIs9*,

when present in the wild-type background induced axon guidance defects, including L/R errors (68% of animals) and neurite outgrowth from VD commissures (Figure 5). When the total amount of FMI-1 was reduced, by crossing the integrant to *fmi-1(tm306)*, many of the defects associated with the integrated chimera were improved. For example, in *lhIs9;juIs76* animals (8/30) had commissural processes that deviated along the anterior/posterior axis, and some of these had ectopic neurites growing out of them (6/30) (Figure 5). This phenotype was not present in wild type, nor in *tm306* alone. The *fmi-1(tm306)lhIs9;juIs76* animals rarely (2/36) had misrouted axons along the A/P axis, and none (0/36) had ectopic neurites (p<0.05). Overall the percentage of animals not displaying any L/R or ectopic neurite outgrowth phenotypes (% wild-type) was higher in the *lhIs9tm306* (24%) animals than in either single mutant background (*lhIs9* – 12% and *tm306* – 10%). We interpret these results along with our loss of function data as an indication that the GABAergic motorneurons were sensitive to the levels of FMI-1 present in the animal. Either too much or too little FMI-1 resulted in axon patterning defects in the GABAergic motorneurons.

FMI-1 protein localization is non-overlapping with synaptic vesicle proteins

To examine the subcellular localization of FMI-1, we generated antisera to the intracellular domain of FMI-1 as well as a full-length GFP tagged genomic clone (see Materials and Methods). Using both methods we found that FMI-1 accumulated to a region of neuropil around the nerve ring and the ventral cord (Figure 6). FMI-1 was also present in the dorsal cord in young animals, but was rarely observed in neuronal cell bodies. We observed no staining in the candidate null alleles, *ju58* (Figure 6), *rh308* (Steimel et al., 2010) or *tm306* (data not shown), indicating our antisera is specific. Because deletions of domains with the extracellular portion of

18

FMI-1 affected protein localization (Steimel et al., 2010) we examined the effects of the missense mutations, *ju43* and *gm188*, that affect the extracellular domain. These animals retain immunoreactivity, and the protein was still localized to axon segments, indicating that the phenotypes in these animals are not due to gross mislocalization of the protein (Figure 6).

To assess the subcellular domain of FMI-1, we co-stained animals with antibodies to FMI-1 and to the synaptic vesicle protein synaptotagmin (SNT-1) (Figure 6). In wild type animals FMI-1 was concentrated in the nervous system, but was not overlapped with SNT-1. We calculated the intensity colocalization coefficient (see materials and methods) for FMI-1 and SNT-1 in the ventral cord and found that in wild-type animals $r=0.27\pm0.08$ (N=6). Because of the *en passant* organization of synapses formed in the ventral nerve cord, it is not possible to determine where FMI-1 is localized with single axon/synapse resolution. Nonetheless, this analysis showed that FMI-1 was not strongly localized to regions containing synaptic vesicles.

Flamingo is expressed in a subset of motor neurons

To determine which motor neurons express *fmi-1,* we fused a 2.6 kb fragment of DNA upstream of the *fmi-1* start codon to GFP. Our expression pattern was consistent with what has been previously reported for *fmi-1* (Steimel et al., 2010). To specifically identify which motorneurons express *flamingo* we co-expressed an RFP (*mCherry)* reporter in GABAergic (*Punc-25)* or cholinergic (*Pacr-2*) neurons (Figure 7). We observed consistent colocalization of GFP and RFP between *Pfmi-1-gfp* and *Pacr-2-rfp* in the DA, VA and VB and weakly in the DB cholinergic neurons (Figure 7). We occasionally observed a limited co-expression of *Punc-25-rfp* and *Pfmi-1-gfp* in the DDs of some L1 animals (<10%) (Figure 7), but never in the VDs (>L2).

Thus, we find no evidence that the *fmi-1* promoter is active in the VD neurons, which are sensitive to mutations in the gene.

fmi-1 might regulate VD development cell non-autonomously

We used the FMI-1::GFP (Steimel et al., 2010) expressed under its endogenous promoter to rescue of the *fmi-1* synaptic defects. We injected the P*fmi-1::fmi-1gfp* (0.5 ng/µl) plasmid into *fmi-1(tm306)* along with a *Punc-25::snb-1dsRed* to visualize GABAergic NMJs. The expression of full-length FMI-1 protein efficiently rescued the synaptic spacing (gaps) (*tm306* − 1.72±0.92 gaps/cord vs. *tm306+fmi-1gfp* − 0.72±0.6, *p*=3x10^{-5}), and rescued the morphology defects (2/2 lines). Interestingly, we found that the intracellular domain deletion FMI-1ΔInt::GFP could also rescue the synaptic clustering defect in the GABAergic neurons (2/3 lines, 0.77±0.71 gaps/cord, *p*=2.1x10^{-4}) (Figure 8). Importantly, we found that in the rescued animals using either full length (data not shown) or the FMI-1ΔInt, the GFP labeled proteins were not detectable in VD neurons (Figure 8). To ensure that this was not due to transgene mosaicism, we integrated the array carrying the P*fmi-1*::FMI-1ΔInt::GFP and Punc-25::SNB-1::RFP, and recovered 4 independent integrated lines. None (0/4) of the integrated lines exhibited any co-expression of the GFP and RFP proteins (Figure 8). This analysis further supports that FMI-1 is not required in VDs for proper synaptogenesis.

To test the site of action of FMI-1 more rigorously we attempted to rescue the defects by expression of FMI-1 in specific cells. We were unable to rescue the synaptic defects in *tm306* when we expressed the *fmi-1* cDNA specifically in the GABAergic neurons (0/3 lines). In fact, even at the lowest concentration tested (0.5 ng/µl) we saw what appear to be more grossly distended synapses in the ventral nerve cord (*tm306* 1.43 µm^2 vs. *tm306+Punc-25::fmi-1* 2.11

μm^2). In contrast we could partially rescue the synaptic morphology defects in the VD neurons of *fmi-1(-)* animals when the cDNA was specifically expressed from a cholinergic promoter (Pacr-2) (4/6 lines) (*tm306* 1.43 μm^2 vs. *tm306+Pacr-2::fmi-1* 1.06 μm^2; $p < 0.05$). Thus, while we cannot formally rule out that a small amount of FMI-1 is produced in the VDs, expression of FMI-1 in non-VD neurons was able to either fully (P*fmi-1*) or partially (P*acr-2*) rescue the VD defects.

In the cell-type specific rescue experiments we used a cytoplasmic RFP to mark the cells expressing the FMI-1 transgene. In *fmi-1* mutants with *Punc-25::fmi-1* we still observed that some axonal regions appeared to lack SNB-1::GFP (Figure 8A), although these processes could also come from the DDs, which also express *unc-25*. We found no gross difference in the severity of synaptic defects in axons that developed normally or those that exhibited guidance defects. In animals expressing *fmi-1* under the cholinergic promoter, occasionally we observed defasciculation of the SNB-1::GFP-labeled GABAergic axons and the RFP labeled cholinergic processes (Figure 8C). This suggested that FMI-1 could be acting locally to influence GABAergic neuron development.

Another possibility that could explain the defects is that FMI-1 functions within cholinergic neurons to maintain axon fasciculation, and that the synaptic defects in GABAergic neurons are secondary to disruptions in the cholinergic fascicle. To address this, we examined *fmi-1(tm306)* mutants with the cholinergic neurons marked by RFP, but lacking the *fmi-1* rescuing transgene. VD neurons exhibited NMJ defects in regions where cholinergic axons were properly fasciculated (Figure 8D), and we found no correlation between cholinergic axon defasciculation and VD synaptic defects ($r=0.16$, $N=50$). Altogether these results suggest that FMI-1 functions locally to influence VD development, rather than simply to maintain cholinergic axon bundling.

Mutations in CDH-4 a Fat-like cadherin exhibit fmi-1-like synaptic defects

Cadherin proteins typically interact homophilically, although there are instances where cadherins exhibit heterophilic interactions (Prakasam et al., 2006). We found that the VD defects in *fmi-1* mutants were rescued when FMI-1 was expressed in neighboring neurons, including the cholinergic neurons, suggesting that FMI-1 likely functions through other proteins in GABAergic neurons. Thus, we examined the other cadherin domain containing proteins to determine if any were functioning in the same genetic pathway with *fmi-1*.

There are 11 genes in the *C. elegans* genome that encode for 12 proteins with cadherin repeats (Yamashita et al., 2004). Of those, 6 are evolutionarily conserved, *fmi-1/flamingo, hmr-1B/N-cadherin, cdh-1/Dachsous, cdh-3/Fat, cdh-4/Fat* and *cdh-11/calsyntenin,* while the remainder (*cdh-5,-7,-9,-10,-12)* appear to be nematode specific. We tested whether systemic RNAi of the conserved cadherin genes phenocopied the *fmi-1* loss-of-function alleles. Using the *eri-1* mutation to potentiate RNAi in the neurons, we found that only the knockdown of *cdh-4(RNAi)* most closely resembled the vesicle accumulation defects in *fmi-1* mutants (Figure 9, Table 1) (*eri-1;cdh-4RNAi* – 1.56 μm^2, 16.7 puncta/100 μm). The knockdown of *cdh-4* in *fmi-1* mutants did not significantly enhance the penetrance of defects (Figure 9) (*tm306*;*eri-1;cdh-4RNAi* – 1.57 μm^2, 17.8 puncta/100 μm).

Two *cdh-4* loss of function alleles, *lq56* and *lq83,* were identified in a screen for Q-cell descendant migration defects (E. Lundquist, unpublished observations). Both alleles result in premature stop codons (*lq83*-R126Amber and *lq56*-L838Amber). We found that the pattern of SNB-1::GFP in GABAergic motor neurons was similar to those observed in the RNAi experiments for *cdh-4* as well as *fmi-1* single mutants (Figure 9, Table 1) (*cdh-4(lq56)* – 1.40 μm^2, 16.7 puncta/100 μm, *cdh-4(lq83)* – 1.82 μm^2, 16.6 puncta/100 μm). NMJs in double

mutants of *cdh-4* and *fmi-1* were similar to the single mutants (*fmi-1(tm306);cdh-4(lq56)* – 1.48 μm², 18.1 puncta/100 μm, *fmi-1(tm306);cdh-4(lq83)* – 1.45 μm², 16.6 puncta/100 μm), consistent with these two molecules functioning in a linear genetic pathway.

Previously Schmitz et al., have described embryonic development, cell migration and axon guidance phenotypes associated with mutations in the *cdh-4* locus (Schmitz et al., 2008). We therefore examined the GABAergic axon patterning in *cdh-4(lq83)* and *cdh-4(lq83);fmi-1(tm306)*. As previously reported we found multiple types of defects in *cdh-4* mutant animals, including animals with L/R defects (*cdh-4* 30%, *fmi-1;cdh-4* 35%) and defasciculations (*cdh-4* 29%, *fmi-1;cdh-4* 22%) (Figure 9, Tables 3,4). Although the percentage of animals with axon guidance defects in the double mutants was similar to the *cdh-4(lq83)* single mutants, in some animals we observed a slight increase in the severity of some phenotypes (Figure 9). Thus, these proteins may function in overlapping pathways for axon guidance.

The cadherin domains of FMI-1 are partially required for their localization to axons. When the cadherin domains are specifically deleted more of the FMI-1::GFP is localized to the cell bodies (Steimel et al., 2010). Therefore, we asked whether CDH-4 might be required for the efficient localization of FMI-1 to axons. However, we observed no gross changes in the localization of FMI-1::GFP when *cdh-4* was removed by mutation or knocked down by RNAi (Figure 9). Thus, our experiments suggest that CDH-4 is not required to localize FMI-1 to axons.

We tested whether *cdh-4* is expressed in the VD motorneurons by examining the expression of *Pcdh-4::gfp* (*hdIs46*) relative to our motoneuron markers (Figure 9). As has been described, *cdh-4* is expressed in a broad set of neurons, including motorneurons, as well as other tissues, such as the epidermis, starting early in development (Schmitz et al., 2008). We find that by the L3/L4 larval transition the expression of *Pcdh-4::gfp* was decreasing in the nervous system, and

was no longer detectable in cholinergic neurons labeled by *Pacr-2::rfp*. In contrast, the remaining neurons labeled by *Pcdh-4::gfp* after this period of development expressed *Punc-25::rfp*, indicating that the VD neurons continued expressing *cdh-4*.

2.4 Discussion

Flamingo cadherins regulate multiple facets of neuronal development

Here we have shown that the single *C. elegans* Flamingo protein regulates multiple aspects of motoneuron development. Mutations in *fmi-1* cause axon outgrowth and synaptic defects in the cholinergic and GABAergic motorneurons. *fmi-1* and *cdh-4,* two conserved cadherin-domain containing proteins both affect GABAergic development, and appear to function in a common genetic pathway. FMI-1 seems to non-autonomously influence GABAergic development, as we find no evidence that *fmi-1* is expressed in the VD GABAergic neurons. Whereas *cdh-4* appears to be expressed within these neurons, but where it is required for GABAergic development remains to be determined. It remains possible that these two molecules may function in receptor-ligand like fashion to facilitate VD development.

Planar cell polarity and synaptogenesis share a common goal

Flamingo was initially isolated as a component of the planar cell polarity pathway, where it functions to establish asymmetric protein localization within a cell. This asymmetry helps break a field of equivalent epithelia into cells polarized to a body axis. On a different scale, synaptogenesis within a VD neuron has a similar goal. The neuron must form synapses along the axon, but interspersed are regions that do not form synapses, i.e. asymmetric localization of protein complexes with the axon. It is interesting to speculate on how a PCP-like activity may have become specialized to ensure patterning of synaptic vs. non-synaptic specializations. For example, these proteins could mark regions of the axon where synapses can or cannot form. Additional evidence for this comes from the identification that Wnt signaling regulates the accumulation of Frizzled receptors to the appropriate segment of the DA9 axon, to ensure the

proper delivery of synaptic components (Klassen and Shen, 2007). Our ultrastructural analysis suggests FMI-1 functions to ensure the proper delivery or assembly of synaptic components, but the precise mechanism by which this occurs remains to be elucidated.

FMI-1 affects both axon extension and synaptic development

We have found that *fmi-1* mutations result in multiple neuronal defects, including altered axon outgrowth and synaptic patterning. Drosophila Flamingo/*fmi* mutants also exhibit both axon pathfinding and synaptogenesis defects in motor neurons (Bao et al., 2007). Interestingly, Flamingo mutants motor axons form ectopic synapses *en passant*, a type of synapses that wild-type Drosophila motor neurons do not form at all. These types of synaptic contacts are also seen in misrouted axons in the brains of *fmi* mutants (Lee et al., 2003, Senti et al., 2003), suggesting that these synapses may occur due to the axon being placed in an unfamiliar context. Similar to our ultrastructural studies, Bao *et al* found that synaptic components can be mislocalized to regions of the axon when it is not contacting its normal target (Bao et al., 2007). Although it's unclear whether this reflects a failure in synaptogenesis or target recognition, it would appear that Flamingo proteins are involved in how synaptic components are directed appropriately within axons.

Axon guidance and synaptogenesis defects occur in many backgrounds where cell adhesion molecules are mutated, *cle-1, nid-1* and *ptp-3*, *unc-40, unc-5* and *unc-6.* Where it has been examined, many have concluded that these defects can be separated (Ackley et al., 2003, Gally and Bessereau, 2003, Ackley et al., 2005, Colon-Ramos et al., 2007, Poon et al., 2008, Killeen, 2009). The synaptic phenotypes in these cell adhesion mutants are distinct from each other as well as from those in *fmi-1*. Although clearly there is an impact of axon pathfinding on synaptic

26

development, it is unlikely that simply being axon guidance defective results in the specific synaptic phenotypes we see in *fmi-1*. Rather, it is more likely that FMI-1 activity patterns both axons and synapses within the nervous system. However, in the absence of *fmi-1* alleles that cause only one phenotype, or downstream effector molecules specific for each function, we cannot rule out that the synaptic phenotypes in *fmi-1* result from the specific combination of axon outgrowth defects present in these animals.

Other genes involved in epithelial polarity have been found to also regulate axon growth and synapse formation in recent years. Vertebrate polarity proteins such as Par3 and Par6 interact with atypical protein kinase C (aPKC), Inscuteable and/or PINS to link signaling from extracellular ligands (*e.g.* NGF or netrin-1) to changes in epithelial polarity (Zhang and Macara, 2006, McCaffrey and Macara, 2009). In some cases these signals indicate to a migrating axon to transition from a migratory, non-synapse forming growth cone, to an adherent synapse forming axon. Synapse formation and axon extension are also linked in *C. elegans* (Grill et al., 2007, Yan et al., 2009, Trujillo et al., 2010). VD neurons are born at the L1 larval stage, and their neurites increase ~3-5 fold in length by the time the animal reaches the adulthood. We find that FMI-1 expression continues throughout development, and that the protein is present into adulthood. This may indicate that FMI-1 functions in the continued development of the nervous system that occurs in those stages, such as axon extension and synaptogenesis.

Cell non-autonomous role of fmi-1

Previously, where it has been examined, Flamingo can interact homophilically, and has been demonstrated to function via self-interactions (Usui et al., 1999, Chen and Clandinin, 2008, Chen et al., 2008). In our study we find that the VD neurons do not produce detectable levels of

Flamingo, yet they are among the most sensitive cells to the absence of FMI-1. The defects in VD neurons were rescued when we use promoters that are not active in the VD neurons (P*fmi-1* and P*acr-2*). FMI-1 lacking the intracellular domain is capable of rescuing the vesicle accumulation defects, even though it is not expressed in the VD neurons. All together these results indicate that FMI-1 is likely functioning cell non-autonomously to regulate the axon and synapse development of the VD neurons.

Flamingo has previously been shown to act cell-non-autonomously, most elegantly in the Drosophila retinal axons (Chen and Clandinin, 2008). They demonstrated that mosaics in which only one of six R neurons was *fmi*(+) exhibit more defects observed in the neurons contacting the FMI containing neuron than in the adjacent neurons, and that over-expression of the FMI-1 ECD was sufficient to induce targeting defects. They concluded that cells are effectively gauging the amount of Flamingo and that asymmetric levels lead to functional consequences. Similarly, we find that, in rescue and overexpression experiments, phenotypes are quite dose-dependent, suggesting that changes in protein levels are important for cellular responses to Flamingo.

FMI-1 interacts genetically with a Fat-like cadherin protein

We find that knockdown of *cdh-4* by RNAi or mutation phenocopies *fmi-1* in synaptic development. In planar cell polarity, Fat and Dachsous have been shown to function together in parallel to Flamingo (Lawrence et al., 2004, Casal et al., 2006). Here we find that during *C. elegans* development Flamingo and CDH-4 appear to have overlapping functions. We see no obvious enhancement of the embryonic or larval lethality caused by *cdh-4* mutations when *fmi-1* is removed from those animals, suggesting no involvement of Flamingo in this process. Our data suggest that *fmi-1* and *cdh-4* primarily function in a linear genetic pathway with regards to the

development of the VD motorneurons, which would be the first indication of such a relationship for these two conserved cadherins.

We find that CDH-4 has a limited, if any, role in the gross localization of FMI-1, although subtle changes in the localization of FMI-1 could be important for its activity. We also find that the promoter of CDH-4 is active in the VD neurons, and that the expression of this gene continues throughout VD development. Because synaptogenesis continues after the axons have become patterned, the continued expression of *cdh-4* in the VDs is consistent with a role for this protein in the formation of VD synapses. The relationship between these proteins could be key to understanding how cholinergic neurons may pattern the GABAergic synapses in the neuromuscular system of *C. elegans.*

2.5 Materials and Methods

***C. elegans* strains**: All *C. elegans* strains were maintained at 20-22.5 ℃ as described (Brenner, 1974), with the exception of *eri-1(mg366)* animals, which were maintained at 18 ℃. The P*fmi-1*::FMI-1venusGFP integrants (*lhIs9* and *lhIs10),* P*fmi-1*::FMI-1Δint::GFP (*lhIs27-lhIs30)* and *Punc-55::*GFP (*lhIs35)* integrants were isolated using trimethyl psoralen/UV mutagenesis and all were out-crossed to wild type six times prior to analyses. The following alleles were used in this work: *fmi-1(ju43), fmi-1(ju58), fmi-1(tm306), fmi-1(rh308), fmi-1(gm188), cdh-4(lq83), cdh-4(lq56), eri-1(mg366), juIs1 [Punc-25::SNB-1::GFP], nuIs94 [Pacr-2::SNB-1::GFP], juIs76 [Punc-25::GFP], juIs14 [Pacr-2::GFP], juIs145 [Pflp-13::GFP], lhIs9* and *lhIs10 [Pfmi-1::FMI-1::venusGFP], lhIs27-lhIs30 [Pfmi-1::FMI-1Δint::GFP+Punc-25::SNB-1RFP], lhIs35 [Punc-55::GFP]* and *hdIs46 [Pcdh-4::GFP].*

Molecular Biology: The *fmi-1* cDNA was prepared by reverse transcription (RT)-PCR using RNA made from mixed-stage of wild type (N2) animals. RNA was isolated using the Trizol reagent Invitrogen (Carlsbad, CA), and RT-PCR conducted using the $dT_{23}VN$ primer and the ProtoScript II RT-PCR Kit NEB (Ipswich, MA). Amplification of the cDNA was conducted using Phusion polymerase (NEB). The resulting *fmi-1* 7.7 kb PCR product was cloned into the pCR8/GW/TOPO vector to generate pEVL89. The plasmid was completely sequenced and determined to be free of PCR-induced mutations. For the *fmi-1* promoter driving GFP clone pBA202, a ~2.6 kb region upstream of the ATG was amplified by PCR and TOPO cloned into pCR8/GW/TOPO (Invitrogen). The plasmid (pBA202) was then cut with *Sph1* and *ClaI* and the *fmi-1* promoter was cloned upstream of the gfp cassette from pPD114.108 in place of the *mec-7* promoter cut with the same enzymes. The *fmi-1* cDNA was independently recombined into

destination expression clones containing the *unc-25* promoter (pBA153) and *acr-2* promoter (pBA223) using LR clonase (Invitrogen). To rescue the synaptic phenotypes associated with *fmi-1(ju58)* we injected a fosmid (WRM066DB07) (GeneService Ltd., UK) that covered the *fmi-1* genomic region, including approximately 1 kb upstream. The fosmid was injected into *fmi-1(ju58);juIs1* animals at a concentration of 2ng/µl along with pBA182 (5ng/µl) as a co-injection marker. The sequence of all primers and plasmids used in this work are available upon request.

FMI-1 Antisera: Antisera were raised against the intracellular domain of FMI-1 corresponding to the entire intracellular domain (AA 2455-2596). We purified the antisera using a maltose binding protein-FMI-1 fusion produced in *E. coli* and purified on an amylose-resin (NEB, Ipswich MA) by column chromatography using the manufacturer's instructions.

Whole-mount immunostaining: Animals were fixed as described (Ackley et al., 2003), with the following modification, the animals were fixed for two hours on ice and the reduction step was performed using 1x borate buffer for two hours at 37 °C. The following primary antisera were used in this report: mouse anti-GFP Roche (Indianapolis, IN) used 1:1000, rabbit anti UNC-10 (Koushika et al., 2001) used 1:1000, mouse anti UNC-10 (Developmental Studies Hybridoma Bank - http://dshb.biology.uiowa.edu/) used 1:1000, rabbit anti-SNT-1 (Nonet et al., 1993) used 1:2000, rat anti-FMI-1 used 1:1000. The following secondary antibodies were purchased from Molecular Probes (Eugene, OR) and were used at 1:2000: Alexa 488 labeled anti-mouse, Alexa 594 labeled anti-rabbit, Alexa 488 anti-rabbit, and Alexa 594 anti-rat. All images were collected on either a Zeiss Pascal confocal microscope (Germany) or an Olympus FV1000 confocal microscope (Center Valley, PA) equipped with Fluoview software. Images were acquired using

31

multi-track parameters, with a 63X Plan-apochromat objective. Deconvolution was done using the "Iterative_Deconvolve_3D" plug-in for Image J (Dougherty, 2005).

Colocalization analysis: We used the "Just Another Colocalization Plug-in" available for Image J (Bolte and Cordelieres, 2006). We used this program to calculate the Pearson's coefficient as well as the percentage of pixels that colocalize from each channel.

GFP analysis: For axon morphology, animals were scored blind to genotype by examining cell-type specific GFP markers (GABAergic – *juIs76[Punc-25-gfp], juIs145[pflp-13-gfp],* and cholinergic – *juIs14[pacr-2-gfp]*) with an Axioplan 2 microscope using a 63x Plan-apochromat objective and a GFP long pass filter set (Chroma, Battleboro, VT) as described (Ackley et al., 2005). Animals that had any differences from the expected wild-type pattern were scored as axon guidance defective. A defasciculation event was counted as a region of the nerve cord where two or more processes appeared to become split from one fascicle and were visible along a distance that was greater than the length of two neuronal cell bodies, which is approximately 10-20 ▯m. Synapse morphology of D-type neurons was visualized by *juIs1* [Punc-25 SNB-1::GFP] and the A/B type neurons were visualized using *nuIs94* [Pacr-2 GFP-SNB-1] and using either a Zeiss Pascal LSM confocal microscope or an Olympus FV1000 confocal microscope. Animals were anesthetized using 0.5% phenoxy-propanol (TCI America, Portland, OR) in M9 and mounted on 5% agar pads. Images were acquired using a 63x Plan-apochromat objective.

Image Quantification: To quantify the area and density of each SNB-1::GFP puncta we generated two-dimensional projections of image stacks acquired by confocal microscopy. The

images were converted to thresholded binary images and the size and location (X-Y coordinates) of single GFP puncta were acquired automatically using the analyze particles command in Image J. Measurements were performed with the experimenter blind to genotype. The procedure was done as described (Ackley et al., 2003) with minor modifications. In ImageJ the files were thresholded, and a region of interest was drawn around the nerve cord. The following measurement options were selected: Area, Center of Mass, Circularity, Perimeter, Fit Ellipse, and Limit to Threshold. The "Analyze Particle" command was used with a minimum of four pixels and no maximum size. The following options were selected: Outline Particles, Ignore Particles Touching Edge, Include Interior Holes and Reset Counter. The resulting measurements were exported to Microsoft Excel (Redmond, WA) for statistical analysis. Significance was determined by a two-tailed Student's t-test or F-test as indicated.

Sequence Alignments: Alignments were performed pairwise using the EMBOSS::needle method (http://www.ebi.ac.uk/Tools/emboss/align/) with the following options selected: Gap Open (10.0), Gap Extend (0.5) and Matrix (Blosum62). The GenBank accession numbers for the non-nematode proteins used are as follows: *Mus musculus* Celsr2 (NP_001004177.2) and *Drosophila melanogaster* Flamingo/starry night (AAF58763.5).

RNAi: Animals with each marker (*juIs1, juIs76* or *lhIs9)* were tested in the *eri-1(mg366)* background to increase RNAi penetrance in the nervous system (Kennedy et al., 2004). Bacteria from the Ahringer RNAi library (Gene Service Ltd., UK) were grown overnight (O/N) in Luria Broth supplemented with 100 μM ampicillin and 25 μM tetracycline, and 100 μl of the saturated culture was placed on NGM plates supplemented with 1mM IPTG, 30 μM carbenecillin and 1

µg/ml nystatin. The plates were incubated at 37 ºC O/N. 3-5 L4 animals of each genotype were placed on the RNAi lawn and allowed to have self-fertilized offspring. The F1 offspring were analyzed for phenotypes. All RNAi experiments were replicated at least two times, each with freshly prepared media.

Electron microscopy: Young adult hermaphrodites of genotype CZ333 *juIs1*, CZ1677 *fmi-1(ju58); juIs1*, CZ460 *fmi-1(ju43); juIs1* were fixed in parallel using glutaraldehyde and osmium fixative as described (Hallam et al., 2002). 300-500 serial 45 nm ultrathin sections were collected from two wild type animals (*juIs1*) and one each of the *fmi-1(ju58)* and *fmi-1(ju43)* mutant worms. Nerve cords were photographed with a Gatan digital camera on a JEOL 1200 electron microscope. NMJs were identified as synapses with muscles as postsynaptic partners (White et al., 1986). GABAergic NMJs have muscles as sole postsynaptic partners, whereas cholinergic NMJs usually have two postsynaptic partners, a muscle and a neuronal process. Small, round, clear vesicles of 30-35nm diameter were counted as synaptic vesicles. Measurement of presynaptic densities was taken as the number of sections that contained recognizable electron-density, multiplied by 45nm. Statistical analysis was conducted using standard t-test (Excel).

Table 2.1

	Ventral Cord			Dorsal Cord		
	Area±S.E.M. (N)[a]	Maximum [a]	Density±S.E.M. (N)[b]	Area±S.E.M. (N)[a]	Maximum [a]	Density±S.E.M. (N)[b]
GABAergic						
wild type	0.80±0.02 (530)	3.9	25.7±1.0 (16)	0.83±0.03 (344)	3.0	22.9±0.9 (10)
fmi-1(ju43)	1.10±0.13 (102)*	8.0	21.7±0.9 (4)*	1.27±0.08 (157)*	4.8	23.4±0.7 (4)
fmi-1(ju58)	1.80±0.14 (328)*	17.4	17.6±2.4 (9)*	1.15±0.06 (233)*	7.0	21.7±3.9 (6)
fmi-1(tm306)	1.43±0.15 (199)*	19.7	19.2±1.9 (5)*	0.89±0.05 (147)	3.4	18.4±3.0 (4)*
fmi-1(rh308)	1.74±0.20 (118)*	18.9	16.3±1.2 (4)*	0.91±0.05 (147)	3.8	19.0±1.5 (3)
fmi-1(ju58)+[WRM066DB07]	1.15±0.10 (167)*‡	9.0	19.9±1.7 (7)*‡	1.24±0.10 (119)*	7.7	17.5±1.8 (4)*
juIs1+[WRM0066DB07]	0.86±0.06 (203)	6.0	26.5±2.0 (6)	0.92±0.06 (184)	6.0	23.1±1.5 (5)
fmi-1(tm306)+[Pacr-2::fmi-1]	1.06±0.07 (129)*‡	4.6	15.5±2.4 (4)*‡	1.22±0.09 (110)*	3.8	17.2±2.2 (4)
fmi-1(tm306)+[Punc-25::fmi-1]	2.11±0.22 (135)*	16.8	12.3±2.4 (5)*	1.14±0.11 (77)*	4.4	20.0±4.4 (4)
juIs1+[Pacr-2::fmi-1 RNAi]	1.42±0.13 (232)*	18.8	19.0±1.9 (6)*	0.84±0.06 (75)	2.5	14.8±5.4 (3)*
juIs1+[Punc-25::fmi-1RNAi]	1.48±0.09 (251)*	11.1	20.7±4.5 (6)*	1.29±0.12 (106)*	8.7	16.5±3.0 (3)*
cdh-4(lq83)	1.82±0.11 (259)*	14.7	16.6±1.6 (7)*	1.24±0.09 (169)*	7.2	20.3±2.0 (4)*
fmi-1(tm306);cdh-4(lq83)	1.45±0.13 (171)*†	13.2	16.6±1.8 (5)*†	0.97±0.07 (134)*	6.0	18.1±2.6 (4)*
cdh-4(lq56)	1.40±0.10 (155)*	6.7	16.7±3.6 (5)*		N/D	
fmi-1(tm306);cdh-4(lq56)	1.48±0.18 (113)*†	12.8	18.1±1.0 (3)*†		N/D	
eri-1(mg366);juIs1;CDH-4(RNAi)	1.56±0.15 (137)*	11.3	16.7±1.8 (4)*		N/D	
fmi-1(tm306); eri-1(mg366);juIs1;CDH-4(RNAi)	1.57±0.24 (101)*†	18.9	17.8±3.1 (4)*†		N/D	
Cholinergic						
wild type	0.90±0.06 (281)	6.2	26.7±2.0 (5)	1.03±0.07 (208)	6.0	26.1±2.8 (4)
fmi-1(ju58)	0.98±0.06 (459)	10.9	23.8±2.1 (9)	1.17±0.09 (323)*	16.6	26.9±2.5 (7)

[a] - measurements μm^2

[b] - average number of puncta observed per $100\mu m$

* - significantly different from wild type (p<0.01)

‡ - significantly different than fmi-1 (p<0.01)

† - not significantly different from fmi-1(tm306)

35

Table 2.1. Measurements of synaptic vesicle accumulation.

Table 2.2

	Type of NMJ	# NMJs	Active Zone Length (nm)	Vesicles Per Active Zone	pse Length (	Vesicles per profile
wild type	GABAergic	11	122.7±15.0	40.7±2.7	1006.2±77.5	26.1±0.9
fmi-1(ju43)	GABAergic	3	75.0±15.0	60.7±11.8	465.0±150.0*	23.4±7.2
fmi-1(ju58)	GABAergic	6	120.0±19.0	21.5±2.6 *	472.5±25.3*	16.6±1.3*
wild type	Cholinergic	23	184.0±14.1	26.5±2.8	637.8±56.4	20.4±1.9
fmi-1(ju43)	Cholinergic	19	165.8±23.1	21.4±1.1	746.1±67.0	21.4±1.1
fmi-1(ju58)	Cholinergic	21	182.1±24.0	27.8±2.5	615.0±55.5	22.2±1.9

[a] defined as consecutive sections with synaptic vesicles

* significantly different from wild type ($p < 0.01$)

Table 2.2. Comparison of neuromuscular junctions by genotype.

Table 2.3

	% wild type	L/R defects	Defasciculation	N
GABAergic (DD and VD)				
wild type	98	2%	0%	50
fmi-1(ju43)	12%	48%	50%	70
fmi-1(tm306)	10%	67%	36%	70
fmi-1(tm306) lhIs9	24%	27%	N/D	76
lhIs9	12%	68%	N/D	70
fmi-1(tm306);FMI-1GFP (high)	16%	64%	N/D	25
fmi-1(tm306);FMI-1GFPDInt (high)	0%	68%	N/D	28
cdh-4(lq83)	15%	30%	29%	79
cdh-4(lq83);fmi-1(tm306)	6%	35%	22%	49
L1 GABAergic (DD only)				
wild type	98%	0%	2%	100
fmi-1(ju43)	92%	5%	3%	100
Cholinergic (DA and DB)				
wild type	90%	8%	2%	60
fmi-1(ju58)	5%	5%	95%	20

Table 2.3. Axon Guidance Defects in *fmi-1* and *cdh-4* mutants.

Table 2.4

	% Gaps	Gaps/Animal	N
GABAergic (DD) [*juIs76* - L1 stage]			
wild type	4%	0.08±0.40	25
fmi-1(ju43)	76%	1.76±1.09	25
fmi-1(tm306)	73%	1.72±1.17	30
fmi-1(tm306) lhIs9	30%	0.36±0.60	33
cdh-4(lq83)	41%	0.55±0.78	29
cdh-4(lq83);fmi-1(tm306)	50%	0.75±0.91	20
GABAergic (DD) [*lhIs35* - L3 stage]			
wild type	0%	0.00±0.00	25
fmi-1(tm306)	88%	1.26±0.85	24

Table 2.4. Axon Extension Defects by Genotype.

Figure 2.1
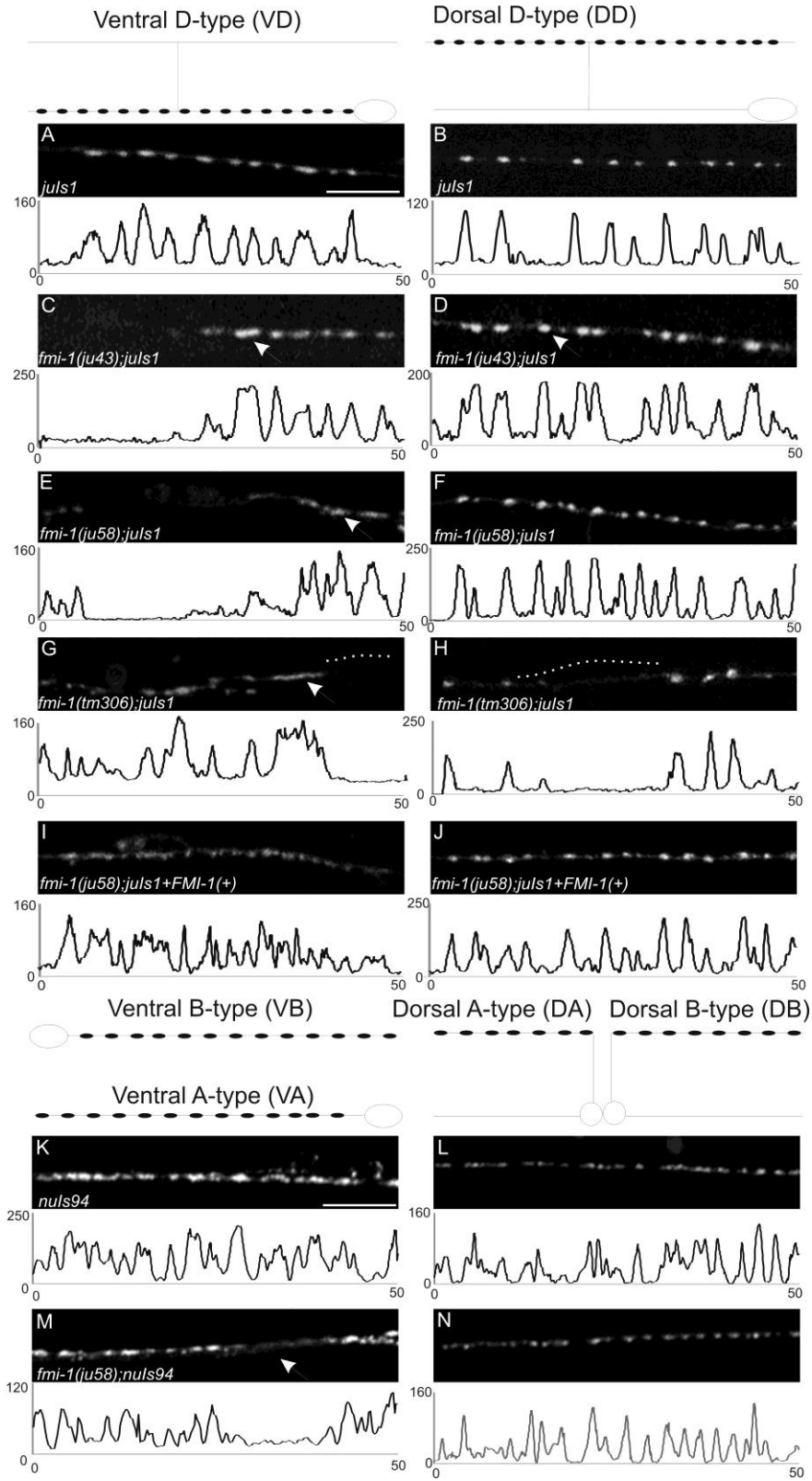
Figure 2.1 GABAergic NMJs are malformed in *fmi-1* mutants. GABAergic (A-J) and cholinergic (K-N) NMJs were examined using SNB-1::GFP to visualize synaptic vesicle clusters. The fusion of the SNB-1 to the GFP and the shape of the VD and DD motorneurons are depicted above panels A-B, respectively, and the location of the synapses within those cells are illustrated (black circles). In all panels left is anterior. (A-J) Images are a 50µm section of the ventral (A, C, E, G, I) or dorsal (B, D, F, H, J) nerve cords, and below each image is a plot profile for each image to demonstrate the approximately similar sized puncta in wild type and how they are divergent in *fmi-1* mutants. Wild-type animals (A, B) had consistently sized puncta that were evenly spaced along the nerve cords. (C-H) In the GABAergic motoneurons of *fmi-1* mutants we observed larger synapses (arrows – C-D) and misshapened (arrows – E, G) puncta. Frequently there were long regions of the nerve cord lacking synapses (dotted lines – G, H). (I, J) We partially rescued the *ju58* defects using a fosmid containing *fmi-1* (WRM0066DB07). These animals had a significant reduction in synaptic size relative to *ju58* alone, and fewer long gaps lacking GFP were found in the nerve cords. (K-N) SNB-1::GFP expressed in the cholinergic neurons appear less defective than in GABAergic neurons. Schematics of the shape and location of synapses within these neurons are shown above panels K and L. Note, the VA and VB synapses, as well as those in the DA and DB neurons would overlap *in vivo,* which is not illustrated here for simplicity. In wild type animals SNB-1::GFP puncta were normally sized and tightly clustered. (M,N) In the *fmi-1(ju58)* animals the puncta were approximately the same size, although we observed a few gaps where puncta are weaker or absent. All scale bars are 10 µm.

Figure 2.2

A

Pfmi-1L
-2662

Pfmi-1S
-1066

1000bp

gm188
G$_{6723}$>A

ju43
G$_{10320}$>A

tm306
Δ$_{10467-11288}$

ju58
G$_{12375}$>A

B

Cadherin Repeats   EGF   EGF   EGF   HomR   GPS   7TM

LamG   LamG

MT1

gm188
G842>R

ju43
G1481>E

ju58
W2150>Opal

100AA

C

									▼											
C.e CD7	835	F R L D R T S **G** T L R V S S K L D R E Q F
D.m CD7	831	F V I D P T S **G** T I R T N K G L D R E S V
M.m CD7	831	F I V E S T S **G** I V R T L R R L D R E N V

D

|									▼											
C.e LG1	1473	D I S N G L F L **G** G R P G T S K Q I E K A
D.m LG1	1701	D L T G P L Q V **G** G L P R I P A H F P V T
M.m LG1	1518	D L T G P L L L **G** G V P D L P E S F P V R

45

Figure 2.2. Lesions identified in the *fmi-1* gene and protein. A) A schematic presentation of the *fmi-1* gene and locations of lesions. Nucleotide numbering is with respect to the start of translation. The promoter regions used for GFP expression (*Pfmi-1L*) and the segment present in the rescuing fosmid (*Pfmi-1S*) are indicated. Exons and their corresponding protein domains are color-coded. **B)** The FMI-1 protein structure was determined using SMART . The extracellular region of the protein is predicted to have nine cadherin repeats (green ovals), 5 EGF-like domains (orange diamonds), 2 LamG domains (yellow ovals) as well as a Hormone receptor related domain (HormR – blue hexagon) and a proteolytic cleavage site that is present in G-coupled protein receptors, *e.g.* latrophilins, (GPS – blue pentagon). FMI-1 has seven predicted transmembrane domains and an intracellular domain of approximately 142 amino acids. **C)** The *gm188* mutation in the seventh Cadherin repeat affects a highly conserved glycine residue (alignment of *C. elegans* (C.e.) FMI-1*, Drosophila* (D.m.) Flamingo, and *Mus musculus* (M.m.) Celsr2). **D)** A partial alignment of the first LamG domain showing the glycine affected by *ju43*.

Figure 2.3

A

VNC

L1 - fmi-1(tm306);juIs1

B

L2 - fmi-1(tm306);juIs1

C

L3 - fmi-1(tm306);juIs1

D

L4 - fmi-1(tm306);juIs1

F

class I

VD6

VD3   VD4   DD2   VD5   class II

class I   class II

VD3   VD4   DD2   VD5   VD6

VD3   VD4   VD5   VD6

G

VNC

hpIs5 - SYD-2::GFP

H

fmi-1(tm306);hpIs5 - SYD-2::GFP

I

NR   VNC

anti-UNC-10/RIM

J

fmi-1(tm306) - anti-UNC-10/RIM
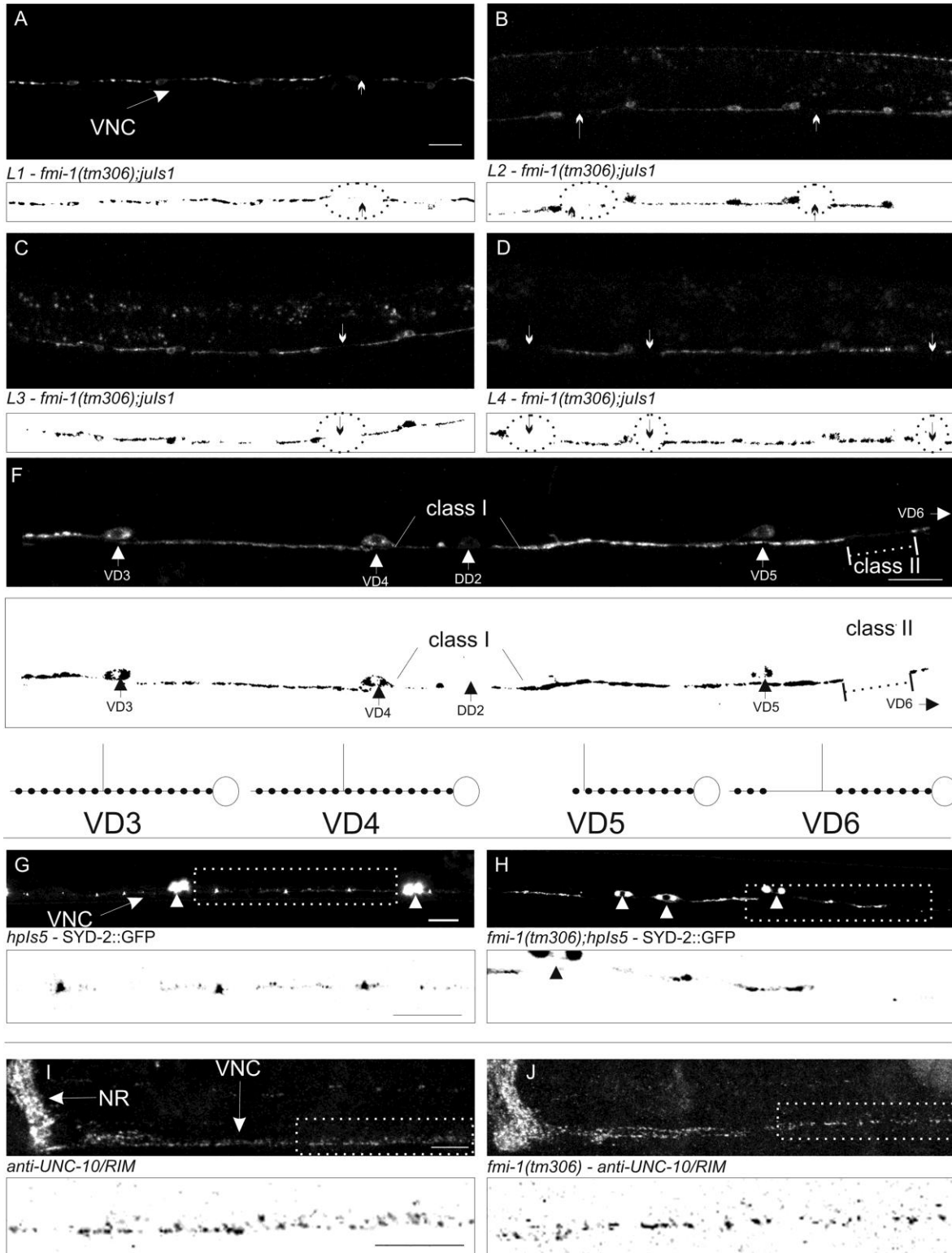
Figure 2.3. FMI-1 causes synaptic defects during development. (A-D) GABAergic neurons in the ventral nerve cord (VNC) in *tm306;juIs1* (Punc-25::SNB-1::GFP) were imaged at each larval stage (L1-4). Regions lacking SNB-1::GFP (circles and arrows) were present in all stages examined. Below each panel is a thresholded mask of the image (black/white inverted). **(F)** An adult animal with both class I and class II gaps is shown. VD5 appears to have a class I gap because the gap extends from end of the synaptic puncta (large arrowhead) to the point of VD4. The small amount of fluorescent material in that region appears to come from the DD2, which is more weakly fluorescent. In comparison the puncta formed in VD4 extend all the way to VD3. VD6 (cell body out of panel) has a class II gap (dotted line) because VD6 forms puncta distal to the gap before VD5. A cartoon illustrating these cells is drawn above and to the right. **(G,H)** SYD-2::GFP accumulates in small puncta in the nerve cord (arrow - **G**) and motor neuron cell bodies (arrowheads – **G,H**). In *fmi-1* mutants **(H)** SYD-2::GFP clustered in larger puncta with bigger gaps between puncta. **(I,J)** UNC-10 localized to discretely sized and spaced puncta in the nerve ring (NR) and ventral cord (VNC). **(J)** UNC-10 localization was grossly wild type in *fmi-1(tm306)*. Boxed regions **(G-J)** are depicted with a black/white inverted image below each panel. All scale bars are 10 μm.

Figure 2.4

A — wild type

B — *fmi-1(ju43)*

MN

MN

Mu

C — *fmi-1(ju58)*

D — *fmi-1(ju43)*

MN1

MN2

Mu

Mu

MN

49
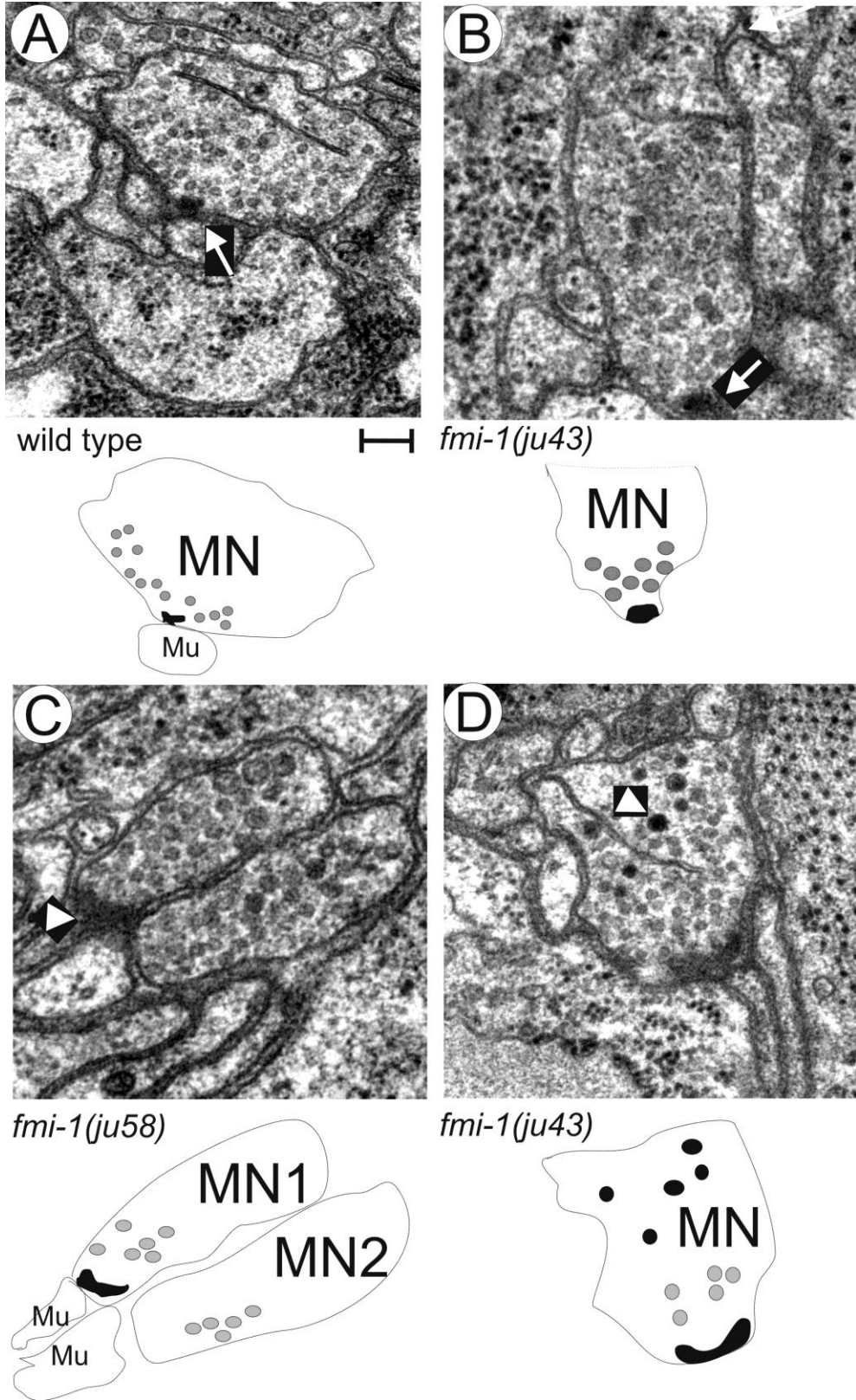
Figure 2.4. Ultrastructural analysis of *fmi-1* synaptic defects. A) Wild-type animals NMJs

formed as a single active zone (arrow) surrounded by evenly sized, clear synaptic vesicles.

Below a schematic is provided to illustrate the motoneuron (MN) and muscle (Mu). The active

zone (black object) was surrounded by synaptic vesicles (grey circles), only some of the vesicles

are illustrated for simplicity. **B-D)** *fmi-1* mutants did have some normal NMJs **(B)**. However,

many *fmi-1* animals also exhibited abnormal junctions **(C,D)**. **C)** In this junction two neurons

had vesicle filled swellings at the point of contact with the muscle; however, only one had an

active zone (arrowhead). This is illustrated below where motoneuron 1 (MN1) has an active

zone, but motoneuron 2 (MN2) does not, despite both having an accumulation of synaptic

vesicles. **D)** Electron dense vesicles were present at *ju43* NMJs (arrowhead), but not in wild-type

animals **(A)**. In the schematic the electron dense structures are illustrated as black circles. Scale

bar is 100 nm.

Figure 2.5

A

NR

DD1 DD2 DD3 DD4 DD5 DD6

juIs76 [Punc-25::GFP] - L1

B

fmi-1(ju43);juIs76 - L1

C

fmi-1(ju58);juIs145 [Pflp-13::GFP] - L1

D

juIs76;fmi-1(tm306)lhIs9 [Pfmi-1::fmi-1::GFP]

E

juIs76

F

fmi-1(ju58);juIs76

G

fmi-1(tm306);juIs76

H

lhIs9;juIs76

I

juIs14 [Pacr-2::GFP]

J

fmi-1(tm306);juIs14
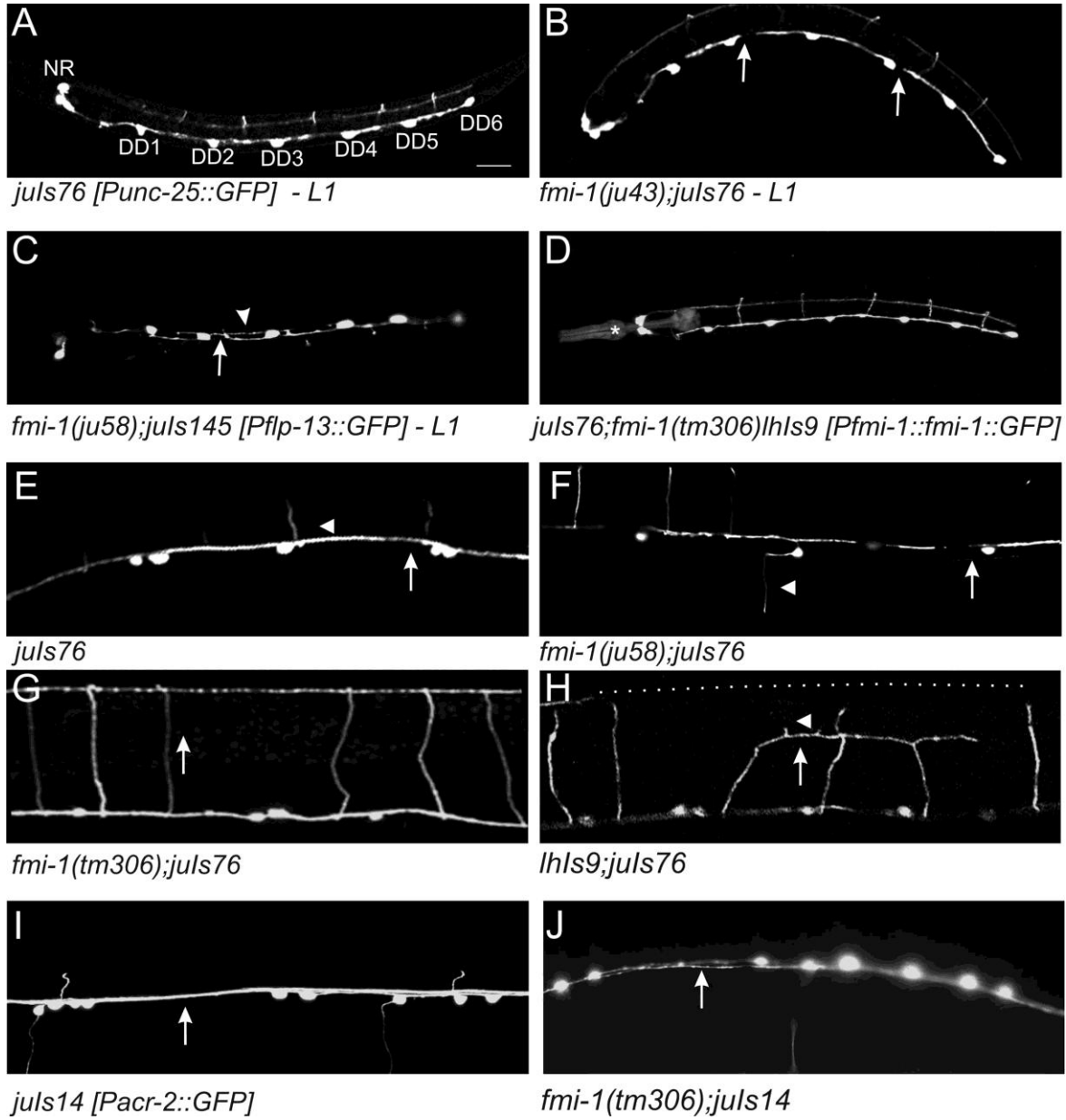
Figure 2.5. Axon guidance defects in *fmi-1*. GABAergic and cholinergic motorneurons were visualized using GFP reporters (**A, B, D-H,** *juIx76 – Punc-25::GFP*, **C** *juIs145 – Pflp-13::GFP* **I, J-** *juIs14 – Pacr-2::GFP* DA, DB, VA and VB). **A-D)** The 6 DD motorneurons are the only GABAergic motorneurons present during L1s (VDs form at the end of the L1 stage, 4 RME neurons are in the nerve ring region – NR). The process of each neuron extends anteriorly to the next cell body, *i.e.* DD3 extends to DD2. **B, C)** DDs in the *fmi-1* mutants often exhibit incomplete axon extension (arrows). **C)** DD axons often defasciculated into two nerve bundles (arrowhead) **D)** DD axon extension defects were rescued by FMI-1::GFP using its endogenous promoter (*lhIs9*). **E)** In wild-type GABAergic axons form as a single, contiguous fascicle in the ventral cord (arrow). Commissures (arrowhead) posterior to DD1 and VD1 grow toward the right side, which is up in this ventral view. **F)** In *fmi-1* mutants GABAergic motorneurons exited the ventral cord on the incorrect side and often had defects in the extension of the axons (arrow). The gap is likely due to the premature termination of both the VD and DD axons. **G)** In wild type animals (not shown) and *fmi-1(tm306)* commissures extend along the dorsal/ventral axis (indicated by arrow) fully to the dorsal cord. **H)** Overexpression of FMI-1::GFP (*lhIs9*) caused aberrant guidance and premature turning and termination of GABAergic commissures (arrow), with some having ectopic neurites (arrowhead). The position of the dorsal cord is indicated by the dotted line. **I)** Cholinergic processes within the ventral cord (arrow) appear as a single, cohesive fascicle in wild type animals. **J)** In the *ju58* animals cholinergic axons of defasciculated (arrow). Scale bar is 10 µm.

Figure 2.6

Figure schematic labels: NR, Pharynx, A,G, VNC, B-F, H

A A' A''

A'''

SNT-1
FMI-1

B LS1 LS2 B'

N2 (SNT-1+FMI-1)

LS1 LS2
SNT-1
FMI-1

B''

C D

C' D'

C'' D''

juIs1 (GFP+FMI-1) *fmi-1(ju58);juIs1* (GFP+FMI-1)

E F

E' F'

E'' F''

fmi-1(gm188) (SNT-1+FMI-1) *fmi-1(ju43)* (SNT-1+FMI-1)

G NR VNC H VNC
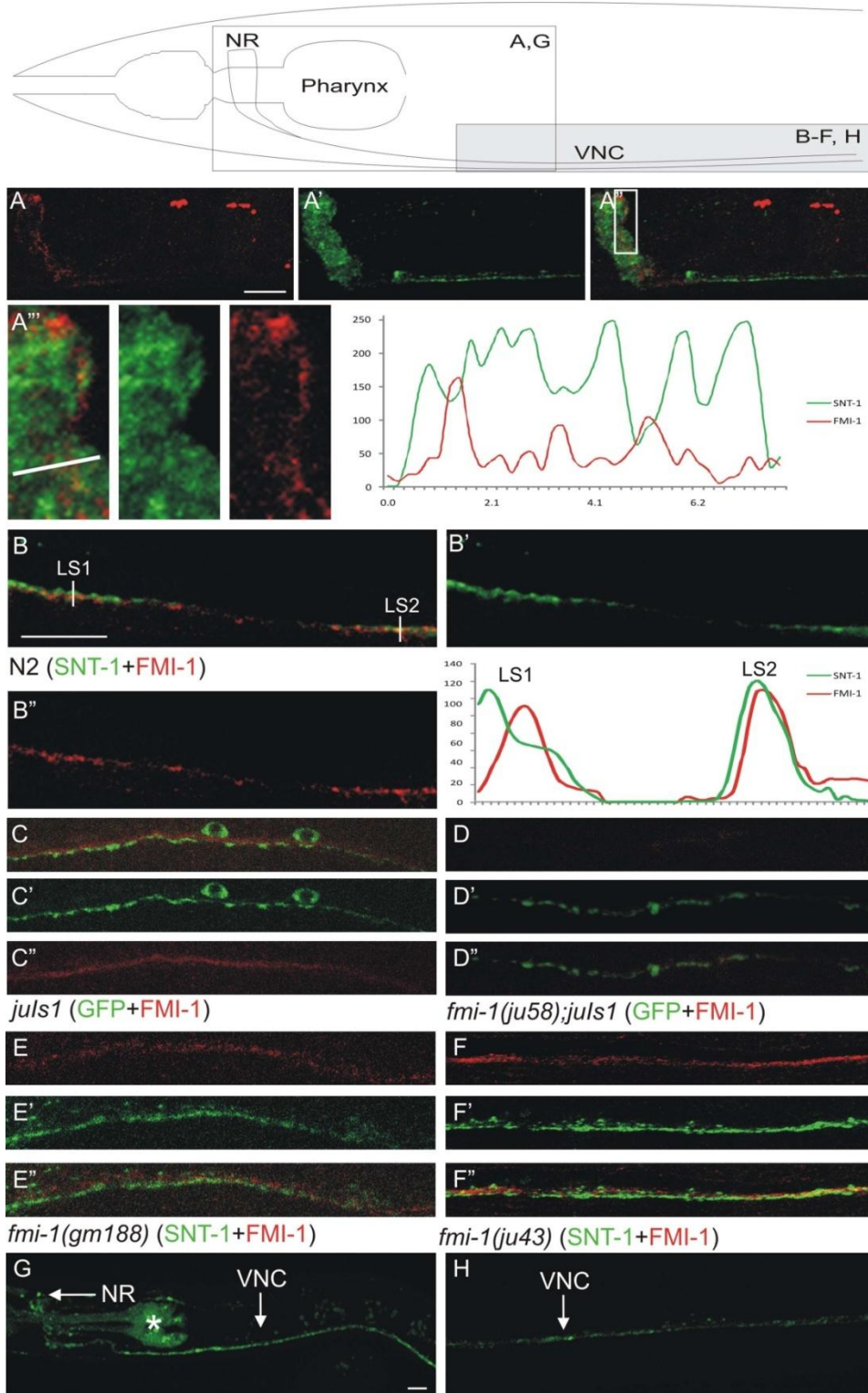
Figure 2.6. FMI-1 is concentrated at non-synaptic regions of the nervous system. Using specific antisera we visualized FMI-1 (red – **A-F**) relative to the synaptic vesicle protein SNT-1 (green – **A, B, E, F**) or *juIs1* (SNB-1::GFP) (green – **C, D**). Above the panels is a schematic to orient the region being examined. In wild type animals **(A, B)** FMI-1 localized to the nerve ring (**A**) and ventral nerve cord (VNC) **(B)**. FMI-1 was predominantly adjacent to, but not overlapping with, SNT-1. **(A''')** An enlarged view of the boxed region from **(A'')** FMI-1 and SNT-1 containing regions have little overlap. An intensity profile corresponding to the line in panel **A'''** is on the right. **(B)** In the ventral nerve cord FMI-1 was adjacent to SNT-1 (line scan 1 – LS1), but occasionally overlapped (*e.g.* line scan 2 – LS2). **(C)** FMI-1 was adjacent to, but not within GABAergic NMJs labeled by SNB-1::GFP. **(D)** The *ju58* allele lacked FMI-1 immunoreactivity; demonstrating the antisera specificity. Results were similar for *tm306* and *rh308* (data not shown). The missense mutations *gm188* **(E)** and *ju43* **(F)** did not grossly affect protein localization, although there is a slight increase in the overlap of the FMI-1 and SNT-1 (colocalization coefficient = 0.38). **G,H)** FMI-1::GFP accumulated in the nerve ring (NR) and ventral cord (VNC) in a pattern similar to the antisera staining. The pharyngeal staining (asterisk) is from the co-injection marker (Pmyo-2-mCherry). All scale bars are 10 μm.
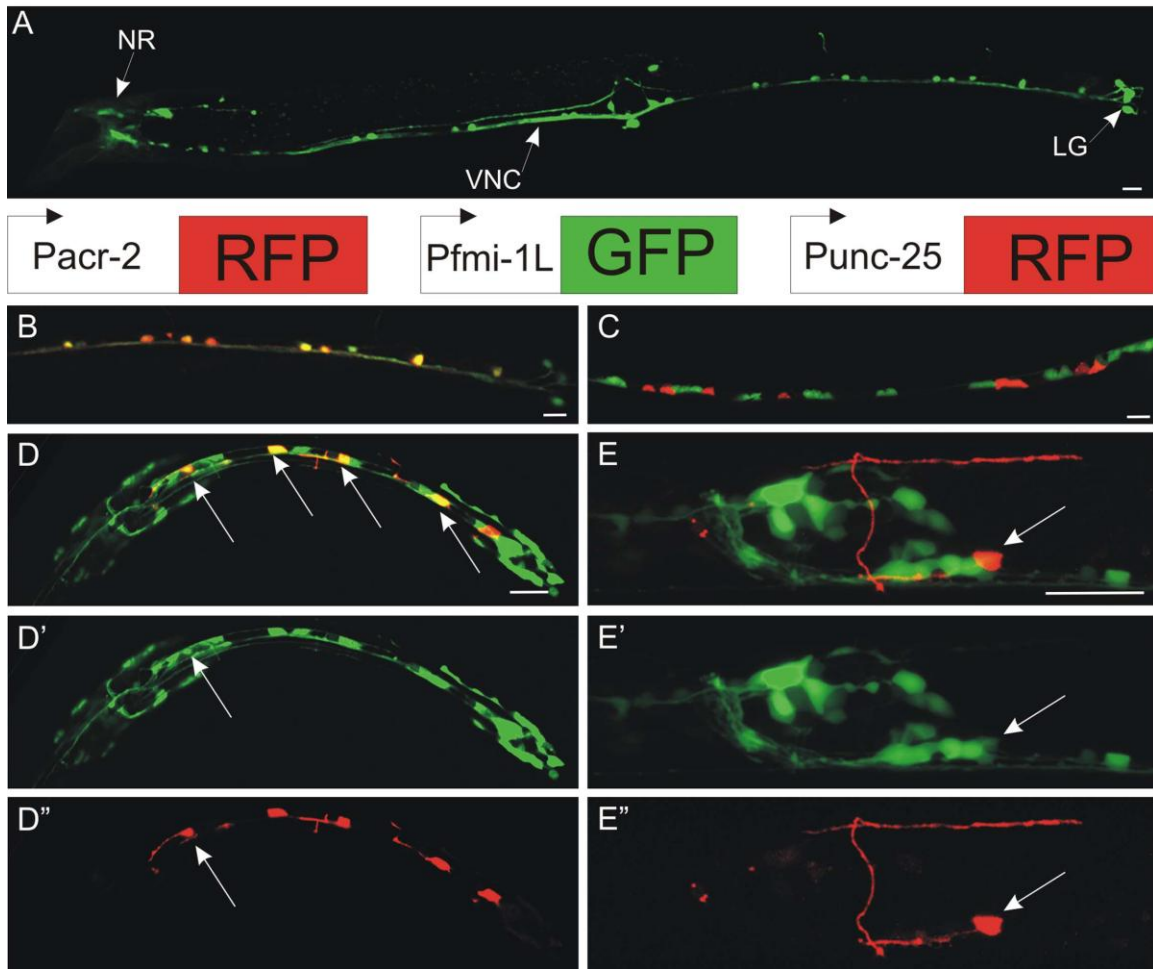
Figure 2.7

Figure 2.7. *fmi-1* **is expressed in the nervous system, but not VD motoneurons. A)** A *Pfmi-1*::GFP was used to determine the spatial expression of *fmi-1*. GFP was observed in a subset of neurons near the nerve ring (NR) along the ventral nerve cord (VNC) and in the lumbar ganglion (LG). To identify which motorneurons were expressing flamingo we co-expressed P*fmi-1-gfp* with either P*acr-2-rfp* **(B)** or P*unc-25-rfp* **(C-E)**. **B,C)** In larva and adults the GFP-positive motorneurons also expressed *Pacr-2-rfp,* but not *Punc-25::rfp* **(D)** In contrast, none of the older larvae or adults co-expressed GFP and RFP when we used *Punc-25-rfp*. **D-D")** In L1 larvae there was limited co-expression P*unc-25-rfp* and P*fmi-1-gfp* in a subset of the DD motorneurons (arrows). The GFP intensity was much reduced relative to other FMI-1(+) cells. The remaining GFP positive cells in the ventral cord are likely the DA motorneurons. **E-E")** By the adult stage DD1 (arrow) no longer expresses GFP. All scale bars are 10 μm.

Figure 2.8

fmi-1(tm306);Punc-25::fmi-1+Punc-25::mCherry

fmi-1(tm306);Pacr-2::fmi-1+Pacr-2::mCherry

fmi-1(tm306);Pacr-2::fmi-1+Pacr-2::mCherry

fmi-1(tm306);Pacr-2::mCherry

fmi-1(tm306);Pfmi-1::fmi-1ΔInt::GFP +Punc-25::SNB-1dsRed

lhIs30;(Pfmi-1::fmi-1ΔInt::GFP +Punc-25::SNB-1dsRed
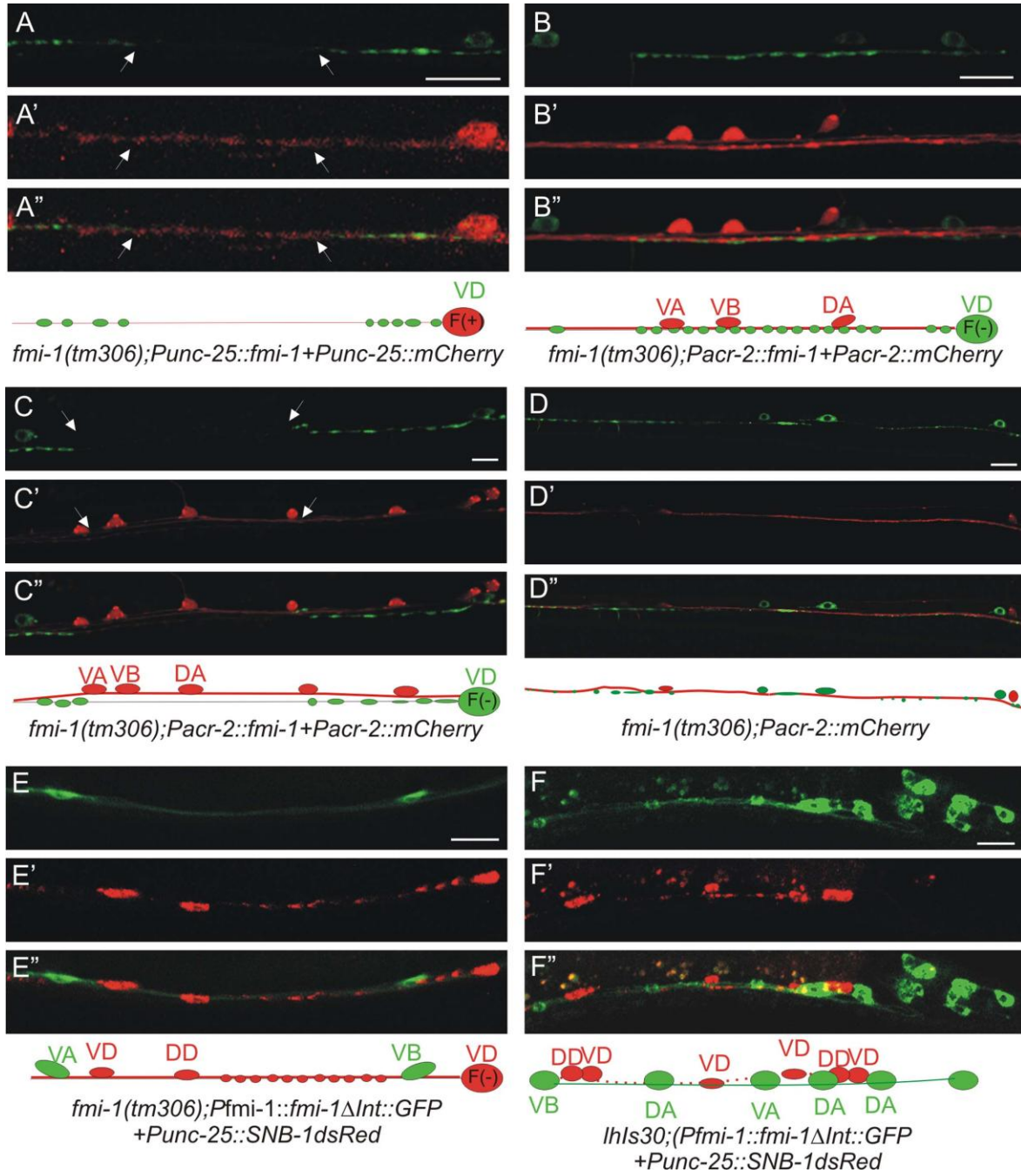
Figure 2.8. FMI-1 functions cell-non autonomously in the VD neurons. (A) VD SNB-1::GFP puncta in *fmi-1(tm306 + Punc-25::fmi-1* were enlarged, and still had gaps (between arrowheads). **(A', A")** RFP was used to mark cells with the transgene. Below is a carton illustrating that the VD neuron (red) is now expressing FMI-1 (F(+)), but we observe long gaps lacking SNB-1GFP. **(B)** When *fmi-1* is specifically expressed in the cholinergic cells, SNB-1::GFP puncta were evenly sized and spaced puncta. **(B', B")** RFP the transgenically positive neurons. **(C-C")** In some cases the cholinergic (red) axons and GABAergic (green) appeared defasciculated. Here, even though the *fmi-1* transgene is present in these cholinergic neurons, the GABAergic synaptic defects are not rescued. **(D-D")** Defects in SNB-1::GFP (green) were present when cholinergic axons (red) were properly fasciculated with the GABA neurons. **(E-E")** FMI-1ΔInt::GFP expressed under its endogenous promoter partially rescued the synaptic defects in GABAergic neurons (as visualized by SNB-1::RFP – **E'**). GFP is not observed in the GABAergic neurons. **(F-F")** We integrated the FMI-1ΔInt::GFP and still found no evidence of expression with the GABA marker (Punc-25::SNB-1::dsRED) confirming that FMI-1 expressed from non-GABAergic neurons is sufficient to rescue the SNB-1 accumulation defects. Scale bar in all panels is 10 μm.

Figure 2.9

A

eri-1(mg366)juIs1 - cdh-4(RNAi)

B

fmi-1(tm306);eri-1(mg366)juIs1 - cdh-4(RNAi)

C

cdh-4(lq83);juIs1

D

fmi-1(tm306);cdh-4(lq83);juIs1

E

cdh-4(lq56);juIs1

F

fmi-1(tm306);cdh-4(lq56);juIs1

G

cdh-4(lq83);juIs76

H

cdh-4(lq83);juIs76

I

fmi-1(tm306);cdh-4(lq83);juIs76

J

fmi-1(tm306);cdh-4(lq83);juIs76

K

eri-1(mg366);FMI-1GFP - fem-1 RNAi

L

eri-1(mg366);FMI-1GFP - cdh-4 RNAi

M M' M''

Pcdh-4::gfp+Punc-25::RFP

N N' N''

Pcdh-4::gfp+Pacr-2::RFP
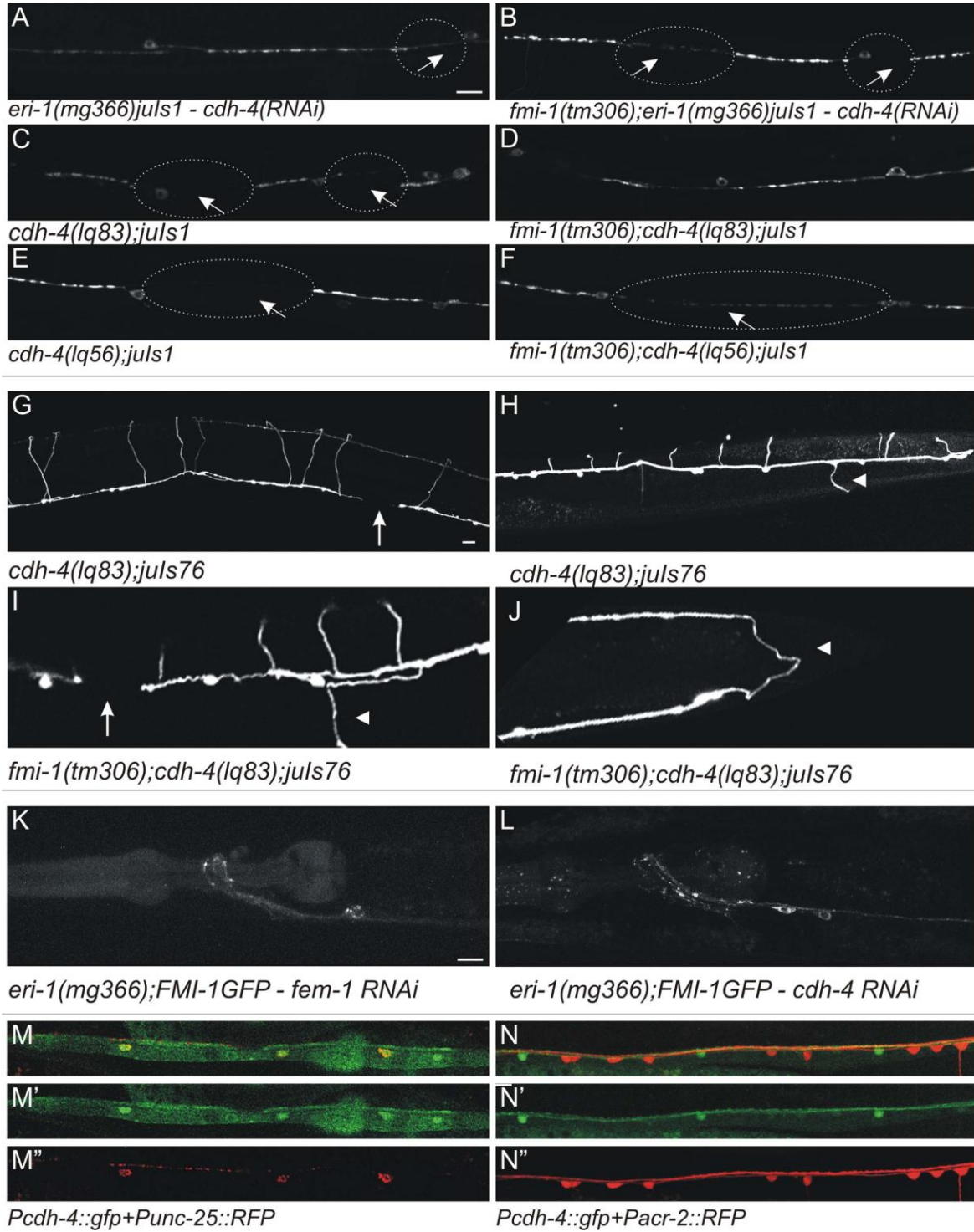
Figure 2.9. *fmi-1* **and** *cdh-4* **mutations cause similar phenotypes in VD patterning. A)** *eri-1(mg366)juIs1* animals treated with *cdh-4* RNAi had elongated SNB-1::GFP puncta interrupted by large gaps (circles and arrows). **B)** *cdh-4* RNAi caused no enhancement of the phenotype present in *eri-1(mg366)juIs1;fmi-1(tm306)* animals. **C-F)** *cdh-4* loss of function mutations, *lq83* **(C,D)** and *lq56* **(E,F)** caused *fmi-1* like phenotypes, but neither enhanced defects present in *fmi-1(tm306)*. **G-J)** *cdh-4(lq83)* caused GABAergic axon pathfinding defects including axon extension failure (arrows – **G, I**) and left/right defects (arrowheads – **H, I**). **I, J)** Animals lacking both *cdh-4* and *fmi-1* have pathfinding defects that are similar to the single mutants. **J)** In this animal the VD13 axon (arrowhead) is extended toward the posterior rather than the anterior. **(K,L)** *cdh-4(RNAi)* does not grossly disrupt FMI-1::GFP localization relative to control – *fem-1(RNAi)*. **(M,N)** In larva and adults *Pcdh-4::gfp* (*hdIs46*) expression overlaps with a marker for the GABAergic neurons (*Punc-25::rfp* – red, **M**), but not the cholinergic (*Pacr-2::rfp* – red **N**). Scale bars in all panels are 10 μm.

Chapter III:

***C. elegans fmi-1/flamingo* and Wnt pathway components interact genetically to control the anteroposterior neurite growth of the VD GABAergic neurons**

3.1 Abstract

Directed axonal growth is essential to establish neuronal networks. During the early development of the VD neurons, an anterior neurite that will become the VD axon extends along the anteroposterior (A/P) axis in the ventral nerve cord (VNC) in *C. elegans*. Little is known about the cellular and molecular mechanisms that are important for correct neurite growth in the VNC. In *fmi-1/flamingo* mutant animals, we observed that postembryonically born VD neurons display a posterior neurite instead of a normal anterior neurite, which caused aberrant VD commissure patterning along the A/P axis. In addition, VD anterior neurites have underextension defects in the VNC in *fmi-1* animals, whereas VD commissure growth along the dorsoventral (D/V) axis occurred normally in these animals, suggesting that *fmi-1* is important for neurite growth along the A/P axis but not the D/V axis. We also uncovered unknown details of the early development of the VD neurons indicating that the neurite defects arose during their early development. Interestingly, though *fmi-1* is present at this time in the VNC, we did not observe FMI-1 in the VD neurons themselves, suggesting that *fmi-1* might be working in a cell-non autonomous fashion. Furthermore, *fmi-1* appears to be working in a novel pathway, independently from the planar cell polarity pathway and in parallel to *lin-17/frizzled* and *dsh-1/dishevelled,* to determine the direction of neurite growth. Our findings indicate that redundant developmental pathways regulate neurite growth in the VNC in *C. elegans*.

3.2 Introduction

During the *in vivo* formation of the nervous system, neurons extend axons in a stereotypical manner. Axons grow along the three main axes of development: left-right; dorsoventral (D/V) and anteroposterior (A/P). Failure to do so has deleterious consequences for the formation of neuronal circuits.

Correct axonal growth along the A/P axis requires both long-range and short-range cues. Recent observations have implicated Wnt signaling in the formation of neuronal processes along the A/P axis (Lyuksyutova et al., 2003, Hilliard and Bargmann, 2006, Pan et al., 2006, Zou, 2006, Kirszenblat et al., 2011). In *C. elegans*, Wnts provide long-range repellent signals, especially during axon growth and pathfinding (Maro et al., 2009).

While Wnt pathways can provide long-range positional cues, adhesion proteins regulate axon growth and pathfinding more locally (Takeichi, 2007). *fmi-1/flamingo* is a conserved non-classical cadherin that contains multiple protein domains, including nine cadherin repeats and a seven transmembrane domain (Steimel et al., 2010, Najarro et al., 2012). In *C. elegans*, mutations in *fmi-1* cause axon growth and guidance defects along the A/P axis in the ventral nerve cord (VNC) in the pioneer, pioneer follower, HSN and GABAergic neurons (Steimel et al., 2010, Najarro et al., 2012). In different contexts, Flamingo proteins function in both a cell autonomous and a cell non-autonomous fashion (Lee et al., 2003, Senti et al., 2003, Chen and Clandinin, 2008, Steimel et al., 2010, Najarro et al., 2012).

fmi-1 homologs can work as part of the planar cell polarity (PCP) pathway to regulate axon growth and guidance. For example, mutations in *celsr3*, a vertebrate *fmi-1* homolog, cause defects in axon growth and guidance of various neurons along the A/P axis that are similar to those observed when other PCP pathway components are mutated (Fenstermaker et al., 2010,

Shafer et al., 2011). Therefore, it appears that in vertebrates, PCP-like pathways control axonal growth and guidance along the A/P axis. It is unknown if similar pathways exist in *C. elegans*.

We study a subset of the D-type GABAergic neurons, the VD neurons. These neurons are born beginning at the late larval 1 stage (L1 stage) in the VNC. A fully differentiated VD neuron contains a ventral axon, a ventrodorsal commissure and a dorsal dendrite, all of which originate from an anterior ventral neurite (AVN) (Hall and Russell, 1991, Knobel et al., 1999). Little is known about the molecular and cellular mechanisms that are essential for the directional growth of the AVN in the VNC.

Here, we report that *fmi-1* is important for the direction of growth of the AVN of the VD neuron. We have observed that VD neurons in *fmi-1* animals displayed a posterior neurite instead of an AVN, causing VD ventrodorsal commissures to be positioned posterior to their cell bodies. We have named this phenotype as the posterior ventral neurite (PVN) phenotype. Developmental sequence experiments suggested that these defects arose when VD neurites were initially extending in the VNC. At this time, FMI-1 was present in neighboring axons in the VNC but not in VD neurons, suggesting that *fmi-1* worked cell non-autonomously to control the direction of neurite growth in the VD neurons. We also show that, in this context, *fmi-1* appeared to work independently from the PCP pathway. Finally, we describe genetic interactions between *fmi-1* and two components of a Wnt pathway, *lin-17/frizzled* and *dsh-1/dishevelled*. Together, these results define a key role for *fmi-1* as well as *lin-17* and *dsh-1* to regulate the direction of neurite growth in the VD neurons along the A/P axis in the VNC in *C. elegans*.

3.3 Results

Patterning of the GABAergic neurons along the A/P axis in *C. elegans*

Beginning at L2 and during the later life stages, the cell bodies and commissures of DD and VD neurons can be separated into six different regions along the A/P axis, corresponding roughly to the areas covered by the longitudinal processes of the 6 DD neurons. Figure 1A shows an example of this pattern using *juIs76*, which is expressed in both DD and VD neurons. Regions 1 to 5 (R1-5) each contains 1 DD and 2 VD neurons, whereas the most posterior region, region 6 (R6), contains 1 DD and 3 VD neurons. In *wt* animals, the commissure for each neuron was always located anterior to its cell body and is typically found within the boundaries of its respective region (Fig. 1A). This pattern is displayed by 99% (*n*=175) of *wt juIs76* animals, suggesting that a robust patterning mechanism or mechanisms is in place. We have used this reliable, natural pattern to detect and score mutations that affect directional neurite growth in the VD neurons.

Abnormal posterior growth of the VD neurites in *fmi-1* mutant animals

As described above, *wt* VD neurons project an AVN. As a result, VD commissures are always located anterior to their cell bodies in *wt*. We observed that in *fmi-1(tm306);juIs76* animals, VD neurons sometimes displayed PVNs, causing VD commissures to be positioned on the posterior side of their cell body, which in turn caused a deviation from the pattern described above (Fig. 1B,C). For example, in Figure 1B, VD4 displays a PVN. As a consequence, the VD4 commissure is present in region R3 instead of in region R2. As a result, regions R2 and R3 now contain 2 and 4 commissures respectively. In contrast, regions R2 and R3 in control animals always contain 3 commissures each (Fig. 1A). Further analysis indicated that these defects were

65

not accompanied by either a change in the total number of cell bodies or commissures (Table S1). In addition, the final position of the cell bodies along the A/P axis in adult animals was grossly similar to *wt* (Fig. 1A, B). 25% (*n=200*) of *tm306* animals had at least one PVN (Fig. 1D) and found throughout the length of the worm (Fig.1E), with around one PVN per defective animal. We confirmed these observations with another *fmi-1* loss-of-function (LOF) allele, *fmi-1(rh308)* (Fig.1D) (Steimel et al., 2010). We also examined the position of the DD commissures using a DD specific marker, *Pflp-13::gfp*, but we did not see differences between *wt* and *fmi-1* animals (0% PVN, *n=100* per genotype). These data suggest that in *fmi-1* animals, VD neurons project PVNs that cause aberrant distribution of the VD commissures along the A/P axis. Furthermore, DD neurons in *fmi-1* animals do not display PVN defects.

juIs76 labels both DD and VD neurons, making it difficult to visualize individual VD neurites. Therefore, in order to find more evidence for the PVN phenotype, we engineered another fluorescent VD marker, *lhIs35* (Fig. 2A). This marker labels two sister cells, VD and AS neurons. AS neurons do not project long ventral neurites, and therefore do not interfere with the quantification of PVN in VD neurons. In agreement with our previous results, VD neurons in L2 *fmi-1* animals displayed PVNs when using the *lhIs35* marker (Fig. 2B). Quantification revealed a higher incidence of animals with PVNs in *lhIs35* compared to *juIs76*, 42% (*n=52*) versus 25% (*n=200*) respectively, perhaps because *lhIs35* allowed us to score the PVN defects more reliably. These results confirm that *fmi-1* mutations affect the direction of neurite growth of VD neurons along the A/P axis. Since we observed the presence of these defects as early as L2 stage, we can also conclude that the neurite defects arose very early during development, at the time when the VD neurites are extending in the VNC (see VD developmental sequence experiments below).

fmi-1;lhIs35 animals also displayed underextension defects in their AVNs, causing gaps to appear in the VNC (Fig. S1). In fact, L2 *fmi-1* animals had on average 2.5 gaps per animal (Table 2). A few gaps were also observed in control animals (Table 2). This result indicates that *fmi-1* is also important for the full extension of the AVN along the A/P axis. In all cases, however, we found that VD neurons did extend a ventrodorsal commissure. Therefore, we concluded that the neurite growth in the D/V axis is not affected by mutations in *fmi-1*.

PVN defects do not occur in *prkl-1* or *vang-1* mutants

We next wondered whether other putative components of the PCP pathway might also be involved in VD neurite growth. However, we did not detect PVN defects in *prkl-1/prickle* and *vang-1/Van Gogh* LOF mutants using *juIs76* (0% PVN defects, *n*=100 per genotype). We also examined double mutant combinations of *fmi-1* with these two genes. Although PVN defects were observed in these animals, we could not confidently score PVN defects because of extensive cell positioning defects. We partially overcame this problem by scoring PVN defects in region R6 in animals with normal cell positioning. There was no increase in the number of animals displaying PVNs in *fmi-1;prkl-1* (2% PVN, *n*=113) or *fmi-1;vang-1* (2 % PVN, *n*=50) compared to *fmi-1* (4% PVN, *n*=200). Thus, *fmi-1* might be working independently from the PCP pathway to control directional neurite growth of the VD neurons.

Overall, these data indicate that *fmi-1* controls the direction of VD neurite growth along the A/P axis in the VNC. When *fmi-1* is mutated, VD neurons display a PVN phenotype. In addition, normal, anteriorly directed VD neurites sometimes fail to fully extend along the A/P axis. Finally, two core components of the PCP pathway do not appear to contribute to the PVN phenotype.

Neuroblast division and VD specification are normal in *fmi-1* mutants

fmi-1 plays a minor role in asymmetric cell division (Wu and Herman, 2006). We investigated whether the defects present in *fmi-1* animals were due to a failure in asymmetric cell division of the VD precursors. To test this, we used the *lhIs35* marker to label both VDs and their sisters, the AS neurons. By cell morphology, VD neurons were always found posterior to the AS neurons in the VNC in *wt* (Zhou and Walthall, 1998) and *fmi-1* animals (*n*=50 per genotype). In addition, the total number of cell bodies remained unchanged in these animals (*n*=50 per genotype). A similar pattern was observed in combination with another AS marker (*Punc-53::tagRFP*) (Fig. 3). These observations suggest that mutations in *fmi-1* do not affect asymmetric cell division as measured by the relative position of sister cells and number of cell bodies.

Given that *lhIs35* expression, along with two other VD differentiation markers, *juIs76* and *oxIs12* (McIntire et al., 1997) (data not shown), were unchanged in *fmi-1* mutant animals, we ruled out VD cell fate errors as a possible cause of the PVN defects. Furthermore, the expression of the AS fluorescent marker was not changed in the AS neurons (Fig. 3C,D), indicating that both daughters of the precursor cell expressed lineage-specific markers. Overall, these data suggest that VD neurite defects are unlikely to be due to problems in asymmetric cell division or cell fate specification.

fmi-1 might function cell-non autonomously to regulate directional VD neurite growth

We next performed transgene-mediated rescue experiments. A GFP-labeled version of *fmi-1* driven by its endogenous promoter was able to fully rescue the PVN phenotype present in *fmi-1* animals (*n*=2 lines) (Fig.4). The VD motoneurons develop during the late L1 and early L2 larval

stages (Knobel et al., 1999) (see also VD developmental sequence described below). We used the GFP-labeled FMI-1 to investigate the distribution of FMI-1 at the same time that VD neurites are undergoing neurite extension (Fig. 5). To do this, we outcrossed one of our *fmi-1* rescuing arrays (*lhEx269*) into *fmi-1* animals expressing a red VD marker (*lhIs44*). FMI-1::GFP was detected in the VNC in early L1s, and was therefore present prior to the birth of the VD neurons (not shown). At early L2 stage, when VD neurons are forming their AVNs, the FMI-1 protein was consistently present along the VNC (Fig. 5A). It was also present in a punctuate pattern along the membrane in the cell bodies of the PVP pioneer and PVQ follower neurons and the cholinergic neurons (not shown). However, we did not observe *fmi-1* expression in the VD neurons (*n*=25) (Fig. 5C). This expression pattern is consistent with previous reports (Steimel et al., 2010, Najarro et al., 2012). In addition, we were unable to rescue the PVN phenotype by expression of FMI-1 specifically in the DD and VD neurons (*n*=6 lines). Since we can rescue the PVN phenotype in *fmi-1* animals with the *fmi-1* promoter, which is not active in the VD neurons, these data suggest that *fmi-1* is working cell-nonautonomously to regulate directional neurite growth of the VD neurons in the VNC. However, we cannot completely rule out that *fmi-1* is being expressed in the VD neurons at undetectable levels.

Since we observed consistent expression of *fmi-1* in the VNC and because *fmi-1* defects are primarily observed there, we wondered if specific expression of *fmi-1* cDNA in the VNC could rescue the PVN phenotype. However, we were unable to rescue the PVN phenotype present in VD neurons when *fmi-1* was expressed specifically in the AVG, the PVP pioneer neurons, PVQ pioneer follower neurons or the cholinergic neurons, all of which have axons that contribute to the VNC (*n*≥3 lines scored per promoter). We concluded that expression of *fmi-1* in these neurons is not sufficient to rescue the PVN defects in *fmi-1* animals.

lin-17 functions in parallel to *fmi-1* in Region 6

A previous study has shown that a canonical Wnt signaling pathway is important for axon growth and pathfinding of the GABAergic neurons in the dorsal nerve cord (DNC) along the A/P axis in *C. elegans* (Maro et al., 2009). We have found that *fmi-1* interacts genetically with components of the Wnt pathway including *lin-17/frizzled* and *dsh-1/dishevelled* (Fig. 6, Fig. 7). In *lin-17;juIs76* animals, we found that 17% (*n*=191) of *lin-17* animals displayed a PVN (Fig. 6C). Unlike *fmi-1* mutants, these defects were predominantly observed in the R6 region (Fig. 7A). In fact, VD13 was primarily affected.

We next performed epistasis analysis between *lin-17* and *fmi-1*. We observed a statistically significant increase in the penetrance of PVNs in R6 from 17% and 4%, in *lin-17* and *fmi-1* respectively, to 52% (*n*=122) in *lin-17;fmi-1* double mutants (Fig. 7A). Double mutant animals did not display a significant increase in the penetrance of PVN defects in any of the remaining regions (R1 to R5) (Fig. S2). These results suggest that *lin-17* and *fmi-1* are working in parallel pathways to regulate the direction of neurite growth of the VD neurons in R6 region.

The R6 region in *lin-17* animals also displayed other types of defects including cell positioning defects and missing cell bodies (data not shown). Although these defects primarily affected VD11 and VD12, we were concerned that these defects might affect the interpretation of our data. Therefore, we calculated the penetrance of the PVN phenotype only in *lin-17* and *lin-17;fmi-1* animals lacking these types of defects in R6. In agreement with our previous observations, we found a significant increase (student's *t* test, p=0.017) in the penetrance of the PVN phenotype in the double mutant compare to the single mutant, 48% (*n*=55) versus 21% (*n*=28) respectively. These results suggest that the observed increase in PVNs occurred independently from the other defects present in *lin-17*.

lin-17;lhIs35 animals also displayed the PVN phenotype on the posterior side of worms (Table 2). We did not score PVN defects in VD13 because the aberrant neurites overlapped with the axon from the PDB neuron, which is also labeled by *lhIs35*, preventing us from confidently scoring these defects. *lin-17* animals also had gaps in the VNC (Table 2; Fig. S1). This result suggests that *lin-17* is also important for directional neurite growth of the VD neurons.

We next performed rescue experiments in the *lin-17;fmi-1* double mutant using a tagRFP-labeled LIN-17, expressed under its endogenous promoter. We were able to fully rescue the PVN phenotype in these animals (*n*=3 lines). In these lines, LIN-17::tagRFP was present in the cell body and neurites of the VD neurons, suggesting that *lin-17* is acting cell autonomously (Fig. 8). However, since we used the endogenous *lin-17* promoter, LIN-17::tagRFP was also present in other parts of the animal including neurons, muscles and epithelium (Fig. 8). Overall, these experiments suggest that *lin-17* works in parallel to *fmi-1* to control the direction of neurite growth of the VD neurons in the R6 region.

dsh-1 is a genetic enhancer of *fmi-1*

We next analyzed the interaction between *fmi-1* and *dsh-1* (Fig.6, Fig.7B). Double mutants of *fmi-1* with *dsh-1* showed a statistically significant increase in the penetrance of the PVN phenotype. In fact, 54% (*n*=100) of *fmi-1;dsh-1juIs76* animals had at least one PVN, whereas, as described above, only 25% of *fmi-1* animals had these defects (Fig. 7B). Unlike the genetic interaction of *fmi-1* with lin-*17*, we observed an increase in the penetrance of the PVN phenotype throughout the length of the animal. We confirmed these results by looking at *dsh-1;fmi-1;lhIs35* animals (Table 1). With this marker, 28% (*n*=29) of the animals had 2-4 VD neurons with PVNs (Fig. 9). This observation contrasted sharply with *fmi-1* animals in which only 4% (*n*=52) of the

worms had 2 VD neurons with PVN defects. We also found an increase in the number of defects per animal (Table 1). Transgenic expression of *fmi-1* was able to fully rescue the PVN phenotype in the *dsh-1;fmi-1* double mutant (Fig. 7B). These data suggest that *dsh-1* is a genetic enhancer of *fmi-1*.

Surprisingly, we did not find PVN defects in *dsh-1* single mutant using either *juIs76* or *lhIs35*. However, a small number of *dsh-1* animals (10-15%) displayed defects in the growth of the dorsal neurites in R6 region (Fig. 6D). In addition, *dsh-1;lhIs35* animals displayed under extension defects or gaps in the VNC like those observed in *fmi-1* mutants (Table 2; Fig. S1). The number and position of the VD cell bodies appear to be normal in *dsh-1;lhIs35* animals (Fig. S1).

We next performed colocalization experiments to find out if *dsh-1* is expressed in the VD neurons. We observed colocalization of a *dsh-1* genomic DNA fragment fused to *gfp* with a red VD marker (Fig. 10). *DSH-1*::GFP was present in the cytoplasm of the VD neurons during early L2 stage with no obvious asymmetric localization (Fig. 10). In addition, expression of this transgene in a *dsh-1juIs76* background caused overextension defects in the DNC in the R6 region (Fig. S3). These experiments indicate that *dsh-1* is expressed in the VD neurons and that it could be acting cell autonomously along with *fmi-1* to regulate the direction of neurite growth. Furthermore, overexpression of *dsh-1* can cause neurite overgrowth on the DNC, suggesting a role for *dsh-1* during neurite growth along the A/P axis. Overall, *dsh-1* appears to work in a parallel pathway to that of *fmi-1* to control the directional neurite growth of the VD neurons.

Mutations in *fmi-1* affect A/P neurite growth during early VD development

72

Our observations suggest that neurite defects in *fmi-1* animals arise during the early development of the VD neurons. Using *lhIs35*, we examined VD neurons during the neuroblast division through neurite extension stages in both *wt* and *fmi-1;dsh-1* animals (Fig. 11). We used *fmi-1;dsh-1* because these animals have a higher incidence of defects (see above). To confirm our observations, *fmi-1* single mutant animals were also examined. In *wt*, neuroblasts divided in the A/P axis during L1, (Fig. 11A). We found no differences in *fmi-1* (not shown) or *fmi-1;dsh-1* mutant animals (Fig. 11D) in the timing or orientation of division.

Shortly after division the lateral aspect of the cell body flattened along the major bundle of the VNC. Then, a neurite process was observed to extend from the anterior part of the flattened lateral aspect where it was contacting the VNC (Fig. 11B) and elongated in the anterior direction, running along the major bundle of the VNC (Fig. 11C). In the *fmi-1;dsh-1* mutants (and *fmi-1* – not shown), VD cells occasionally had a posterior projection from the lateral edge (Fig. 11E), and neurites extending posteriorly (Fig. 11F). It was not uncommon (~15-20% of VDs examined) to observe both anterior and posterior projections in VDs in *wt* animals (Fig. 11G). We measured the lengths of these projections and found that in *wt*, on average, the anterior process was 2.2-fold longer than the posterior (*n=12*) and only in 1/12 cases was the posterior process longer than the anterior. In *fmi-1;dsh-1* mutants the ratio was 0.86 (*n=12*) and 6/12 cases the posterior process was longer than the anterior. It is likely that this gives rise to the PVN phenotype in older animals.

3.4 Discussion

A fundamental step during the early development of the VD neurons is the polarized anterior growth of a single neurite which differentiates following a developmental program to generate a ventral axon, a ventrodorsal commissure and a dorsal dendrite. All of the processes formed by the VD neurons are located anterior to the cell body, indicating that these neurons must contain systems that detect and process information in terms of their relative position in the animal. Thus, abnormalities in these systems can affect proper neuronal development. VD neurons are inhibitory motor neurons, and each single cell covers a unique segment of the body. Thus, VD neurites that extend posteriorly leave segments of the ventral muscles without inhibitory input. In this study, we have shown that *fmi-1*, *lin-17/frizzled* and *dsh-1/dishevelled* are involved in directional neurite growth in the VD neurons, suggesting that multiple molecular cues contribute to the proper VD neurite growth along the A/P axis in the VNC in *C. elegans*.

fmi-1 and neurite growth along the A/P axis

To visualize VD neurite growth in the VNC, we used a VD marker that permitted visualization of the ventral processes. *fmi-1* animals had VD neurons that projected a PVN instead of an AVN. In spite of being misdirected, these posterior neurites were still able to extend ventrodorsal commissures which resulted in a different commissure pattern of the D-type GABAergic neurons along the A/P axis. *fmi-1* VD neurites also displayed highly penetrant underextension defects. These results suggest that the loss of *fmi-1* negatively affects neurite growth along the A/P axis whereas ventrodorsal neurite growth is not affected by *fmi-1* mutations. In contrast, netrin UNC-6 and its receptors, UNC-5 and UNC-40, have been previously shown to guide the VD commissures along the D/V axis (Hedgecock et al., 1990,

Norris and Lundquist, 2011). Therefore, VD neurite growth may be mechanistically separated along these two axes of development.

Recent studies have shown that *celsr3*, the vertebrate homologue of *fmi-1*, plays important roles during axon growth and guidance along the A/P axis in the embryonic mouse system (Fenstermaker et al., 2010, Shafer et al., 2011). Similarly, our study reveals that *fmi-1* is important for neurite growth along the A/P axis in *C. elegans*, suggesting a conservation of function across species. However, unlike these previous studies, our data does not support the involvement of two PCP pathway components, *prkl-1* or *vang-1*, in this developmental process in *C. elegans*. We show here that neither *prkl-1* nor *vang-1* LOF alleles displayed a *fmi-1*-like phenotype in the VD neurons. In addition, double mutant combinations of *fmi-1* with either of these two genes did not enhance or suppress the PVN defects in the VD neurons. Therefore, it is possible that *fmi-1* might be working in a novel developmental pathway to control neurite growth. This is not the first time that *fmi-1* has been shown to function independently from the PCP pathway. For instance, in *C. elegans*, mutations in *fmi-1* cause axon growth and guidance defects in the pioneer and pioneer follower neurons, whereas neither *prkl-1* nor *vang-1* appears to have a role here (Steimel et al., 2010). Moreover, mutations in *flamingo*, the *Drosophila* ortholog of *fmi-1*, cause axonal defects in the photoreceptor neurons that are not phenocopied by mutations in other components of the PCP pathway (Senti et al., 2003).

Studies on *celsr3* also revealed that this protein could be acting cell autonomously to regulate axon growth and guidance in vertebrate systems (Fenstermaker et al., 2010, Shafer et al., 2011). In contrast, our colocalization data suggest that FMI-1 is not present in the VD neurons, suggesting that *fmi-1* could be acting cell non-autonomously to regulate directional neurite growth in *C. elegans*. In fact, specific expression of *fmi-1* cDNA in the VD neurons was not able

to rescue the PVN defects whereas expression of *fmi-1* under a promoter that is inactive in the VD neurons was still able to fully rescue the PVN defects in the VD neurons. The cell non-autonomous function of *fmi-1* has been previously reported in both *C. elegans* and *Drosophila* (Chen and Clandinin, 2008, Steimel et al., 2010, Najarro et al., 2012).

fmi-1 and axon tract formation

How does *fmi-1* control neurite growth in the VD neurons? The VNC in *C. elegans* is comprised of two longitudinal axon tracks that run across the anteroposterior axis. The right and left axon tracks are pioneered by AVG and PVPR axons respectively (Steimel et al., 2010). Previous studies have shown that axon navigation of later born neurons rely on these pioneer neuron axons (Hutter, 2003, Steimel et al., 2010). For example, mechanical or genetic disruption of the AVG neuron can affect the guidance of various neurons in the VNC including the DD GABAergic neurons (R. M. Durbin, PhD Thesis, University of Cambridge, 1987) (Hutter, 2003). Moreover, as described above, a study has shown that pioneer-dependent navigation of follower axons is controlled by *fmi-1* (Steimel et al., 2010). Since VD neurons are born postembryonically, at a time when the pioneer neurons are already present in the VNC, it is possible that the neurite growth defects in the VD neurons are due to a failure in axon track formation. In agreement with this idea, we detected consistent presence of FMI-1 in the right axon bundle during the initial extension of the VD neurite. In addition, our data from the early development of the VD neurons reveals that AVN extends while closely following a marker for the right axon track. In order to know if the AVN of the VD neurons use the pioneer axons as guidance for their outgrowth, we transgenically expressed the *fmi-1* cDNA in the AVG and PVP pioneer neurons. However, expression of *fmi-1* in these neurons did not rescue the PVN defects

76

in the VD neurons. Similar results were found when *fmi-1* was expressed in the PVQ or cholinergic neurons. Therefore, it is possible that *fmi-1* in these neurons is not sufficient for the normal VD neurite extension. It is also possible that we have not yet found the optimal concentration required to rescue the PVN defects in the VD neurons in a cell specific manner. In fact, there is evidence that tight regulation of protein levels is required for the different functions of *flamingo* in the *Drosophila* model (Berger-Muller and Suzuki, 2011). At this point, it remains to be determined which cell or cells express *fmi-1* that is important for the direction of growth of the VD neurons.

How can a protein that appears to be evenly distributed in the VNC regulate neurite growth toward a specific direction in a cell-non autonomous fashion? One possible explanation is that *fmi-1*, through the adhesive properties of its cadherin domain, promotes anterior growth of a preexisting VD neurite. In this context, *fmi-1* could be partnering with a protein that is located on the anterior VD neurite to ensure anterior neurite growth. One prediction of this model is that the loss of *fmi-1* will cause underextension defects in the VNC. In fact, we observed extensive underextension defects in the VD neurons. However, this model does not explain the presence of PVN in *fmi-1* VD neurons. Our data from the early development of the VD neurons suggest that in addition to an AVN, VD neurons appear to have a small posterior process. Therefore, it is possible that *fmi-1*, in addition to promoting anterior neurite extension, might also inhibit posterior neurite growth. However, we only rarely saw *fmi-1* VD neurons containing both an AVN and a PVN. Finally, another possibility is that *fmi-1* is involved in VD neuronal polarity. We are confident that the identification and characterization of genes that work in the *fmi-1* pathway will shed light on the molecular mechanisms of directional neurite growth in the VNC.

Redundant developmental pathways control VD neurite growth along the A/P axis in *C. elegans*

Mounting evidence indicate that Wnt signaling regulates axon guidance and growth along the A/P axis (Zou, 2006). In *C. elegans*, there are multiple Wnt pathways that play redundant roles during axon growth along the A/P axis (Maro et al., 2009). We have found that *lin-17 and dsh-1* work in parallel to *fmi-1* to regulate the direction of growth of the VD neurites in the VNC. Although mutation in either of these two genes enhanced the PVN defect present in *fmi-1* animals, one clear difference between these interactions was that *lin-17;fmi-1* animals displayed PVN defects primarily in the R6 region whereas PVN defects in *dsh-1;fmi-1* animals were found throughout the animal. *lin-17* can work as a receptor for the *lin-44* and *egl-20* Wnt ligands (Maro et al., 2009, Kirszenblat et al., 2011), which form protein gradients along the A/P axis that can act as repellent signals during neurite growth (Maro et al., 2009). The R6 region coincides with the place where both LIN-44 and EGL-20 proteins are detected in *C. elegans* (Harterink et al., 2011), so this could be the reason why the VD neurons located there are more affected by the loss of *lin-17*.

RMEV and RMED are two GABAergic neurons whose cell bodies are located in the nerve ring in *C. elegans*. They extend a longitudinal neurite along the VNC and DNC respectively. Previous studies have shown that *dsh-1* is important for the extension of the RMEV and RMED neurites along the A/P axis (Song et al., 2010). Similarly, we have found that *dsh-1* animals display VD neurite defects such as underextension in the VNC and DNC. *dsh-1* single mutant animals do not display PVN defects on their own. We only saw PVN defects in the VD neurons when this mutation is combined with the *fmi-1* mutation. These observations clearly suggest that these two genes work in parallel pathways to regulate directional neurite growth.

In summary, we have uncovered an important function for *fmi-1* during directional neurite growth of the VD neurons in the VNC. Furthermore, two known components of the Wnt pathway contribute to the correct growth of the VD neurites along the A/P axis in the VNC.

3.5 Materials and Methods:

C. elegans strains: All _C. elegans_ used were hermaphrodites, and strains were maintained at 20–22.5°C as described (Brenner, 1974). _lhIs35[Punc-55::gfp]_ and _lhIs44[Punc-25::mcherry]_ were isolated using trimethylpsoralen/UV mutagenesis, and out-crossed to wild-type (_wt_) six times prior to analyses. The following alleles were used: _fmi-1(tm306)_ V, _fmi-1(rh308)_ V, _prkl-1(ok3182)_ IV, _vang-1(ok1142)_ X, _lin-17(n671)_ I, _dsh-1(ok1445)_ II, _juIs76[Punc-25::gfp]_ II, _lhIs35[Punc-55::gfp]_, _lhIs44[Punc-25::mcherry]_, _juIs145[Pflp-13::gfp]_.

Molecular biology: The _fmi-1::gfp_ (Steimel et al., 2010) was injected into _fmi-1(tm306);juIs76_ animals at 0.5 ng µl^{-1} along with coinjection markers at 10 ng µl^{-1} of _Pstr-1::gfp_ and 5 ng µl^{-1} _Pmyo-2::rfp_ to generate extrachromosomal arrays named _fmi-1(+) line #1_ and _fmi-1(+) line#2_ respectively. _fmi-1(+) line #1_ (_lhEx269_) was crossed into _fmi-1(tm306);lhIs44_ and _dsh-1(ok1445)juIs76;fmi-1(tm306)_ to perform colocalization and rescue experiments respectively. Constructs to express _fmi-1_ cDNA in the pioneer (_Podr-2_), pioneer follower (_Psra-6_) and cholinergic (_Pacr-2_) neurons are described in (Steimel et al., 2010) and (Najarro et al., 2012) respectively. Each of these constructs was injected into _fmi-1(tm306);juIs76_ animals at two different concentrations, 0.5 and 2.0 ng µl^{-1}, along with 10 ng µl^{-1} of _Pstr-1::gfp_ as a coinjection marker. At least three extrachromosomal arrays per injection were generated. The _dsh-1::gfp_ (Sanchez-Alvarez et al., 2011) was expressed in _dsh-1(ok1445)_ animals carrying either _juIs76_ or _lhIs44_. _lin-17::tagRFP_ was generated from _lin-17::gfp_ (Wu and Herman, 2006) and was injected into _lin-17(n671);fmi-1(tm306);juIs76_ mutant animals at 0.5 ng µl^{-1} with 10 ng µl^{-1} of the _Pstr-1::gfp_ coinjection marker to generate _lin-17(+) line #1_ to _#3_. The AS marker was created by expressing _tagRFP_ under a _Punc-53_ promoter (Stringham et al., 2002). _Punc-53::tagRFP_ was

injected into *wt* animals at 30 ng µl^{-1} with 5 ng µl^{-1} of the *Pmyo-2::rfp* to generate *lhEx240*. Details of the cloning are available upon request.

Phenotype quantification: PVN defects using *juIs76* were scored as follows. Adults were visually separated in six regions (R1 to R6 region) along the A/P axis. Cell body number, commissure number and positions were noted. In *wt* animals, the DD and VD commissures are always located anterior to their somas such that regions R1-R5 each contain 3 commissures, whereas region R6 typically contains 4 commissures (occasionally, the VD12 and DD6 commissures fasciculate). If a region expected to have three commissures contained only two commissures, this was scored as a PVN defect, as long as we were able to find the mispositioned commissure in the region immediately posterior. Of the total PVN defects observed, <4% were found within regions.

The expression pattern of *lhIs35[Punc::55::gfp]* was similar to previous observations (Zhou and Walthall, 1998) except that VD precursor cells were also labeled. GFP was detected in the 13 VD neurons, 11 AS neurons, VA1 and PDB. *Punc-55* activity was highest during L2, and was not detected beyond L4, as reported (Zhou and Walthall, 1998). We scored PVNs in L2 animals. We acquired Z sections by confocal microscopy followed by a close examination of the presence or absence of PVNs. We did not score defects in the VD1 and VD2 because their cell bodies are located close to each other, so their neurites cannot be visualized individually. VD12 and VD13 have similar resolution constraints. Finally, we used the images to score underextension or gap defects in the VNC. Gaps had to be at least half size of a VD cell body ($\approx$ 1.5-2.0 µm) to be considered.

81

Early development of the VD neurons: Using *lhIs35,* we acquired Z-stacks of the early VD neurons by confocal microscopy. The VNC was marked by *Punc-53::tagRFP* that labels DA motoneurons (and later AS). Late L1 and early L2 animals were picked based on size, then confirmed by examination of the gonad primordium. Images were acquired on an Olympus FV1000 using multi-tracking parameters and a 60x Plan-apochromat objective. Images were exported to ImageJ for analysis and rotation. To measure the anterior and posterior neurites an oval/circle was drawn around the cell body in ImageJ. Measurements were made from the center of the circle to the anterior and posterior most tip of the neurite via a straight line.

In all images in this manuscript, anterior is to the left.

Table 3.1

Genotype	n	VD1-2	VD3	VD4	VD5	VD6	VD7	VD8	VD9	VD10	VD11	VD12-13	total	defects/animal
N2	24	N/D	0%	0%	0%	0%	0%	0%	0%	0%	0%	N/D	0%	0.00
fmi-1	52	N/D	0%	8%	4%	4%	12%	13%	4%	4%	0%	N/D	44%	0.48
lin-17	44	N/D	0%	0%	0%	0%	0%	0%	0%	5%	5%	N/D	9%	0.09
dsh-1	25	N/D	0%	0%	0%	0%	0%	0%	0%	0%	0%	N/D	0%	0.00
fmi-1; dsh-1	29	N/D	14%	28%	10%	10%	14%	10%	14%	3%	0%	N/D	59%	1.00 *

* Value different from *fmi-1* animals by Student's t test, *p* =0.02.
(N/D) not determined

3.1. Posterior ventral neurite (PVN) defects in animals expressing *lhIs35* marker.

Table 3.2

Genotype	n	VD1-2	VD3	VD4	VD5	VD6	VD7	VD8	VD9	VD10	VD11	VD12-13	total	gaps/animal
N2	24	N/D	4%	4%	4%	0%	4%	17%	8%	0%	0%	N/D	30%	0.29
fmi-1	52	N/D	38%	48%	23%	29%	29%	42%	15%	15%	10%	N/D	100%	2.56
lin-17	44	N/D	5%	9%	5%	0%	5%	18%	7%	14%	5%	N/D	55%	0.73
dsh-1	25	N/D	24%	16%	12%	12%	12%	4%	12%	12%	0%	N/D	64%	1.00

(N/D) not determined

85

3.2. Neurite underextension defects or gaps in the VNC in animals expressing *lhIs35*

marker.

Table 3.S1.

Genotype	Number of cell bodies per Region (penetrance %)						
	Region 1	Region 2	Region 3	Region 4	Region 5	Region 6	# commissures
N2	3(100%)	3(100%)	3(100%)	3(100%)	3(100%)	4(99%)	19(93%)*
fmi-1(tm306)	3(100%)	3(99%)	3(100%)	3(100%)	3(100%)	4(100%)	19(91%)**

* 19 commissures per animal were observed in 93% of the control animals. 6% of the remaining control animals displayed18 commissures per animal. In these animals, VD13 commissures appear to be fasciculated with DD6 commissures.

** 19 commissures per animal were observed in 91% of the *fmi-1* animals. 6% of the remaining *fmi-1* animals displayed 18 commissures per animal. In these animals, VD13 commissures appear to be fasciculated with DD6 commissures.

$n \geq 100$

3.S1. Number of cell bodies per Region and total number of commissures per animal.

Figure 3.1
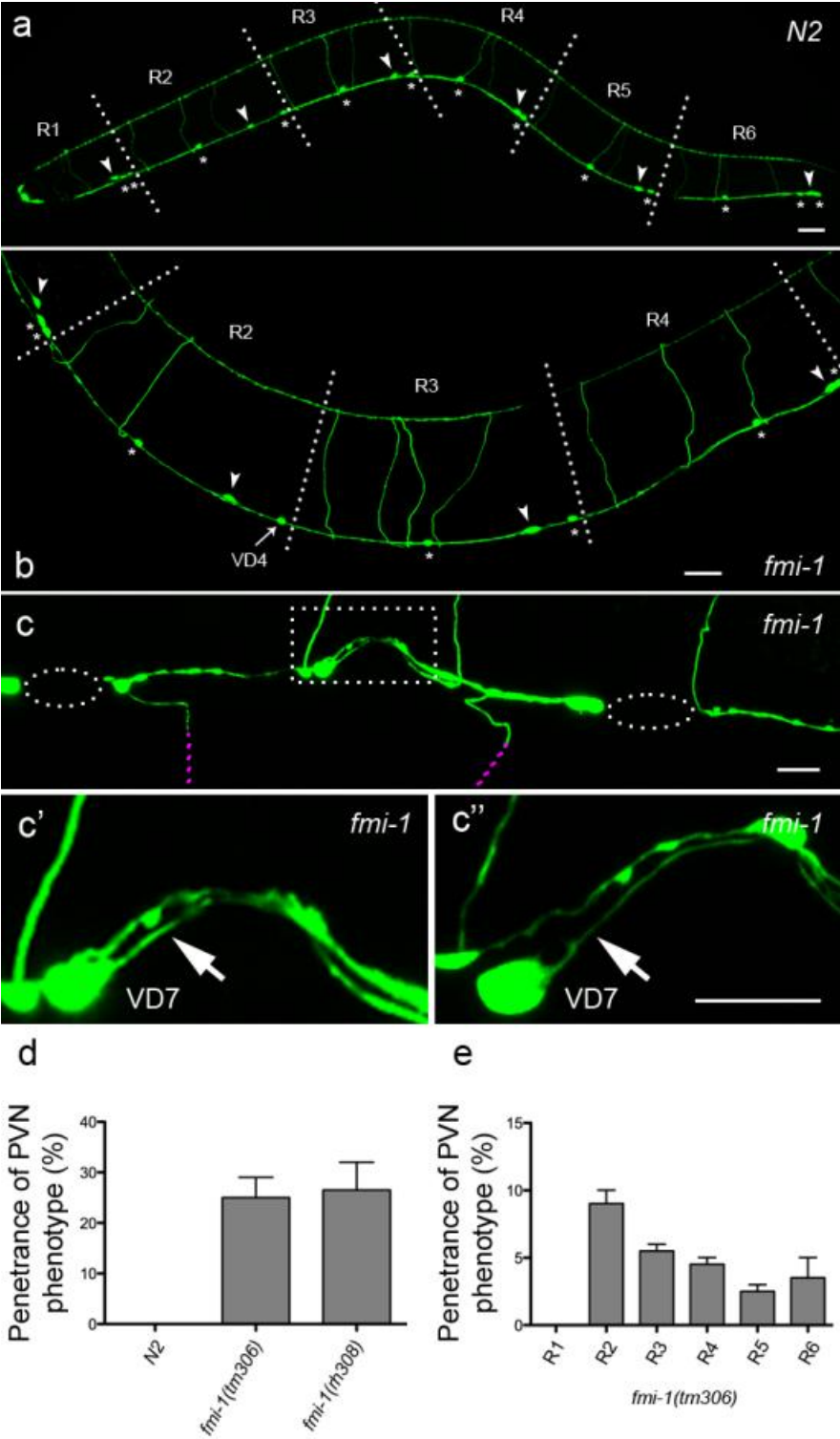
Figure 3.1. PVN defects in *fmi-1* animals. **(A)** In *juIs76* animals, the D-type GABAergic neurons can be organized in six regions (R1-R6) along the A/P axis. Regions R1-R5 each contain one DD (arrowheads) and two VDs (asterisks) whereas region R6 contains one DD and three VDs. VD and DD commissures are positioned anterior to their respective cell body. **(B)** In this *fmi-1* animal, VD4 commissure is in region R3 instead of R2. As a result, R2 and R3 contain 2 and 4 commissures respectively. In contrast, R2 and R3 in *wt* always contain three commissures as depicted (A). **(C-C')** Ventral view of another *fmi-1* animal where VD7 is displaying a PVN (arrow). **(C'')** Rotated version of (c'). **(D)** Quantification of the PVN phenotype penetrance. **(E)** Quantification of the PVN phenotype per region. Dashed ellipse indicates regions lacking neuronal processes in the VNC whereas purple dashed lines show commissures out of focus. Dashed square show region magnified and depicted in (C'-C''). Scale bar is 20 μm in (A,B) and 10 μm in (C-C''). Anterior is to the left.

Figure 3.2
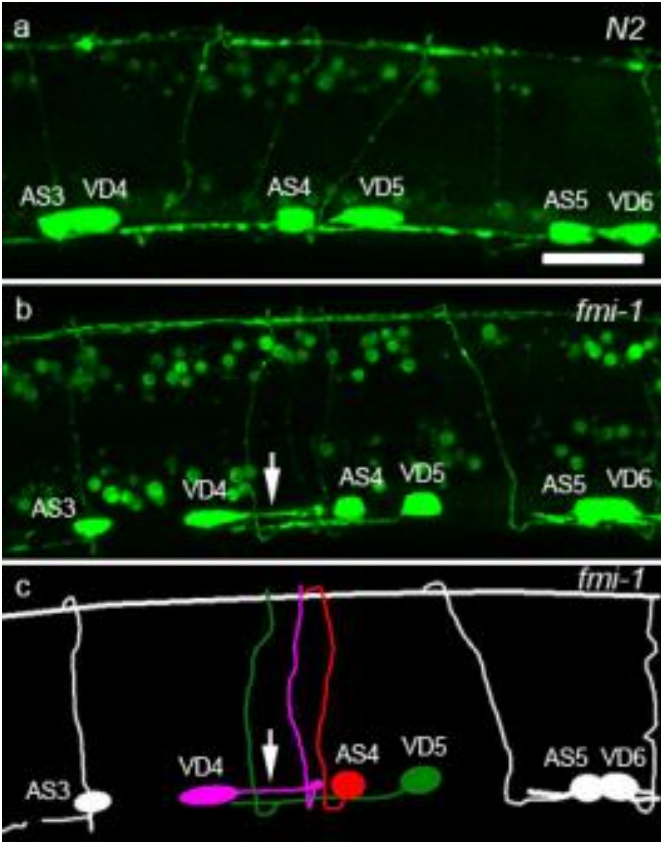
Figure 3.2. VD neurons display PVN defects in *fmi-1;lhIs35* animals. (A) L2 *wt* animal expressing the *lhIs35* marker. VD neurons are posterior to AS neurons. **(B)** VD4 displaying a PVN defect (arrow) in an L2 *fmi-1* animal. In spite of this defect, VD4 still projects a ventrodorsal commissure. VD5 has a normal AVN. Note that VD6 commissure is not shown in the *fmi-1* animal **(C)** A cartoon of (B). Scale bar is 10 μm.
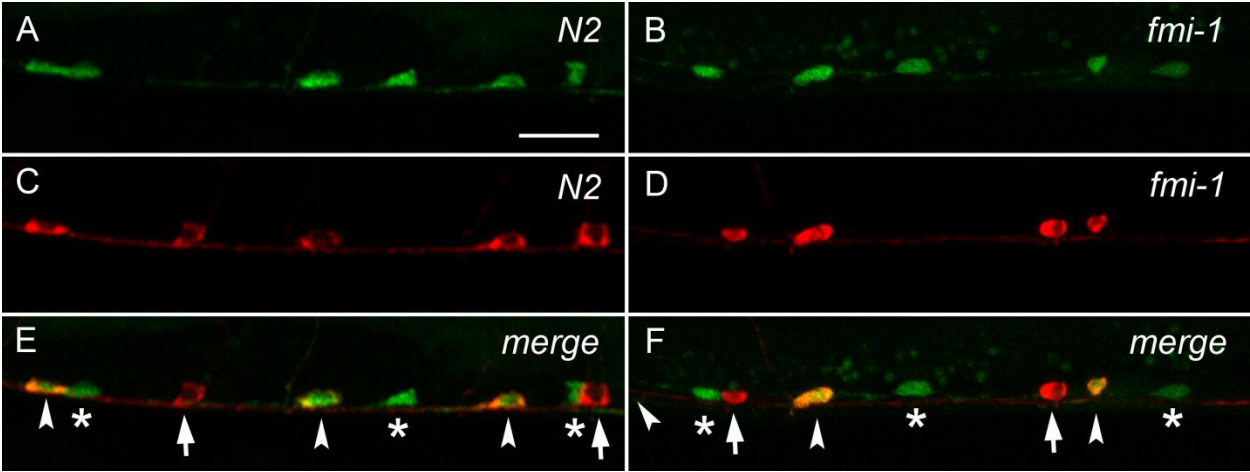
Figure 3.3

Figure 3.3. VD neurons are positioned posterior to AS neurons in *wt* and *fmi-1* animals. **(A,B)** *lhIs35* labels VD and AS neurons in *wt* (A) and *fmi-1* (B). **(C,D)** AS and DA neurons are labeled by RFP (*Punc-53::tagRFP*) in *wt* (C) and *fmi-1* (D). **(E,F)** Merge views. VD neurons (asterisks) are located posterior to AS (arrowheads) in both backgrounds. Notice that the first AS neuron, from left to right, is not shown in (F). Red marker is also expressed in the DA neurons (arrows in E and F). Scale bar is 10 μm.
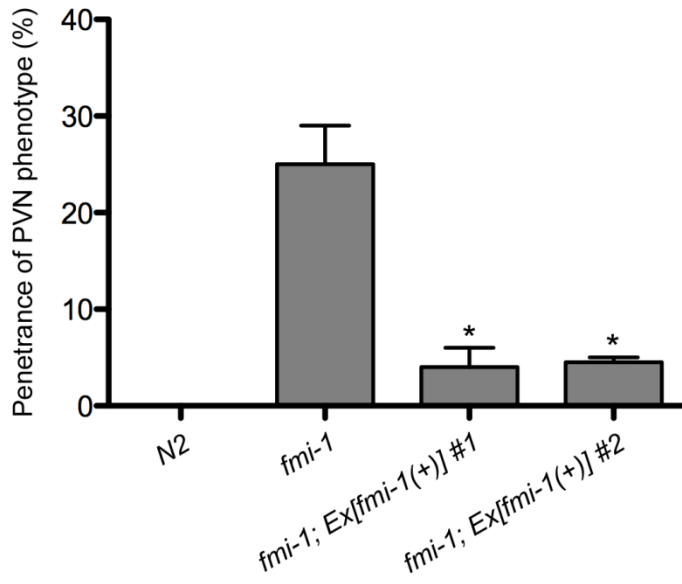
Figure 3.4

Figure 3.4. **Transgenic rescue of PVN defects in *fmi-1* adults.** For each data set, *n* represents at least 100 animals. Asterisks indicates significantly different from *fmi-1* by Student's *t* test, *p*<0.05.

Figure 3.5
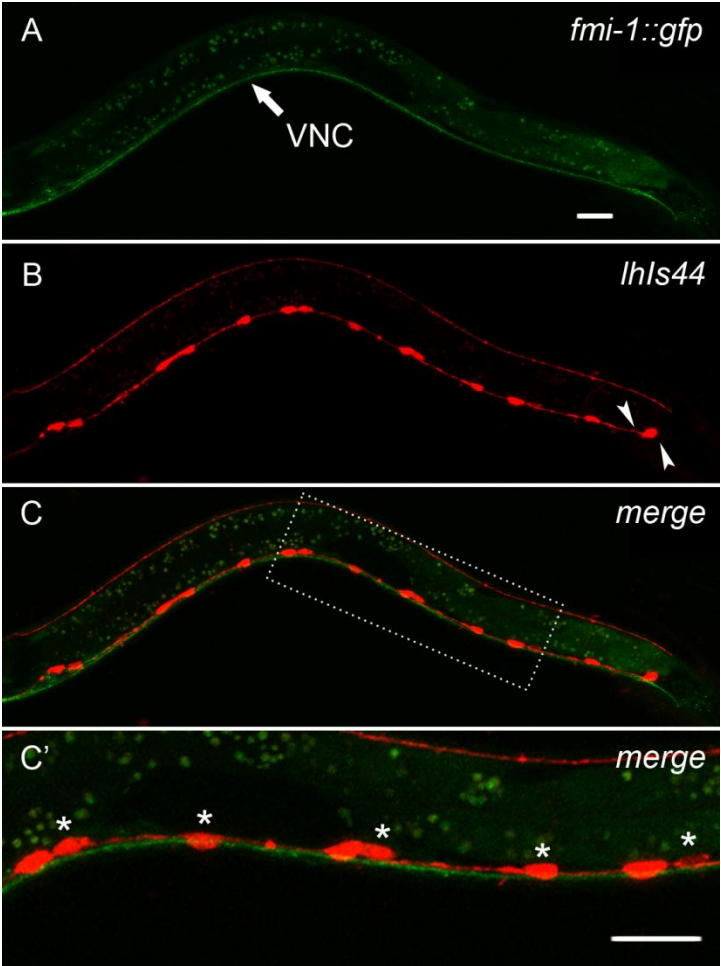
Figure 3.5. FMI-1 is in the VNC at early L2 stage during AVN growth. (A) An early L2 *fmi-1* animal expressing a rescuing FMI-1::GFP. GFP-labeled FMI-1 is consistently present in the VNC. **(B)** Same animal coexpressing a red VD marker (*lhIs44*). Arrowheads indicate the position of VD12 and VD13 which have yet to develop in this early L2 animal. **(C-C')** FMI-1::GFP is not detectable in the VD neurons but is present in neighboring axons in the VNC. Dashed rectangle show inset depicted in (C'). Asterisks indicate VD neurons. Scale bar is 10 μm.
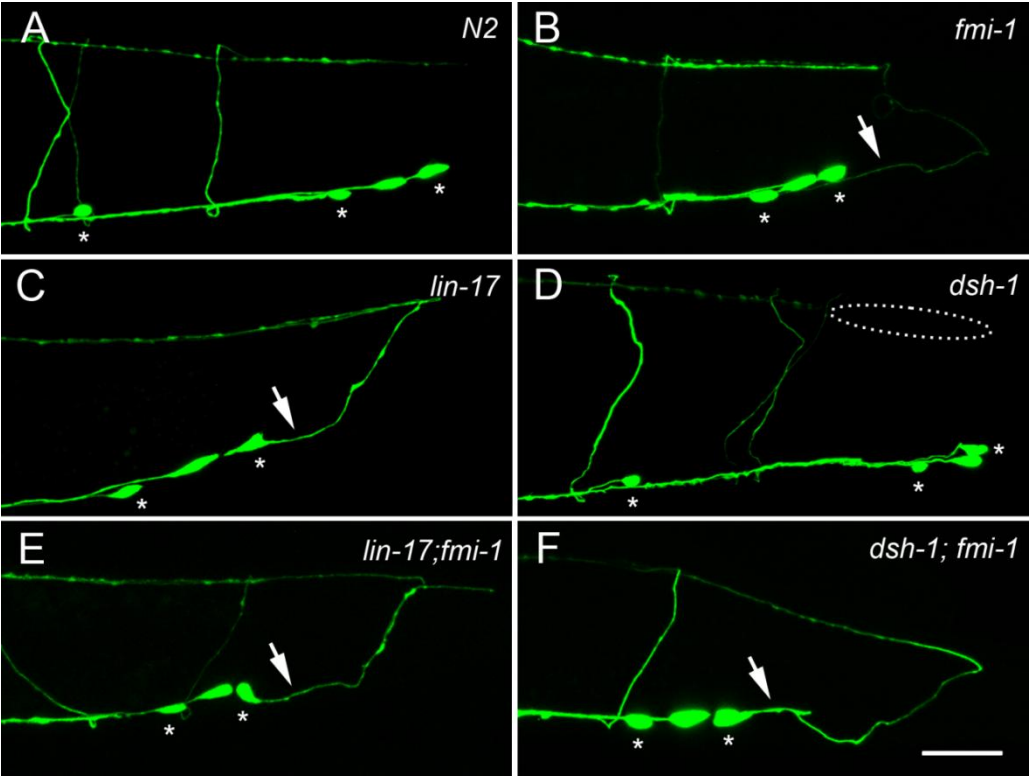
Figure 3.6

Figure 3.6. A/P neurite growth defects in *fmi-1, lin-17* and *dsh-1*. **(A)** Region R6 in *wt*. **(B)** An *fmi-1* animal displaying a PVN phenotype in R6. **(C)** A *lin-17* animal displaying *fmi-1*-like defects in R6. **(D)** *dsh-1* animals display defects in dorsal neurite extension (dashed ellipse), but not PVNs. PVN defects are present in the *lin-17;fmi-1* **(E)** and *dsh-1;fmi-1* animals **(F)**. Asterisks indicate VD neurons. Scale bar is 20 μm.
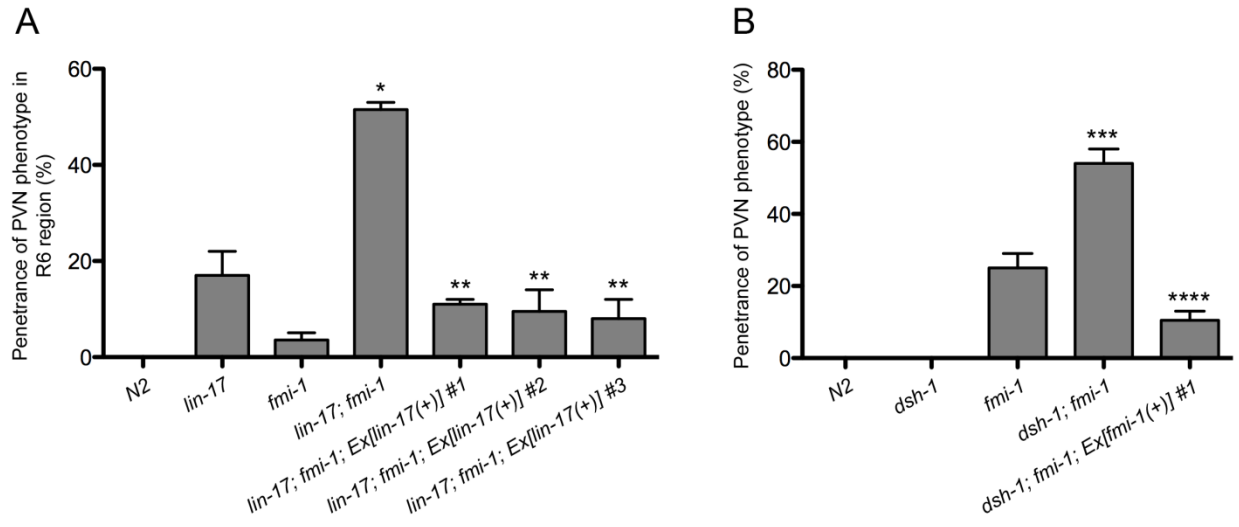
Figure 3.7

Figure 3.7. *fmi-1* genetically interacts with *lin-17* and *dsh-1*. (A) Quantification of the PVN

phenotype in region R6 in *lin-17* and *fmi-1* mutants and *lin-17;fmi-1* double mutants using

juIs76. *lin-17* expression, under its endogenous promoter, rescues defects in *lin-17;fmi-1* double

mutants (third bars from right to left). (*) indicates value different from *lin-17* and *fmi-1* single

mutant animals, *p*<0.05. (**) indicates values different from *lin-17;fmi-1* mutant animals,

p<0.05. **(B)** Penetrance of PVN defects in regions R1-R6 in *dsh-1;fmi-1* double mutant animals.

Defects were rescued by transgenic expression of *fmi-1* in the double mutants (first bar from

right to left). PVNs are not present in either *dsh-1* or *N2* control animals. (***) indicates value

different from *fmi-1* mutants, p<0.05. (****) indicates values different from *dsh-1;fmi-1* mutants,

p<0.05.

Figure 3.8

A

*

juIs76

B

*

lin-17::tagRFP

C

*

merge
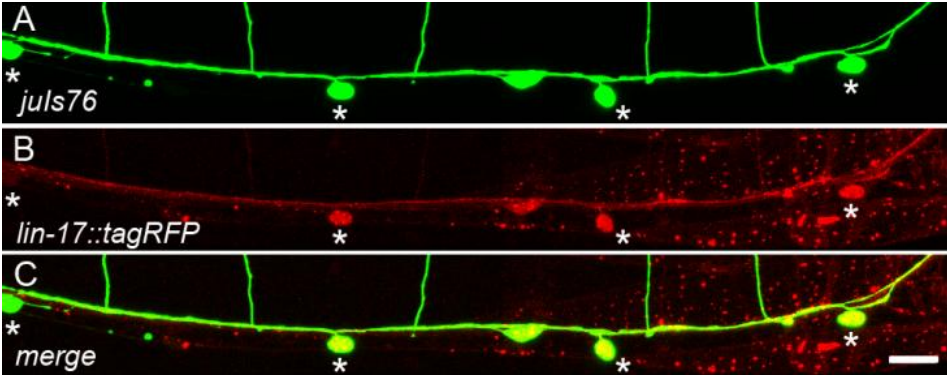
Figure 3.8. *lin-17::tagRFP* **is expressed in VD. (A)** Ventral view of an adult *juIs76* animal, DDs and VDs (asterisks) are green. **(B)** Same animal coexpressing *Plin-17::lin-17::tagRFP*. **(C)** Colocalization (yellow) indicates LIN-17::tagRFP is present in the VD neurons. Scale bar is 10 μm.
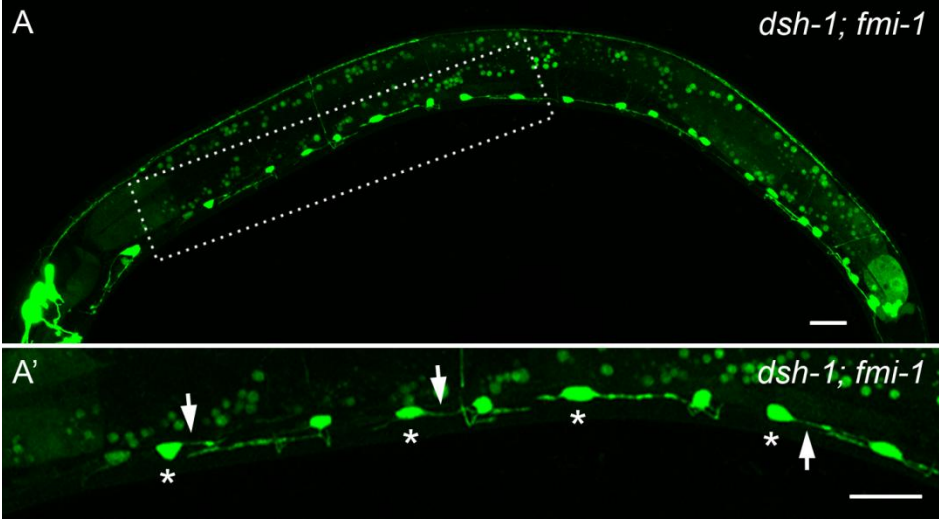
Figure 3.9

Figure 3.9. *dsh-1* is an enhancer of *fmi-1*. (A-A') *dsh-1;fmi-1* double mutant animal displaying

multiple PVN defects in the VDs (asterisks). Arrows mark PVN defects. Scale bar is 10 µm.
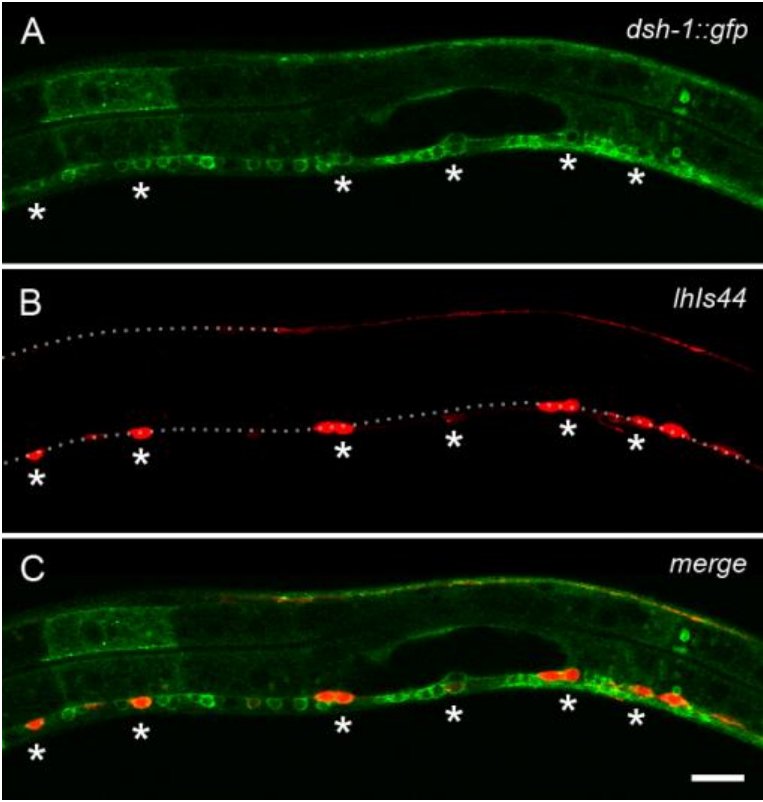
Figure 3.10

Figure 3.10. DSH-1::GFP is present in the VDs at early L2 stage. (A) *Pdsh-1::dsh-1::gfp* labels neurons along the VNC. **(B)** Same animal coexpressing a red GABAergic marker (*lhIs44*). **(C)** DSH-1::GFP is present in the VD neurons (asterisks). Yellow indicates colocalization. Dashed lines in (B) indicate the DNC and VNC. Scale bar is 10 μm.
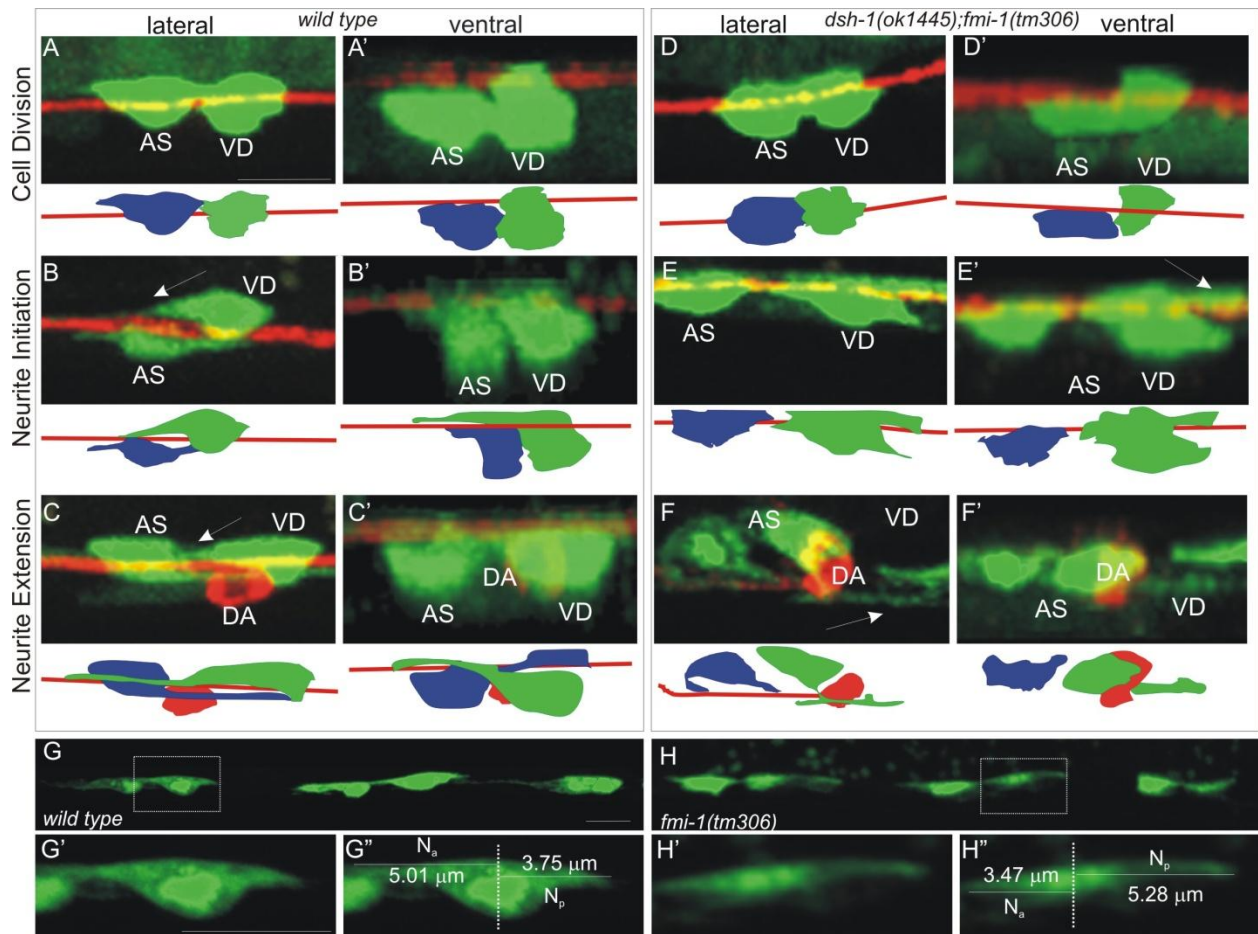
Figure 3.11

Figure 3.11. Early VD development. *lhIs35* (AS and VD neurons) and *Punc-53::tagRFP* (DA neurons) were visualized in *wt* and *dsh-1;fmi-1* mutants (A-I). In all panels anterior is left. **(A-F).** Early VD development was classified into stages: cell division (A,D), neurite initiation (B,E) and neurite extension (C,F). No differences were found in cell division. However, during neurite initiation, at a time when cells were forming AVNs (B – arrow), mutants more often formed posteriorly extended neurites (E – arrow). During neurite extension, at a time when *wt* VDs displayed an AVN (C - arrow), we found PVNs in mutant animals (F – arrow). For each panel we have provided a cartoon where VD (green), AS (blue) and VNC (red) are illustrated. **(G,H)** As the VDs flattened along the VNC, it was possible to observe anterior and posterior projections from the cells in wild-type (G) and *fmi-1(tm306)* (H). **(G',H')** Individual VD neurons (boxed regions-G,H). **(G",H")** We measured the anterior neurite length (Na) and posterior neurite length (Np). Scale bar is 5 μm.
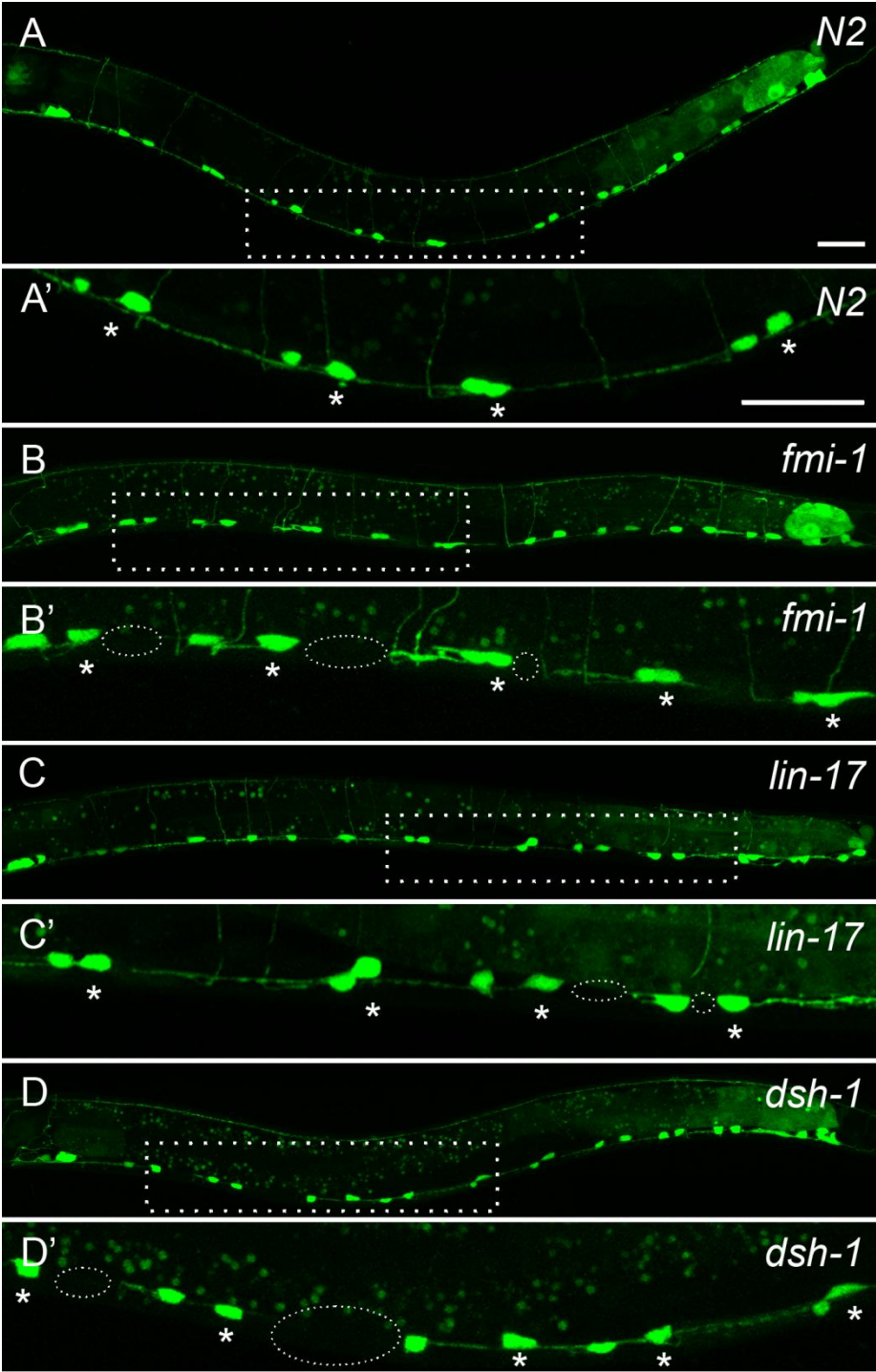
Figure 3.S1

Figure 3.S1. Mutations in *fmi-1*, *lin-17* and *dsh-1* cause neurite underextension defects or gaps in VNC. (A,A') *lhIs35 wt* animals typically do not display gap defects in the VNC. **(B-D)** Gap defects are present in *fmi-1* (B,B'), *lin-17* (C,C') and *dsh-1* (D,D') animals. Asterisks indicate VD neurons. Dashed rectangles highlight the insets displayed below each genotype. Dashed ellipses mark gap defects. Scale bar is 10 µm.
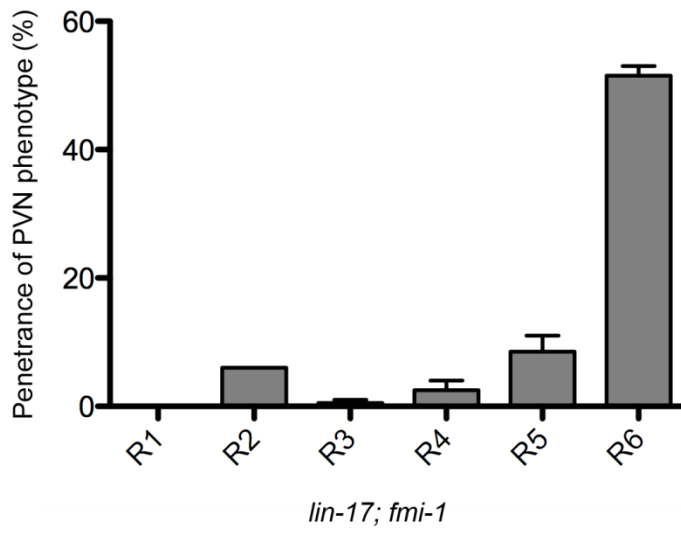
Figure 3.S2

Figure 3.S2. *lin-17;fmi-1* double mutant animals display PVN defects primarily in R6 region.

**Figure 3.S3**

dsh-1; Ex[dsh-1(+)]
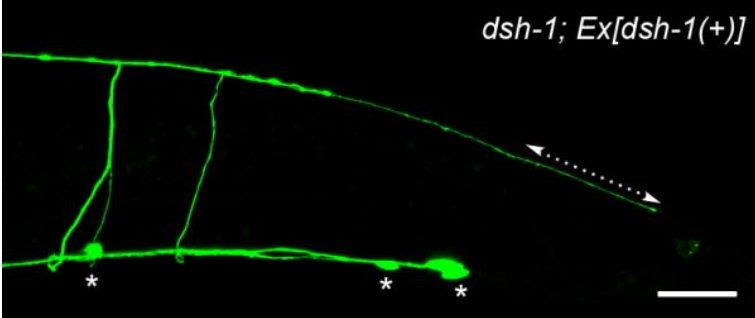
Figure 3.S3. **Overexpression of *dsh-1* causes dorsal neurite overgrowth.** An adult *dsh-1* mutant animal displaying overextended dorsal neurite caused by the overexpression of *dsh-1* gene. Dashed arrow indicates the extent of neurite overextension. Scale bar is 20 µm.

Chapter IV

Conclusions

More than a century ago, the distinguish neurobiologist, Ramon y Cajal, was able to use the Golgi staining to visualize the nervous system in unprecedented detail. These observations led him to the realization of the enormous architectural complexity that is displayed by the nervous systems of many organisms, including human beings. One of the outstanding questions that arose from these early observations is: What are the molecular and cellular mechanisms that are important for the formation of fully assembled and functional neuronal networks? In order to answer such a challenging scientific problem, the development of neuronal networks has being separated into consecutives steps, including neurulation, cell fate acquisition, cell migration, cell differentiation, axon growth, synaptogenesis and so on. Many, if not all of these developmental steps, require cell-cell contact and adhesion. Therefore, molecules that permit and facilitate cell-cell contact are important during the formation of the nervous system. Cadherins are such proteins.

Here I have described the characterization of the atypical cadherin *fmi-1* in the context of its role during the development of the D-type GABAergic neurons in *C. elegans*. Our main discoveries include a role for *fmi-1* during early neurite/axon growth along the anterior-posterior axis and that it carries out this function in parallel to components of the Wnt pathway. In addition, *fmi-1* animals display synaptic defects. Overall, these observations indicate that *fmi-1* is involved in various aspects of neural development and function.

The development of the VD neurons has many parallels with what is known about neuronal development in other systems. *In vivo* and *in vitro* data have shown that right after neurulation, a neurite emerges from the cell body, which in turn, marks the appearance of a second neurite located 180 degrees from the first neurite and so forth (Caceres et al., 2012). Generally, the first neurite develops further to become the axon whereas the other neurites may become dendrites

118

(Caceres et al., 2012). Similarly, we have found that right after cell division, a VD neuron extends two neurites located at either side of the cell body along the A/P axis. The anterior VD neurite develops further to give rise to an axon whereas the posterior neurite appears to collapse. VD neurons also have other neuronal processes, including a ventrodorsal commissure and a dorsal dendrite, but these arise from the anterior neurite. Although all these cellular behaviors appear to be primarily directed by intracellular mechanisms, there is evidence that extracellular cues influence some of these processes including neurite and axon growth. In fact, there is evidence that adhesive complexes via cadherin and laminin play a role here (Caceres et al., 2012).

How does *fmi-1* influence neurite growth? We hypothesize that *fmi-1*, which is located in the VNC in the neighboring axons, promote growth of the anterior neurite by interacting with another adhesion protein that may be asymmetrically localized in the anterior neurite. In this context, *fmi-1* could be important for the early polarization of the VD neurons. *fmi-1*-like proteins are involved in epithelial polarization (Vladar et al., 2009), therefore it is possible that *fmi-1* has such function in the VD neurons. How can we determine if *fmi-1* has a role in neuronal polarization? One way to test this hypothesis is by the use of neuronal polarity markers such as the centrosome, whose intracellular position has being shown to determine the place where the first neurite emerges (de Anda et al., 2005). We tested whether the same is true in the VD neurons, but we got inconclusive results. Two centrosome-like structures were observed in each VD neuron and they were located in either side of the cell body along the A/P axis (data not shown). Because a neuron is a differentiated cell, it should only contain one centrosome. So, it is possible that the observed centrosome-like structures may represent an artifact due to the overexpression of the centrosomal proteins. The problems associated with the overexpression of

119

proteins in *C. elegans* can be minimized by using the newly developed single copy insertion of transgenes in this organism. Another way to narrow down the specific role of *fmi-1* during the development of the VD neurons is the identification of genes that might be working in the *fmi-1* pathway. In this regard, it would be extremely important to identity the *fmi-1* receptor or receptors that are present in the VD neurons. Luckily for us, the phenotype displayed by *fmi-1* mutant animals along with the markers developed here in this work provide us with rational approaches to carry out forward and reverse genetic screen to identify genes that work in the *fmi-1* pathway. For example, the newly developed VD marker, *Punc-55::gfp*, could be used to perform a forward genetic screen. This genetic screen should be able to identify genes that are important for VD neurite growth in the VNC.

Here we have also implicated components of the Wnt pathway in directional neurite growth. Mutations in *lin-17/frizzled* and *dsh-1/disheveled* enhance the penetrance of the aberrant neurite phenotypes present in *fmi-1* animals. Our preliminary results suggest that the Wnt ligands *lin-44* and *egl-20,* along with downstream components, such as *bar-1* and *mig-5*, are also involved in VD neurite growth (data not shown). These observations clearly indicate that multiple pathways participate to direct the growth of the VD neurites in the VNC. Further experiments are needed to understand how these pathways collaborate to influence neurite growth at the cellular and molecular levels. These genetic interactions also provide strategies to identify genes that might be part of the *fmi-1* pathway. For example, *dsh-1* animals can be used as a sensitized background to carry out forward and reverse genetic screens.

We have also found that *fmi-1* animals display synaptic defects. Because neurite/axon growth precedes synaptogenesis, the absence of the presynaptic marker, SYNAPTOBREVIN::GFP, in some regions in the VNC can be explained by neurite/axon extension defects. However, we also

120

found some evidence that even when the axon is present, VD synapses displayed some morphology defects (Najarro et al., 2012). Therefore, it is possible that *fmi-1* has a synaptic function that might be independent from that of its axon growth function. In fact, *fmi-1*-like proteins are also being shown to have synaptic functions (Bao et al., 2007). Future experiments should be designed to identify genes that work in the *fmi-1* pathway that primarily affects synaptogenesis.

Finally, this study also demonstrates, one more time, that *C. elegans* is a powerful tool to characterize the function of cadherin proteins in the development of the nervous system.

References

Ackley BD, Harrington RJ, Hudson ML, Williams L, Kenyon CJ, Chisholm AD, Jin Y (2005) The two isoforms of the Caenorhabditis elegans leukocyte-common antigen related receptor tyrosine phosphatase PTP-3 function independently in axon guidance and synapse formation. J Neurosci 25:7517-7528.

Ackley BD, Kang SH, Crew JR, Suh C, Jin Y, Kramer JM (2003) The basement membrane components nidogen and type XVIII collagen regulate organization of neuromuscular junctions in Caenorhabditis elegans. J Neurosci 23:3577-3587.

Bao H, Berlanga ML, Xue M, Hapip SM, Daniels RW, Mendenhall JM, Alcantara AA, Zhang B (2007) The atypical cadherin flamingo regulates synaptogenesis and helps prevent axonal and synaptic degeneration in Drosophila. Molecular and cellular neurosciences 34:662-678.

Berger-Muller S, Suzuki T (2011) Seven-pass transmembrane cadherins: roles and emerging mechanisms in axonal and dendritic patterning. Molecular neurobiology 44:313-320.

Bolte S, Cordelieres FP (2006) A guided tour into subcellular colocalization analysis in light microscopy. Journal of microscopy 224:213-232.

Brenner S (1974) The genetics of Caenorhabditis elegans. Genetics 77:71-94.

Brown HM, Van Epps HA, Goncharov A, Grant BD, Jin Y (2009) The JIP3 scaffold protein UNC-16 regulates RAB-5 dependent membrane trafficking at C. elegans synapses. Developmental neurobiology 69:174-190.

Caceres A, Ye B, Dotti CG (2012) Neuronal polarity: demarcation, growth and commitment. Current opinion in cell biology 24:547-553.

Casal J, Lawrence PA, Struhl G (2006) Two separate molecular systems, Dachsous/Fat and Starry night/Frizzled, act independently to confer planar cell polarity. Development 133:4561-4572.

Chen PL, Clandinin TR (2008) The cadherin Flamingo mediates level-dependent interactions that guide photoreceptor target choice in Drosophila. Neuron 58:26-33.

Chen WS, Antic D, Matis M, Logan CY, Povelones M, Anderson GA, Nusse R, Axelrod JD (2008) Asymmetric homotypic interactions of the atypical cadherin flamingo mediate intercellular polarity signaling. Cell 133:1093-1105.

Colon-Ramos DA, Margeta MA, Shen K (2007) Glia promote local synaptogenesis through UNC-6 (netrin) signaling in C. elegans. Science 318:103-106.

Curtin JA, Quint E, Tsipouri V, Arkell RM, Cattanach B, Copp AJ, Henderson DJ, Spurr N, Stanier P, Fisher EM, Nolan PM, Steel KP, Brown SD, Gray IC, Murdoch JN (2003) Mutation of Celsr1 disrupts planar polarity of inner ear hair cells and causes severe neural tube defects in the mouse. Curr Biol 13:1129-1133.

de Anda FC, Pollarolo G, Da Silva JS, Camoletto PG, Feiguin F, Dotti CG (2005) Centrosome localization determines neuronal polarity. Nature 436:704-708.

Dougherty RP (2005) Extensions of DAMAS and benefits and limitations of deconvolution in beamforming. In: AIAA Paper, pp 2005-2961.

Fenstermaker AG, Prasad AA, Bechara A, Adolfs Y, Tissir F, Goffinet A, Zou Y, Pasterkamp RJ (2010) Wnt/planar cell polarity signaling controls the anterior-posterior organization of monoaminergic axons in the brainstem. The Journal of neuroscience : the official journal of the Society for Neuroscience 30:16053-16064.

122

Formstone CJ, Mason I (2005) Expression of the Celsr/flamingo homologue, c-fmi1, in the early avian embryo indicates a conserved role in neural tube closure and additional roles in asymmetry and somitogenesis. Dev Dyn 232:408-413.

Gally C, Bessereau JL (2003) GABA is dispensable for the formation of junctional GABA receptor clusters in Caenorhabditis elegans. J Neurosci 23:2591-2599.

Gao FB, Kohwi M, Brenman JE, Jan LY, Jan YN (2000) Control of dendritic field formation in Drosophila: the roles of flamingo and competition between homologous neurons. Neuron 28:91-101.

Grill B, Bienvenut WV, Brown HM, Ackley BD, Quadroni M, Jin Y (2007) C. elegans RPM-1 regulates axon termination and synaptogenesis through the Rab GEF GLO-4 and the Rab GTPase GLO-1. Neuron 55:587-601.

Hall DH, Russell RL (1991) The posterior nervous system of the nematode Caenorhabditis elegans: serial reconstruction of identified neurons and complete pattern of synaptic interactions. The Journal of neuroscience : the official journal of the Society for Neuroscience 11:1-22.

Harterink M, Kim DH, Middelkoop TC, Doan TD, van Oudenaarden A, Korswagen HC (2011) Neuroblast migration along the anteroposterior axis of C. elegans is controlled by opposing gradients of Wnts and a secreted Frizzled-related protein. Development 138:2915-2924.

Hedgecock EM, Culotti JG, Hall DH (1990) The unc-5, unc-6, and unc-40 genes guide circumferential migrations of pioneer axons and mesodermal cells on the epidermis in C. elegans. Neuron 4:61-85.

Hilliard MA, Bargmann CI (2006) Wnt signals and frizzled activity orient anterior-posterior axon outgrowth in C. elegans. Developmental cell 10:379-390.

Huang X, Cheng HJ, Tessier-Lavigne M, Jin Y (2002) MAX-1, a novel PH/MyTH4/FERM domain cytoplasmic protein implicated in netrin-mediated axon repulsion. Neuron 34:563-576.

Huang X, Huang P, Robinson MK, Stern MJ, Jin Y (2003) UNC-71, a disintegrin and metalloprotease (ADAM) protein, regulates motor axon guidance and sex myoblast migration in C. elegans. Development 130:3147-3161.

Hutter H (2003) Extracellular cues and pioneers act together to guide axons in the ventral cord of C. elegans. Development 130:5307-5318.

Inaki M, Yoshikawa S, Thomas JB, Aburatani H, Nose A (2007) Wnt4 is a local repulsive cue that determines synaptic target specificity. Curr Biol 17:1574-1579.

Jin Y (2005) Synaptogenesis. WormBook 1-11.

Jin Y, Jorgensen E, Hartwieg E, Horvitz HR (1999) The Caenorhabditis elegans gene unc-25 encodes glutamic acid decarboxylase and is required for synaptic transmission but not synaptic development. The Journal of neuroscience : the official journal of the Society for Neuroscience 19:539-548.

Kennedy S, Wang D, Ruvkun G (2004) A conserved siRNA-degrading RNase negatively regulates RNA interference in C. elegans. Nature 427:645-649.

Killeen MT (2009) The dual role of the ligand UNC-6/Netrin in both axon guidance and synaptogenesis in C. elegans. Cell Adh Migr 3:268-271.

Kim K, Li C (2004) Expression and regulation of an FMRFamide-related neuropeptide gene family in Caenorhabditis elegans. The Journal of comparative neurology 475:540-550.

Kirszenblat L, Pattabiraman D, Hilliard MA (2011) LIN-44/Wnt directs dendrite outgrowth through LIN-17/Frizzled in C. elegans Neurons. PLoS biology 9:e1001157.

Klassen MP, Shen K (2007) Wnt signaling positions neuromuscular connectivity by inhibiting synapse formation in C. elegans. Cell 130:704-716.

Knobel KM, Jorgensen EM, Bastiani MJ (1999) Growth cones stall and collapse during axon outgrowth in Caenorhabditis elegans. Development 126:4489-4498.

Koushika SP, Richmond JE, Hadwiger G, Weimer RM, Jorgensen EM, Nonet ML (2001) A post-docking role for active zone protein Rim. Nat Neurosci 4:997-1005.

Lawrence PA, Casal J, Struhl G (2004) Cell interactions and planar polarity in the abdominal epidermis of Drosophila. Development 131:4651-4664.

Lee RC, Clandinin TR, Lee CH, Chen PL, Meinertzhagen IA, Zipursky SL (2003) The protocadherin Flamingo is required for axon target selection in the Drosophila visual system. Nature neuroscience 6:557-563.

Lewis A, Wilson N, Stearns G, Johnson N, Nelson R, Brockerhoff SE (2011) Celsr3 is required for normal development of GABA circuits in the inner retina. PLoS Genet 7:e1002239.

Lu B, Usui T, Uemura T, Jan L, Jan YN (1999) Flamingo controls the planar polarity of sensory bristles and asymmetric division of sensory organ precursors in Drosophila. Curr Biol 9:1247-1250.

Lyuksyutova AI, Lu CC, Milanesio N, King LA, Guo N, Wang Y, Nathans J, Tessier-Lavigne M, Zou Y (2003) Anterior-posterior guidance of commissural axons by Wnt-frizzled signaling. Science 302:1984-1988.

Maro GS, Klassen MP, Shen K (2009) A beta-catenin-dependent Wnt pathway mediates anteroposterior axon guidance in C. elegans motor neurons. PloS one 4:e4690.

McCaffrey LM, Macara IG (2009) Widely conserved signaling pathways in the establishment of cell polarity. Cold Spring Harb Perspect Biol 1:a001370.

McIntire SL, Reimer RJ, Schuske K, Edwards RH, Jorgensen EM (1997) Identification and characterization of the vesicular GABA transporter. Nature 389:870-876.

Najarro EH, Wong L, Zhen M, Carpio EP, Goncharov A, Garriga G, Lundquist EA, Jin Y, Ackley BD (2012) Caenorhabditis elegans flamingo cadherin fmi-1 regulates GABAergic neuronal development. The Journal of neuroscience : the official journal of the Society for Neuroscience 32:4196-4211.

Nonet ML, Grundahl K, Meyer BJ, Rand JB (1993) Synaptic function is impaired but not eliminated in C. elegans mutants lacking synaptotagmin. Cell 73:1291-1305.

Norris AD, Lundquist EA (2011) UNC-6/netrin and its receptors UNC-5 and UNC-40/DCC modulate growth cone protrusion in vivo in C. elegans. Development 138:4433-4442.

Pan CL, Howell JE, Clark SG, Hilliard M, Cordes S, Bargmann CI, Garriga G (2006) Multiple Wnts and frizzled receptors regulate anteriorly directed cell and growth cone migrations in Caenorhabditis elegans. Developmental cell 10:367-377.

Pettitt J (2005) The cadherin superfamily. WormBook 1-9.

Poon VY, Klassen MP, Shen K (2008) UNC-6/netrin and its receptor UNC-5 locally exclude presynaptic components from dendrites. Nature 455:669-673.

Prakasam AK, Maruthamuthu V, Leckband DE (2006) Similarities between heterophilic and homophilic cadherin adhesion. Proc Natl Acad Sci U S A 103:15434-15439.

Richmond J (2005) Synaptic function. WormBook 1-14.

Sanchez-Alvarez L, Visanuvimol J, McEwan A, Su A, Imai JH, Colavita A (2011) VANG-1 and PRKL-1 cooperate to negatively regulate neurite formation in Caenorhabditis elegans. PLoS genetics 7:e1002257.

Schmitz C, Wacker I, Hutter H (2008) The Fat-like cadherin CDH-4 controls axon fasciculation, cell migration and hypodermis and pharynx development in Caenorhabditis elegans. Dev Biol 316:249-259.

Senti KA, Usui T, Boucke K, Greber U, Uemura T, Dickson BJ (2003) Flamingo regulates R8 axon-axon and axon-target interactions in the Drosophila visual system. Current biology : CB 13:828-832.

Shafer B, Onishi K, Lo C, Colakoglu G, Zou Y (2011) Vangl2 promotes Wnt/planar cell polarity-like signaling by antagonizing Dvl1-mediated feedback inhibition in growth cone guidance. Developmental cell 20:177-191.

Shen K, Fetter RD, Bargmann CI (2004) Synaptic specificity is generated by the synaptic guidepost protein SYG-2 and its receptor, SYG-1. Cell 116:869-881.

Shima Y, Kawaguchi SY, Kosaka K, Nakayama M, Hoshino M, Nabeshima Y, Hirano T, Uemura T (2007) Opposing roles in neurite growth control by two seven-pass transmembrane cadherins. Nat Neurosci 10:963-969.

Shima Y, Kengaku M, Hirano T, Takeichi M, Uemura T (2004) Regulation of dendritic maintenance and growth by a mammalian 7-pass transmembrane cadherin. Dev Cell 7:205-216.

Song S, Zhang B, Sun H, Li X, Xiang Y, Liu Z, Huang X, Ding M (2010) A Wnt-Frz/Ror-Dsh pathway regulates neurite outgrowth in Caenorhabditis elegans. PLoS genetics 6.

Steimel A, Wong L, Najarro EH, Ackley BD, Garriga G, Hutter H (2010) The Flamingo ortholog FMI-1 controls pioneer-dependent navigation of follower axons in C. elegans. Development 137:3663-3673.

Stringham E, Pujol N, Vandekerckhove J, Bogaert T (2002) unc-53 controls longitudinal migration in C. elegans. Development 129:3367-3379.

Sudhof TC (2001) alpha-Latrotoxin and its receptors: neurexins and CIRL/latrophilins. Annu Rev Neurosci 24:933-962.

Takeichi M (2007) The cadherin superfamily in neuronal connections and interactions. Nature reviews Neuroscience 8:11-20.

Tissir F, Bar I, Jossin Y, De Backer O, Goffinet AM (2005) Protocadherin Celsr3 is crucial in axonal tract development. Nat Neurosci 8:451-457.

Trujillo G, Nakata K, Yan D, Maruyama IN, Jin Y (2010) A Ubiquitin E2 Variant Protein Acts in Axon Termination and Synaptogenesis in Caenorhabditis elegans. Genetics.

Usui T, Shima Y, Shimada Y, Hirano S, Burgess RW, Schwarz TL, Takeichi M, Uemura T (1999) Flamingo, a seven-pass transmembrane cadherin, regulates planar cell polarity under the control of Frizzled. Cell 98:585-595.

Vladar EK, Antic D, Axelrod JD (2009) Planar cell polarity signaling: the developing cell's compass. Cold Spring Harbor perspectives in biology 1:a002964.

White JG, Southgate, E., Thomson, J.N. and Brenner, S. (1986) The Structure of the Nervous System of The Nematode Caenorhabditis elegans. Philos Trans R Soc Lond B Biol Sci 314:1-340.

Wu M, Herman MA (2006) A novel noncanonical Wnt pathway is involved in the regulation of the asymmetric B cell division in C. elegans. Developmental biology 293:316-329.

Wu Z, Ghosh-Roy A, Yanik MF, Zhang JZ, Jin Y, Chisholm AD (2007) Caenorhabditis elegans neuronal regeneration is influenced by life stage, ephrin signaling, and synaptic branching. Proc Natl Acad Sci U S A 104:15132-15137.

Yamashita H, Goto A, Kadowaki T, Kitagawa Y (2004) Mammalian and Drosophila cells adhere to the laminin alpha4 LG4 domain through syndecans, but not glypicans. Biochem J 382:933-943.

Yan D, Wu Z, Chisholm AD, Jin Y (2009) The DLK-1 kinase promotes mRNA stability and local translation in C. elegans synapses and axon regeneration. Cell 138:1005-1018.

Yeh E, Kawano T, Weimer RM, Bessereau JL, Zhen M (2005) Identification of genes involved in synaptogenesis using a fluorescent active zone marker in Caenorhabditis elegans. J Neurosci 25:3833-3841.

Zhang H, Macara IG (2006) The polarity protein PAR-3 and TIAM1 cooperate in dendritic spine morphogenesis. Nat Cell Biol 8:227-237.

Zhen M, Jin Y (1999) The liprin protein SYD-2 regulates the differentiation of presynaptic termini in C. elegans. Nature 401:371-375.

Zhou HM, Walthall WW (1998) UNC-55, an orphan nuclear hormone receptor, orchestrates synaptic specificity among two classes of motor neurons in Caenorhabditis elegans. The Journal of neuroscience : the official journal of the Society for Neuroscience 18:10438-10444.

Zou Y (2006) Navigating the anterior-posterior axis with Wnts. Neuron 49:787-789.